CHALMERS
UNIVERSITY OF TECHNOLOGY

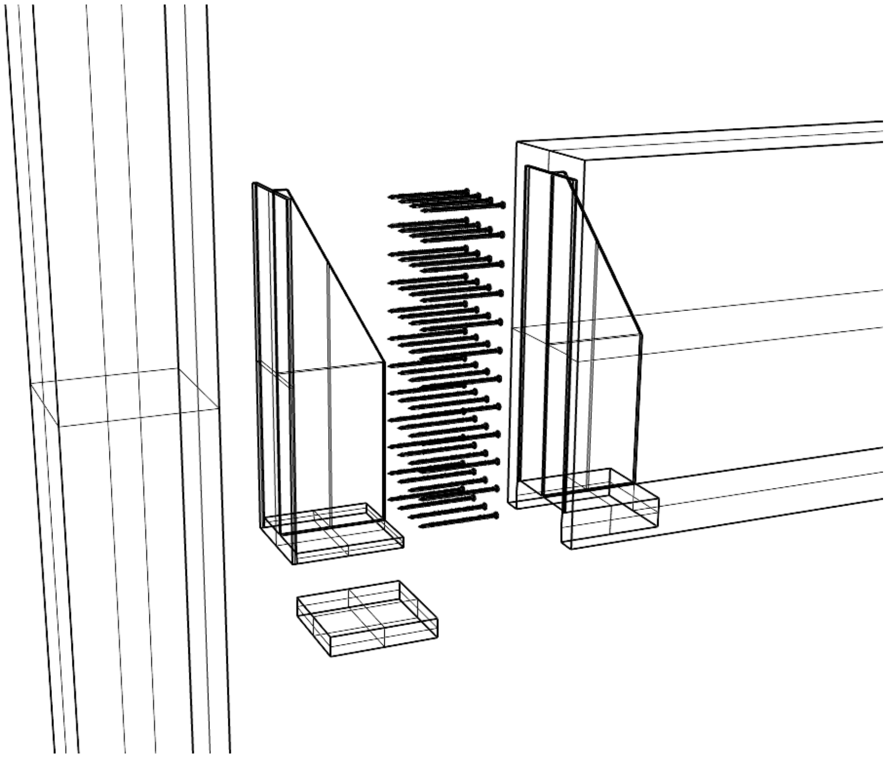

# Beam–Column Connections with Concealed Steel Components in Timber Structures

Master's Thesis in the Master's Programme Structural Engineering


MATTIS SUNDQVIST

SEBASTIAN BRÅTEN

DEPARTMENT OF ARCHITECTURE AND CIVIL ENGINEERING
DIVISION OF STRUCTURAL ENGINEERING AND BUILDING TECHNOLOGY

CHALMERS UNIVERSITY OF TECHNOLOGY



Master's thesis ACEX30
Gothenburg, Sweden 2026

MASTER'S THESIS ACEX30

# Beam–Column Connections with Concealed Steel Components in Timber Structures

*Master's Thesis in the Master's Programme Structural Engineering*

MATTIS SUNDQVIST
SEBASTIAN BRÅTEN

Department of Architecture and Civil Engineering
*Division of Structural Engineering and Building Technology*
CHALMERS UNIVERSITY OF TECHNOLOGY
Gothenburg, Sweden 2026

Beam–Column Connections with Concealed Steel Components in Timber Structures
*Master's Thesis in the Master's Programme Structural Engineering*

MATTIS SUNDQVIST
SEBASTIAN BRÅTEN



Supervisor: Ondrej Novotny, Tyréns AB
Examiner: Mahbube Subhani, Chalmers Department of Civil Engineering

Examensarbete ACEX30
Institutionen för Arkitektur och Samhällsbyggnadsteknik
Chalmers Tekniska Högskola, 2026

Department of Architecture and Civil Engineering
Division of Structural Engineering and Building Technology
Chalmers University of Technology
SE-412 96 Göteborg
Sweden
Telephone +46 31 772 1000

Cover:
Schematic illustration of the exploded assembly of the beam–column connection showing the internal beam shoe, screw arrangement, timber beam, column, and filler block prior to installation.
Department of Architecture and Civil Engineering
Göteborg, Sweden, 2026

Beam–Column Connections with Concealed Steel Components in Timber Structures

*Master's thesis in the Master's Programme Structural Engineering*

MATTIS SUNDQVIST

SEBASTIAN BRÅTEN

Department of Architecture and Civil Engineering
Division of Structural Engineering and Building Technology
Chalmers University of Technology

ABSTRACT

In timber structures, concealed beam-to-column connections may be attractive in applications where high load-carrying capacity must be combined with a seamless architectural expression. However, such connections are challenging to design, since the connection must provide sufficient resistance in both the steel components and the surrounding timber. In particular, compression perpendicular to the grain in the beam-side contact zone may become governing in bearing-type solutions.

This thesis investigates concealed beam-to-column connections in timber structures for high-load applications. Different concealed connection families were first reviewed and qualitatively screened with respect to load transfer, structural behaviour, and degree of concealment. Based on this screening, a bearing-type concept was selected for further study and developed in the form of an internal beam shoe integrated within the beam cross-section.

The connection behaviour was then studied through a combination of analytical and numerical methods. Simplified analytical models were used to describe the principal load-transfer mechanisms and to provide reference quantities for validation of a numerical model developed in Abaqus. The numerical analysis was used to investigate the force transfer to the timber column and to identify the governing steel components and fasteners. The results showed that the fasteners satisfied the governing shear, axial, and combined interaction checks for the studied load case, while the bearing plate was identified as the critical steel component due to local bending stresses.

On the beam side, the unreinforced timber did not provide sufficient resistance against compression perpendicular to the grain. Reinforcement strategies were therefore studied analytically through parametric analyses and genetic-algorithm-based optimization. The results showed that fully threaded screws, rods with wood screw thread, and bonded-in rods could increase the beam-side capacity sufficiently to carry the applied load, whereas wooden dowels could not. Among the feasible alternatives, screw reinforcement was found to be the most efficient solution with respect to capacity increase and associated $CO_2$-emissions.

Key words:
concealed timber connections, beam-to-column connection, compression perpendicular to grain, internal beam shoe, reinforcement optimization, timber structures

# Contents

# List of Figures

# List of Tables

# Notations

The main symbols and abbreviations used in the thesis are listed below.

### Abbreviations

| | |
|---|---|
| CPG | Compression perpendicular to grain |
| EWP | Engineered wood products |
| FEM | Finite element method |
| GA | Genetic algorithm |

### Roman upper-case letters

| | |
|---|---|
| $F$ | Force |
| $M$ | Bending moment |
| $N$ | Normal force |
| $V$ | Shear force |

### Roman lower-case letters

| | |
|---|---|
| $b$ | Width |
| $d$ | Fastener diameter |
| $h$ | Height |
| $l_w$ | Penetration depth / withdrawal length |
| $n$ | Number of fasteners |

### Greek letters

| | |
|---|---|
| $\sigma$ | Normal stress |
| $\theta$ | Rotation angle |
| $\gamma_M$ | Partial material factor |

# 1 Introduction

In recent years, sustainability has become a central consideration in structural engineering. In response, timber structures are experiencing renewed interest, driven by environmental imperatives and advances in engineered wood products (EWP) (Kuda & Petřičková, 2020). Glue laminated timber (Glulam) is a widely used EWP known for its high strength-to-weight ratio, dimensional stability, and design flexibility (A.Pranata et al., 2025). These properties have enabled high-rise and long-span timber constructions. In such structures, the beam-to-column connection plays a decisive role in load transfer and overall structural stability.

The growing use of timber in larger-scale buildings increases the demand for high-strength beam-to-column connections. Many connections in mass timber construction rely on externally mounted steel components, such as dowels, bolts, screws, nails, pins, plates, brackets, and hangers, which are often visible at the timber surface (WoodWorks, 2024). While such solutions can provide reliable load transfer and ease of assembly, visible steel elements may conflict with architectural intentions that prioritize a clean and homogeneous timber appearance. Concealed steel connections or all-wood solutions may help preserve such an expression, but high loads and large spans make their design challenging.

Timber also has an inherent weakness in compression perpendicular to the grain (CPG), which is particularly critical in concealed beam-to-column connections (Kanagaki et al., 2025). Reinforcement of the beam-side timber may therefore be required to prevent local crushing and ensure adequate load transfer in such connections.

These challenges are relevant in an ongoing timber project by Tyréns in central Stockholm, where the architectural ambition is to achieve a seamless and exposed timber expression. The project serves as a reference case with regard to span lengths, load levels, and structural dimensions. However, the scope of this thesis is not limited to the specific requirements of this project. Instead, the reference case is used to define realistic boundary conditions, while the findings aim to provide broader applicability to similar timber structures.

## 1.1 Aim and objectives

The aim of this thesis is to investigate concealed beam-to-column connections in timber structures, with particular focus on applications requiring high load-carrying capacity and a seamless architectural expression. The work aims to contribute to the development of structurally efficient and practically feasible concealed connection solutions for modern timber construction. Furthermore, the thesis investigates whether reinforcement of the beam-side timber can improve the structural performance of the connection, with particular focus on increasing the CPG-capacity while minimizing the associated $CO_2$-emissions of the reinforcement strategy.

The objectives of this thesis are to:

- evaluate different concealed beam-to-column connection families for timber structures and identify a suitable direction for further detailed investigation,

- develop and assess a selected concealed connection concept with respect to its structural behaviour and load transfer,
- evaluate how the selected concealed connection concept transfers forces to the column, identify the governing steel components and fasteners, and assess whether the concept provides sufficient design resistance, and
- investigate reinforcement strategies for the beam-side timber in order to identify which parameters most effectively increase the compression-perpendicular-to-grain capacity while minimizing the associated $CO_2$-emissions.

## 1.2 Research questions

Based on the aim and objectives of the thesis, the following research questions are addressed:

- Which concealed beam-to-column connection family is most suitable for high-load timber applications with respect to load transfer, structural behavior, and degree of concealment?
- In what way does the connection concept distribute shear and axial forces to the column, and what are the influencing factors?
- What are the most critical components and to what extent can the selected connection concept provide sufficient load transfer and resistance, considering column-side force transfer (steel and fasteners) as well as both column-side and beam-side compression perpendicular to the grain?
- Which reinforcement strategy is most material efficient in terms of minimizing $CO_2$-emissions while increasing the beam-side compression perpendicular-to-grain capacity, and what are the most influencing design parameters?

## 1.3 Methodology

The methodology of this thesis is divided into four main phases. These phases are structured to move from an initial screening of concealed timber connection families to a detailed investigation of a selected concept, followed by feasibility assessment of both the steel-side and beam-side response, and finally a study of reinforcement strategies for the beam-side timber.

1. **Literature review and screening of connection families.** The first phase consists of a review of relevant literature, design standards, and existing concealed beam-to-column connection solutions in timber structures. Based on this review, different connection families are qualitatively assessed with respect to load transfer mechanisms, structural behaviour, and degree of concealment. The purpose of this phase is to identify a suitable connection family for further detailed investigation.
2. **Concept development, numerical modelling, and analytical validation.** In the second phase, a selected concealed connection concept is developed in greater detail. A numerical model of the column-side of the connection is established in Abaqus, including the steel components and fasteners. In parallel, simplified analytical models are developed to describe selected response quantities in the connection. These include the fastener shear force distribution, the fastener ax-

ial force distribution, and the bending stress in the bearing plate. The purpose of these analytical models is to support subsequent validation of the numerical model through comparison with the corresponding numerical results.

3. **Feasibility assessment of the connection.** In the third phase, the feasibility of the selected connection concept is assessed. On the steel side, the governing forces and stresses obtained from the numerical model are compared with the corresponding design resistances of the fasteners and steel components according to applicable Eurocode provisions. On the beam side, an analytical model is developed for the unreinforced beam in order to assess whether the beam can resist compression perpendicular to the grain without reinforcement. Together, these assessments are used to determine whether the selected concealed connection concept is feasible as a whole connection.

4. **Reinforcement analysis and optimization.** In the final phase, analytical models are developed for the reinforced beam-side of the connection. Different reinforcement strategies are then studied through analytical modelling, parametric analyses, and genetic-algorithm-based optimization. The purpose of this phase is to determine which reinforcement strategies most effectively increase the beam-side compression-perpendicular-to-grain capacity while remaining compatible with concealed detailing and minimizing the associated $CO_2$-emissions.

## 1.4 Limitations / Demarcations

This thesis is subject to a number of deliberate limitations intended to ensure a focused and feasible investigation within the available timeframe.

The study is limited to concealed beam-to-column connections in timber structures and does not aim to provide an exhaustive survey of all possible connection solutions. The detailed structural investigation is limited to one selected connection concept. The analytical and numerical studies are therefore focused on this concept and are not extended to full design verification of alternative solutions.

The structural assessment is carried out primarily by analytical and numerical methods supported by existing literature and design standards. Experimental testing is not included in the scope of the thesis. The results should therefore be interpreted as analytical and numerical assessments of the proposed concept rather than as experimentally validated design values.

The loading considered in this thesis is limited to the transverse load transferred from the beam to the column. Lateral loading and eccentric loading causing rotation about the longitudinal axis of the beam are not included in the detailed analysis.

The numerical analysis is limited to selected parts of the connection. The timber beam is not included in the finite element model. Instead, the transferred load is applied directly at the contact interface. Consequently, the CPG-behavior of the timber is assessed analytically according to applicable Eurocode provisions rather than numerically.

The reinforcement analysis is based on analytical modeling, parametric studies, and genetic algorithm optimization, and is not validated through numerical modeling or experimental testing.

Long-term effects such as creep, moisture variations, shrinkage, and aging are not considered in the detailed analysis.

## 1.5 Societal, ethical and ecological consideration

In the process of formulating this degree project, it is necessary to reflect upon the broader implications of the work beyond its technical objectives. Although the thesis is conducted in collaboration with Tyréns and addresses practical design challenges relevant to industry, the purpose of the study is not solely to promote a particular technical solution. Instead, the work must be evaluated within a broader societal, ethical, and ecological context.

From a societal perspective, structural engineering solutions directly affect safety, reliability, and long-term performance of buildings. The development and evaluation of connection solutions must therefore prioritize structural safety, robustness, and compliance with established design standards where applicable. Questions that need to be addressed include whether the proposed solutions contribute to safe and sustainable construction practices, and whether their implementation could influence cost efficiency, resource use, or accessibility within the construction sector.

From an ecological perspective, timber construction is often promoted as a climate-efficient alternative to conventional building materials. However, reinforcement strategies involving steel components or additional material use may affect the overall environmental footprint of a structure. The study must therefore consider how different connection solutions influence material consumption, potential carbon impact, durability, and the possibility of reuse or recycling.

From an ethical research perspective, it is essential that the study is conducted objectively and transparently. The collaboration with industry must not influence the scientific integrity of the work. Assumptions, limitations, and uncertainties in analytical models, optimization procedures, and numerical simulations must be clearly stated. Furthermore, no results should be selectively reported to favor a predetermined outcome. The objective is to provide a balanced and technically justified comparison of alternative solutions.

By addressing these societal, ecological, and ethical dimensions, the thesis aims to ensure that the proposed connection solutions are not only structurally efficient, but also responsibly developed and evaluated.

## 1.6 Use of AI in the project

AI-based tools were used as support for writing, language revision, and presentation preparation. They were mainly used to improve the formulation and structure of text and to support brainstorming around research questions, methodology, and discussion points. All technical assessments, modeling, result interpretation, and conclusions were carried out and critically evaluated by the authors.

# 2 Background and literature review

This chapter first presents the material and connection behavior required to understand the investigated structural problem. Previous research on moment-resisting, hanger-type, and bearing-type concealed timber connections is then reviewed, with emphasis on their structural behavior, advantages, limitations, and remaining research gaps. Finally, the governing failure mechanisms and relevant design provisions for timber connections are introduced.

## 2.1 Mechanical properties of wood

Wood is an anisotropic material, meaning its mechanical properties depend on the direction of loading relative to the grain (Swedish Wood, 2022). Therefore, stresses and deformations are evaluated with respect to the longitudinal, radial and tangential directions of the material, see Figure 2.1.

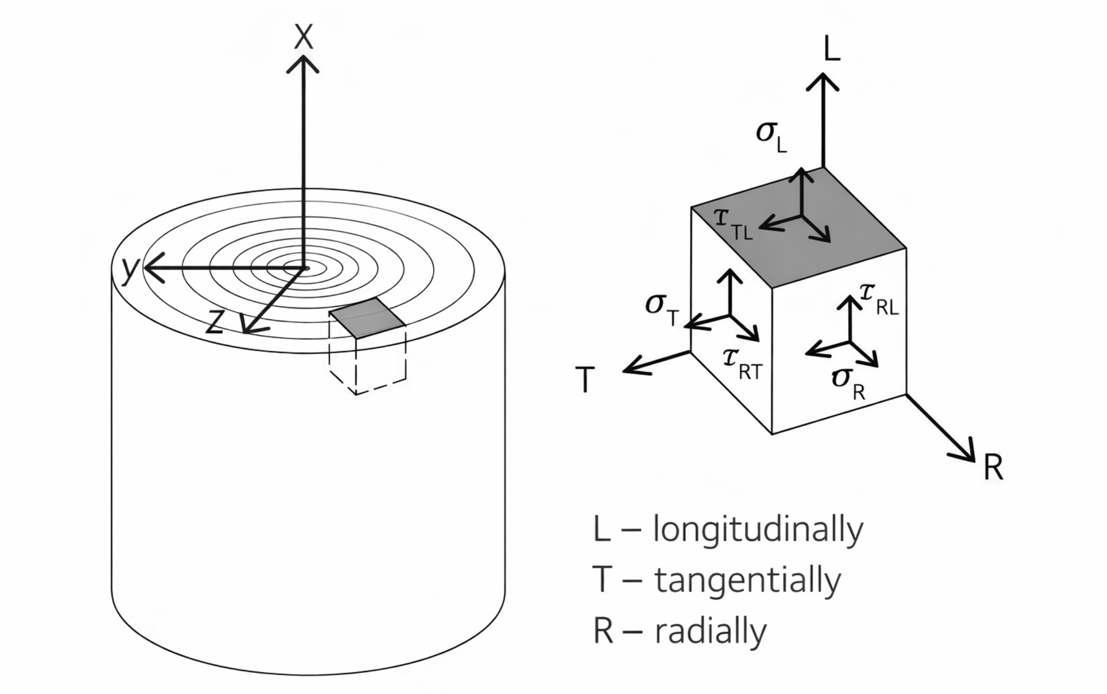


**Figure 2.1:** Normal and shear stresses in longitudinal, tangential and radial direction in wood.

For structural applications, the material response is often simplified to behavior parallel to the grain and perpendicular to the grain (Swedish Wood, 2022). The modulus of elasticity and strength differ greatly between these directions, which explains why timber performs well in some load cases, and poorly in others.

As shown in Figures 2.2a and 2.2b, wood loaded in tension parallel to the grain shows high strength and an almost linear stress-strain relationship up to brittle failure. In contrast, tension perpendicular to the grain results in much lower strength, with failure occurring at significantly lower stress levels. Studying Figures 2.2c and 2.2d, in compression parallel to the grain the wood fibres act as tubular elements with relatively high strength up until instability begins, after which non-linearity develops. By comparison, the compression perpendicular to the grain is governed by local crushing of the cellular structure and shows much lower strength.

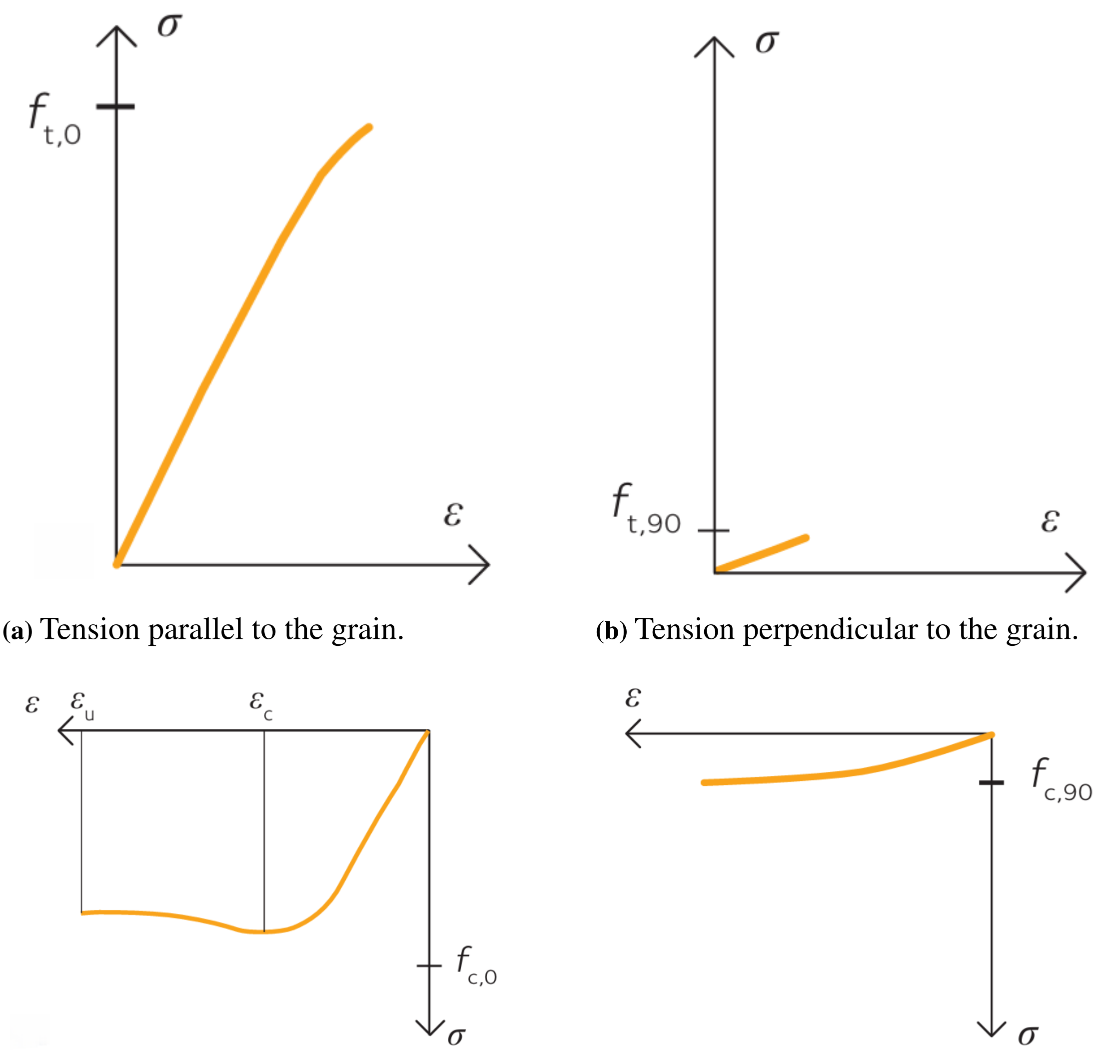


**(a)** Tension parallel to the grain.

**(b)** Tension perpendicular to the grain.

**(c)** Compression parallel to the grain.

**(d)** Compression perpendicular to the grain.

**Figure 2.2:** Stress-strain relationship for clear wood loaded in tension and compression, parallel and perpendicular to the grain.

## 2.2 Glued laminated timber

Glued laminated timber (glulam) is an engineered wood product that consists of several sawn timber laminations which are bonded together with adhesive, such that the grain direction runs along the longitudinal axis of the member (Swedish Wood, 2022). This manufacturing method enables the production of structural members with larger and more versatile cross-sections than ordinary sawn timber. In homogeneous glulam, laminations of similar quality are used throughout the cross-section, while combined glulam places stronger laminations in the outer regions of the member, where bending stresses are highest. Together, these form the two main types of glued laminated timber.

Regarding mechanical behaviour, its main advantage lies in the reduced variability of strength, meaning that defects that would strongly weaken a single solid member are distributed among many smaller pieces when the material is divided into laminations (Swedish Wood, 2022). As a result, the local weaknesses become less fatal and the structural behaviour becomes more uniform and reliable.

## 2.3 Timber connection behavior

In basic structural analysis, a rigid joint is defined as a connection in which the structural members in the joint maintain their relative positions even as the connected structural members deform (Leichti et al., 2000). Thus, the joint transfers moment and the connected members rotate together. This differs from a pinned joint, which does not transfer moment. The connected members are free to rotate relative to one another when subjected to loads that cause deformation. A semi-rigid joint lies between these two behaviors, transferring some moment and both member rotation and limited joint rotation may occur. The level of connection rigidity affects the bending moment and the deformation in the beam as shown in Figure 2.3.

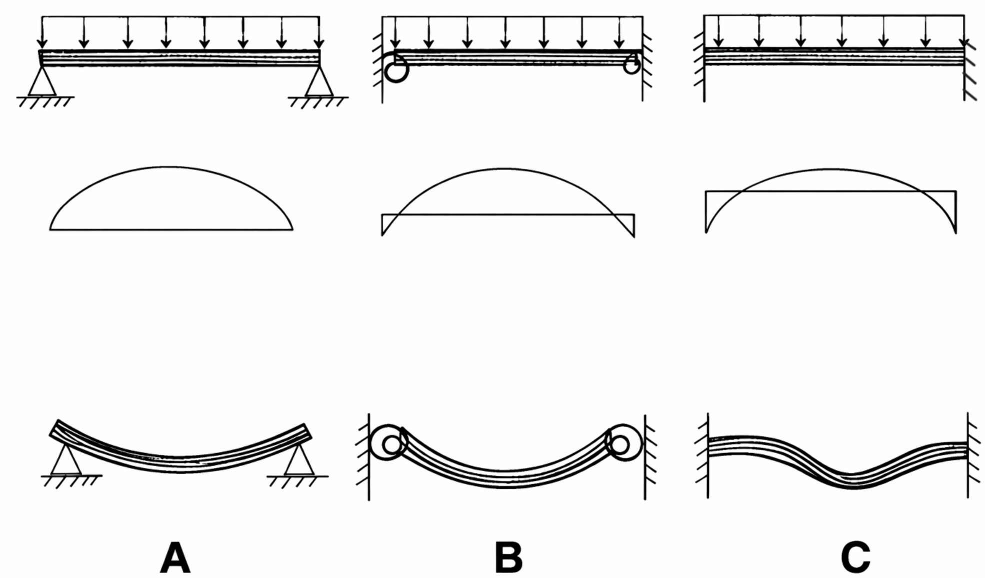


**Figure 2.3:** Diagrams of beams having (A) pinned, (B) semi-rigid, and (C) rigid end showing; loading, bending moment, and deformed shape.

However, for timber connections, fully rigid joints are rare due to the orthotropic stiffness of the wood. At the same time, joints are not free to rotate fully either, they generally exhibit a measurable degree of stiffness. Thus, in practice, timber connections are neither pinned nor rigid, but are instead semi-rigid to varying degrees depending on their connection stiffness.

## 2.4 Literature review of concealed timber connections

Connections can be categorized based on their load transfer mechanisms. From this perspective, concealed connections are divided into three connection families: moment-resisting, hanger-type, and bearing-type connections. In this section, relevant research on these connection families is reviewed, focusing on their structural behavior, advantages, limitations, and remaining research gaps.

### 2.4.1 Moment-resisting concealed connections

This section reviews relevant research on moment-resisting concealed timber connections, focusing on their structural behavior, advantages, limitations, and remaining research gaps.

#### 2.4.1.1 Current state of research

Moment-resisting beam-to-column connections are designed to transfer bending moments in addition to shear and axial forces. They can therefore contribute to the lateral stiffness of timber frames and reduce the dependence on diagonal bracing or structural walls. However, their performance is strongly influenced by the rotational stiffness, strength, ductility, and failure mode of the connection. Reboucas et al. (2022) reviewed two commonly investigated approaches to ductile moment-resisting timber connections: reinforced bolted connections with slotted-in steel plates and connections using glued-in steel rods. Their review showed that both approaches can provide substantial moment resistance and rotation capacity, although their failure mechanisms and levels of ductility differ.

Gauthier-Turcotte et al. (2022) experimentally investigated full-scale glulam beam-to-column connections using glued-in steel rods. Three configurations with different numbers of rods and member dimensions were tested. The connections behaved as semi-rigid moment-resisting joints, and their stiffness and capacity were influenced by the number and arrangement of rods, the dimensions of the members, and the resistance of the surrounding timber. The bending moment was transferred through a combination of rods subjected to tension, rods subjected to compression, and compressive stresses in the timber. The experiments showed that ductile behavior could be achieved when failure developed in the steel rods, whereas splitting of the timber anchorage region resulted in brittle failure.

A different steel-based concept was studied by Stamatopoulos et al. (2022), who developed a moment-resisting beam-to-column connection using inclined screwed-in threaded rods and metallic coupling components. The threaded rods transfer tensile and compressive forces associated with the bending moment and provide high axial stiffness within the connection. The authors developed analytical expressions for the rotational stiffness and forces in the rods using the component method. The predicted stiffness was subsequently compared with full-scale experimental results, for which good agreement was reported. This study demonstrates how concealed or highly integrated rod systems can be described using component-based analytical models rather than relying exclusively on experimental characterization.

In addition to steel-based solutions, Hawasly et al. (2023) investigated a bio-inspired, wood-only moment-resisting connection. The joint consisted of a stepped conical mortise-and-tenon interface combined with bent laminated beech plies that extended between the glulam beam and column. The conical interface was intended to distribute shear across the contact surface, while the bent plies transferred tensile and compressive forces associated with moment resistance. The connection was tested under cyclic bending, and its performance was compared by the authors with calculated reference values for glued-in-rod and lag-screw-bolt connections. The best-performing wood-only configuration achieved a moment capacity close to the glued-in-rod reference used in the comparison, although its initial rotational stiffness was considerably lower.

#### 2.4.1.2 Advantages

A principal advantage of moment-resisting connections is their ability to contribute to the global stiffness and stability of the structural frame. By transferring bending moments at the beam-to-column interface, these connections may reduce lateral displacements and allow more open structural layouts than systems that depend entirely on walls or diagonal bracing. Reboucas et al. (2022) further emphasized that adequate ductility is important for structural robustness and energy dissipation, particularly when moment-resisting timber frames are subjected to cyclic or seismic loading.

Connections based on glued-in or screwed-in rods can also provide architectural advantages because much of the load-transferring system is integrated within the timber members. Gauthier-Turcotte et al. (2022) identify mechanical performance, fire resistance, and architectural appearance as relevant advantages of glued-in-rod systems. In comparison with externally mounted steel plates and brackets, integrated rods can preserve a more continuous exposed-timber surface.

The wood-only concept proposed by Hawasly et al. (2023) represents an alternative approach in which steel accessories are eliminated entirely. Its bent plies provide a continuous timber load path through the joint, while the conical interface distributes shear over a larger surface. The study therefore demonstrates that substantial bending resistance can also be achieved through geometrically integrated timber components. Nevertheless, this concept should be regarded as an experimental alternative rather than an established replacement for conventional steel-based systems.

#### 2.4.1.3 Limitations

The main limitation of moment-resisting timber connections is that moment transfer produces high tensile and compressive forces within a relatively small connection region. The resulting stress concentrations may cause brittle timber failures before ductile deformation develops in the steel components. In the tests by Gauthier-Turcotte et al. (2022), failure of the steel rods provided comparatively ductile behavior, while splitting of the timber around the anchorage resulted in brittle failure. Rod spacing, edge distances, timber cover, anchorage length, and the relationship between steel and timber resistance are therefore important design parameters.

The behavior of glued-in-rod joints is further complicated by the anisotropy of timber, the discontinuity between the connected members, stress concentrations, adhesive behavior, and time-dependent deformation. Fragiacomo and Batchelar (2012) investigated the long-term behavior of glued-in-rod moment joints and found that creep, stress redistribution, and local deformation of timber loaded perpendicular to the grain may influence the overall joint response. This makes the prediction of long-term rotational stiffness and deformation more complex than the analysis of an idealized rigid connection.

The wood-only system studied by Hawasly et al. (2023) also illustrates limitations associated with highly integrated connection geometries. Splitting developed in the bent plies, while cracks and transverse tensile stresses occurred in the column region. The performance was sensitive to the geometry and glued surface of the conical interface. Furthermore, manufacture required bent lamination, several adhesive interfaces, CNC-machined channels, and controlled fitting tolerances. The authors therefore concluded that the system required further analytical, parametric, and manufacturing development and acknowledged that its production was more complicated than conventional steel-added alternatives.

#### 2.4.1.4 Research gap

The reviewed studies demonstrate several feasible approaches to moment-resisting timber connections, including reinforced slotted-in plates, glued-in steel rods, inclined threaded rods, and wood-only systems with continuous bent plies. However, the studies primarily evaluate moment capacity, rotational stiffness, ductility, cyclic response, or the behaviour of individual connection concepts. Within the literature reviewed for this thesis, comparatively limited attention is given to the systematic comparison of moment-resisting, hanger-type, and bearing-type concealed connections using common criteria such as load-transfer efficiency, robustness, constructability, tolerance sensitivity, and degree of concealment.

Furthermore, moment-resisting systems are generally developed to provide rotational restraint and lateral frame stiffness. These characteristics may provide limited benefit in applications where the principal requirement is to transfer a high vertical beam reaction. The additional components and anchorage required to establish a tension–compression couple may then introduce structural and manufacturing complexity without directly improving the transfer of the governing vertical load.

The literature therefore provides a strong basis for understanding the behavior of individual moment-resisting concepts but does not by itself establish whether this connection family is the most suitable for the high-load application considered in the present thesis. A comparative screening of the connection families is consequently carried out in Chapter 3, where moment-resisting, hanger-type, and bearing-type solutions are assessed using common evaluation criteria before one family is selected for further development.

### 2.4.2 Hanger-type concealed connections

This section presents a review of previous research on hanger-type concealed timber connections, focusing on their structural behavior, advantages, limitations, and remaining research gaps.

#### 2.4.2.1 Current state of research

Hanger-type beam-to-column connections are primarily designed to transfer vertical shear forces from the supported beam to the column or another primary member. Modern systems commonly consist of two pre-installed steel or aluminum components attached to the beam and supporting member using self-tapping screws. During assembly, the two components are engaged through sliding, interlocking, or clamping mechanisms. When the connector is recessed into the timber, the metal components can be concealed, while the connection is generally treated as a nominally pinned support at the structural level.

Recent research has investigated the behavior of proprietary pre-engineered beam hangers under loading conditions extending beyond their conventional vertical-shear design function. Ganjali et al. (2025) conducted 12 full-scale tests on RICON and MEGANT beam hangers subjected to combined shear and axial tension. The connectors maintained their resistance when simultaneously subjected to their factored shear resistance and an axial force corresponding to 5% of that resistance. Considerable axial resistance was also measured, and both connector systems exhibited ductile global behavior and residual deformation capacity. Although the connectors were surface-mounted in the experimental specimens, the results provide information about the biaxial behavior of systems that may also be installed in concealed configurations.

The conventional assumption that hanger-type connections behave as ideal pins was examined by Walters et al. (2025). The authors investigated a full-scale, single-storey, two-bay glulam frame connected using fully concealable MEGANT beam hangers. Experimental testing was combined with finite-element analysis to study how the rotational stiffness of the hangers influenced the connected columns. The frame sustained repeated cycles up to a storey drift of 3.0% without structural instability or connection failure. However, the numerical analysis showed that rotational restraint from hangers positioned on both sides of an interior column generated substantial bending moments. The authors therefore concluded that the studied hanger should be treated as semi-rigid rather than perfectly pinned when assessing the frame response.

The deformation compatibility of pre-engineered hanger connections was investigated further by Woods and Wierzbowski (2026). Bolt-and-collar and interlocking-jaw connectors were tested under combined gravity shear and cyclic rotation. The bolt-and-collar connections consistently reached rotations exceeding 0.06 rad before losing their shear-carrying capacity, while the interlocking-jaw connections exceeded 0.08 rad without losing that capacity. These results demonstrate that pre-engineered hangers can accommodate substantial frame deformation while maintaining gravity-load transfer. However, their rotational stiffness and capacity depend on factors such as connector geometry, screw arrangement, gravity loading, and connection detailing.

In addition to ambient structural performance, the fire behavior of concealed hanger connections has received recent attention. du Plessis et al. (2025) tested 16 concealed beam-to-column connections incorporating a proprietary aluminum hanger and gaps of 0, 3, 6, and 10 mm between the connected members. The specimens were exposed to the ISO 834 standard fire for 60 minutes, with half protected using an intumescent sealant. The results showed that unprotected gaps of 6 and 10 mm caused substantially greater temperature development around the connector and should therefore be avoided. The sealant significantly reduced connector temperatures and improved the predictability of the thermal response.

#### 2.4.2.2 Advantages

Pre-engineered beam hangers form part of the gravity-load-resisting system and are designed primarily to transfer vertical shear forces from the supported beam to the primary member. The load is transferred through the connector plates and self-tapping screws, resulting in a connection response governed mainly by connector and fastener action under gravity loading (Ganjali et al., 2025).

Because pre-engineered systems can be attached to the members before delivery, on-site installation may be completed by positioning the beam and engaging the corresponding connector components. For example, the RICON and MEGANT systems studied by Ganjali et al. (2025) consist of separate components installed on the primary and secondary members before the beam-side component is slid into position. This can simplify on-site assembly compared with connections requiring extensive installation of individual fasteners after the members have been positioned

Recessing the connector components within the timber provides a high degree of architectural concealment. The timber cover can also protect the embedded metal components from fire exposure. However, this protection may be compromised by gaps at the beam-to-column interface, particularly when the gaps expose the connector directly to fire (du Plessis et al., 2025).

Recent testing also indicates that pre-engineered hangers may provide useful performance beyond their nominal vertical-shear function. Ganjali et al. (2025) showed that the studied systems could resist concurrent shear and axial forces, while Woods and Wierzbowski (2026) demonstrated substantial rotational capacity without premature loss of gravity-load resistance. These characteristics are beneficial in buildings where the gravity frame must accommodate deformation imposed by the lateral-force-resisting system.

#### 2.4.2.3 Limitations

Despite being commonly represented as pinned connections, hanger systems may develop non-negligible rotational stiffness through interlocking connector components and deformation of the plates and fasteners. As demonstrated by Walters et al. (2025), this restraint can transfer bending moments into columns during lateral frame deformation. Neglecting this behavior may therefore underestimate the combined bending and axial-force demand in the supporting members.

The structural response also depends on the behavior and arrangement of several individual components. Potential failure mechanisms include connector yielding, screw withdrawal or tensile failure, and splitting of the surrounding timber. In the full-frame tests discussed by Walters et al. (2025), typical connector damage was characterized by yielding of the connector plates followed by failure of several screws. Although the frame maintained stability up to the maximum investigated drift, the results demonstrate that the force transfer during lateral deformation may differ considerably from an idealized vertical-shear load path.

Concealment may introduce further practical challenges. Recesses must be manufactured and aligned accurately so that the connector components engage during assembly and bear as intended. Gaps may be planned for constructability or develop because of moisture-related shrinkage and swelling, but such gaps can expose the connector to fire and reduce the protection otherwise provided by the surrounding timber. du Plessis et al. (2025) showed that variations in gap size significantly influenced the thermal response. Manufacturing tolerances, moisture-related dimensional changes, installation accuracy, and fire-protection detailing should therefore be considered together rather than independently.

Pre-engineered hangers are commonly proprietary systems with connector-specific geometries, fastener arrangements, capacities, and installation requirements. The studies reviewed here also concern particular RICON, MEGANT, and aluminium hanger configurations. Findings obtained for one connector type or size may therefore not be directly transferable to another system, particularly when the connection must resist unusually high beam reactions.

#### 2.4.2.4 Research gap

The reviewed research demonstrates that concealed hanger-type connections can provide efficient vertical-load transfer, relatively simple assembly, considerable deformation capacity, and a high degree of architectural concealment. However, recent studies have mainly examined individual proprietary systems under particular loading or exposure conditions, including combined shear and tension, cyclic frame deformation, or fire.

Within the literature reviewed for this thesis, limited research combines these aspects in a unified assessment of high-capacity concealed connections. In particular, the interaction between vertical resistance, rotational stiffness, installation tolerances, fire protection, and structural robustness is not described through a general framework applicable across different proprietary hanger systems. The available results also indicate that idealizing such connections as perfectly pinned may not adequately represent their influence on the surrounding frame.

The literature therefore establishes hanger-type systems as a technically viable family of concealed connections, but it does not determine whether they are preferable to moment-resisting or bearing-type solutions for the high vertical reaction considered in this thesis. The three connection families are consequently compared using common evaluation criteria in Chapter 3.

### 2.4.3 Bearing-type concealed connections

This section presents a review of previous research on bearing-type concealed timber connections, focusing on their structural behavior, advantages, limitations, and remaining research gaps.

#### 2.4.3.1 Current state of research

Bearing-type beam-to-column connections transfer the vertical beam reaction primarily through compressive contact. The contact may occur directly between timber members or through an intermediate bearing component integrated into the connection. At the beam-side support, the timber is typically loaded in compression perpendicular to the grain, while the force may be transferred to the supporting column through timber bearing, an internal steel component, mechanical fasteners, or a combination of these mechanisms. Auxiliary fasteners may provide positional restraint, uplift resistance, or stability during assembly, but the principal vertical load path remains the bearing interface.

Blass and Görlacher (2004) investigated timber contact joints subjected to partial compression perpendicular to the grain. They described such joints as comparatively easy to manufacture and assemble and found that their load–deformation behavior is generally ductile compared with many mechanically fastened timber connections. Their study distinguished several loading and support configurations and showed that local bearing resistance depends not only on the basic timber strength but also on the contact geometry and the availability of unloaded timber adjacent to the loaded area. Following initial local compression, the specimens could continue to resist increasing loads, although this was accompanied by increasing permanent deformation.

More recent research has continued to examine the influence of geometry and deformation on compression perpendicular to the grain. Pasca et al. (2024) conducted experimental investigations on solid timber, glued laminated timber, and cross-laminated timber, combined with a parametric finite-element study. The authors investigated the effects of support type, load position, contact dimensions, loading arrangement, and member height. Their results confirmed that the apparent bearing capacity is influenced by the accepted deformation level and by the extent to which stresses can spread into the surrounding timber. The study also identified a need to limit the effective height assumed in stress-spreading models for deep members.

A practical application of direct timber-to-timber bearing was presented by Blomgren et al. (2023). In the connection described by the authors, glulam beam ends bear directly on notches formed in the supporting columns, with screws used to provide positive fixing. At the horizontal bearing interface, the beam is loaded perpendicular to the grain while the column is loaded parallel to the grain. The authors identified reduced cost, relatively simple fabrication, architectural appearance, and high load-carrying capacity as advantages of this form of connection in mass-timber structures.

A bearing-type connection incorporating an internal steel component was experimentally investigated by Madland et al. (2023b). The authors tested five full-scale glulam beam-to-column connection systems under combined gravity and lateral loading. One of the custom-designed systems, denoted C1-KP, consisted of a bracketed steel knife plate connected to the timber column using screws. The beam reaction was transferred through bearing on the built-up steel angle of the knife-plate assembly, after which the load was transferred into the column through the vertical plate and its fasteners. The beam was locally notched to accommodate the internal plate.

Although the system was described as a knife-plate connection, it is relevant to the bearing-type family because the principal vertical reaction was transferred through bearing on a concealed steel component rather than solely through fastener shear. The tests primarily examined deformation compatibility under combined gravity and lateral actions. Both the monotonic and cyclic investigations showed that the connection could maintain its gravity-load-carrying function during substantial imposed frame deformation (Madland et al., 2023a, 2023b).

Since compression perpendicular to the grain may limit the capacity of bearing-type connections, reinforcement of the loaded timber region is sometimes required. Research has shown that self-tapping screws can increase bearing capacity and initial stiffness, although the reinforcement effect depends on screw dimensions, arrangement, thread configuration, timber properties, and loading conditions. The analytical prediction of reinforced capacity and failure modes also remains uncertain. Reinforcement strategies and their design models are therefore reviewed separately in Sections 2.6 and 2.7.3.

#### 2.4.3.2 Advantages

The principal structural advantage of bearing-type connections is their direct load path. The vertical beam reaction can be transferred through compressive contact rather than relying entirely on fasteners subjected to shear, withdrawal, or axial tension (Blomgren et al., 2023; Madland et al., 2023b). Local compression does not necessarily cause an immediate loss of load-carrying capacity, and timber contact joints may therefore exhibit a comparatively gradual load–deformation response. This behavior can provide deformation capacity, provided that the resulting bearing deformation remains compatible with the surrounding structure (Blass & Görlacher, 2004).

Bearing-type connections can be developed using either direct timber-to-timber contact or a concealed steel bearing component. The notched connection presented by Blomgren et al. (2023) demonstrates direct bearing between timber members, whereas the bracketed knife-plate connection studied by Madland et al. (2023b) demonstrates how the beam reaction can be introduced through an internal steel bearing surface. These alternatives provide opportunities to integrate the principal load-transferring components within the timber members while maintaining a concealed architectural expression.

The dimensions and position of the bearing surface may also be adapted to the required load and available member geometry. These parameters influence the nominal compressive stress and the extent of stress spreading within the timber. Auxiliary screws, plates, or other concealed components may additionally be introduced to provide positive fixing, lateral restraint, or force transfer to the supporting member while retaining the principal compressive load path (Blass & Görlacher, 2004; Blomgren et al., 2023; Madland et al., 2023b).

#### 2.4.3.3 Limitations

The main limitation of bearing-type connections is the relatively low strength and stiffness of timber perpendicular to the grain. Local compression can produce substantial support deformation before the resistance of the other connection components is reached. Depending on the structural configuration, this may primarily represent a serviceability problem, but the deformation may also influence the internal force distribution or initiate failure elsewhere in the structural member. Bearing resistance should therefore not be considered independently of the acceptable deformation level.

The effective capacity is also sensitive to the geometry surrounding the contact zone. Contact length, load position, member height, distance from the end of the member, neighboring loaded areas, and the amount of unloaded timber influence stress spreading. Consequently, a calculation based only on the physical contact area may neglect beneficial redistribution, whereas an overly generous assumed effective area may overestimate the resistance. This is particularly relevant for concealed bearing components because internal recesses may limit both the available contact area and the remaining timber cross-section.

Effective bearing further requires accurate fabrication and assembly. Uneven contact may cause the reaction to be introduced over only part of the intended surface, resulting in increased local stresses. At adjacent vertical interfaces, gaps may be required to accommodate fabrication tolerances, installation, structural rotation, and moisture-related dimensional changes. Blomgren et al. (2023) reported typical vertical gaps of approximately 2–6 mm in notched connections. Such gaps may also permit fire penetration unless suitable protection is provided.

A direct bearing load path does not necessarily result in a simple complete connection. In the knife-plate system investigated by Madland et al. (2023b), the vertical reaction was transferred through the steel bearing component, the vertical knife plate, and the column-side fasteners. Additional components were also required to provide lateral restraint. The performance of such a connection therefore depends on several interacting steel, fastener, and timber components and cannot be assessed through a compression-perpendicular-to-grain verification alone.

The Madland studies also focused primarily on deformation compatibility under a prescribed gravity load rather than on determining the ultimate vertical resistance of the bearing mechanism. Consequently, the tests provide valuable evidence that the connection can maintain gravity-load transfer during lateral deformation, but they do not establish a general design method for the bearing plate, column-side fastener forces, or the maximum vertical capacity of this type of connection (Madland et al., 2023a, 2023b).

#### 2.4.3.4 Research gap

The reviewed literature provides substantial knowledge concerning timber subjected to compression perpendicular to the grain, including the effects of partial loading, geometry, stress spreading, and accepted deformation. Practical studies further demonstrate that bearing-type connections can transfer vertical loads through either direct timber contact or concealed internal steel components.

However, much of the available research examines either the local bearing behavior of timber specimens or individual connection configurations developed for particular structural applications. The knife-plate connection investigated by Madland et al. (2023b) is particularly relevant because it combines beam-side bearing on an internal steel component with force transfer through a vertical plate and fasteners to the supporting column. Nevertheless, the study was primarily concerned with deformation compatibility and did not provide a general component-level assessment of high vertical resistance.

Within the literature reviewed for this thesis, limited research therefore addresses the complete behavior of concealed bearing-type beam-to-column connections by simultaneously considering beam-side compression perpendicular to the grain, deformation and resistance of the internal steel bearing component, and force transfer from the steel component into the timber column. Although the literature indicates that bearing-type connections can provide an efficient and concealable load path for high vertical loads, it does not establish whether this family is more suitable than alternative concealed systems. A comparative assessment of the different connection families is therefore carried out in Chapter 3 before a concept is selected for further development.

## 2.5 Governing behavior and failure mechanisms

The structural performance of timber connections is governed by a combination of material behavior and load transfer mechanisms. As introduced in the previous sections, different connection types exhibit distinct structural responses depending on how loads are transferred and resisted.

In order to assess the capacity and performance of such connections, it is necessary to understand the governing deformation mechanisms and potential failure modes. In particular, compression perpendicular to the grain and the behavior of mechanical fasteners play a central role in determining the load-carrying capacity of timber connections (CEN, 2025).

### 2.5.1 Compression perpendicular to grain

Compression perpendicular to grain refers to the loading of timber elements in a direction orthogonal to the wood fibers. In beam-to-column connections, this occurs when the reaction force from a beam is transferred to a supporting member, either through direct contact or via intermediate components such as steel bearing plates. This results in localized compressive stresses that act perpendicularly to the grain of the wood (Swedish Wood, 2022).

As described in Section 2.1, due to the anisotropic nature of wood, the strength and stiffness perpendicular to the grain are significantly lower than in the parallel direction. As a result, the behavior under such loading is typically governed by localized crushing and deformation of the timber. This leads to stress redistribution within the member, where the load is transferred over an increasing effective area. In design, this behavior is accounted for through simplified stress spreading models, where the load is assumed to spread into the member at a defined angle, see Figure 2.4 (CEN, 2025).

However, due to the non-uniform stress distribution in the contact region, local stress concentrations may occur, particularly near edges or geometric discontinuities (Jockwer & Dietsch, 2018). These effects may give rise to tensile stresses perpendicular to the grain, which can lead to cracking or splitting of the timber, representing a brittle failure mode. In practical design, such effects are typically addressed through appropriate detailing and reinforcement of the connection.

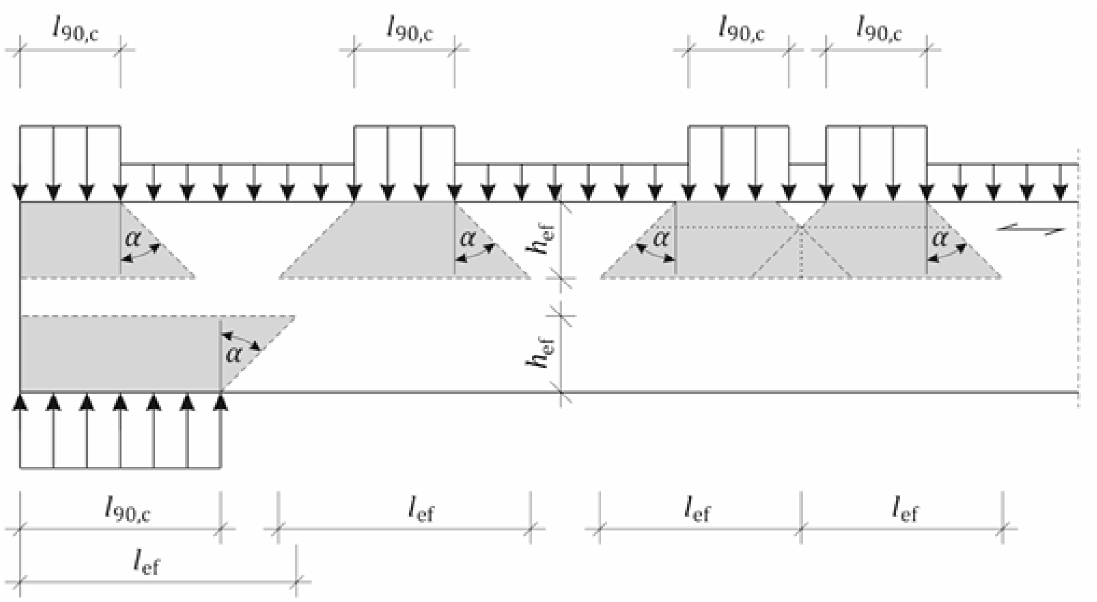


**Figure 2.4:** Effective load-spreading length and stress gradient in members supported by discrete supports.

### 2.5.2 Fastener behavior

Fasteners such as screws, bolts, and dowels are used to transfer loads between timber members or between timber and steel components through localized contact stresses and shear forces. The load-carrying capacity of these connections is governed by a number of characteristic failure modes, including embedment (crushing) of the timber, yielding of the fastener, and combined mechanisms involving both timber crushing and fastener plastic deformation (CEN, 2025). Figure 2.5 illustrates these typical failure modes for dowel-type fasteners in single shear.

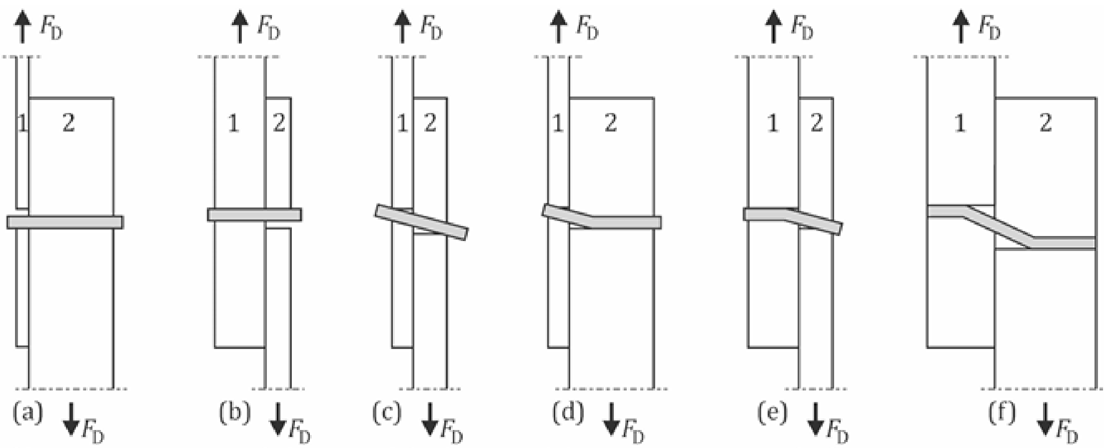


**Figure 2.5:** Failure modes for fastener loaded in single shear a) to f).

In addition to shear, fasteners in beam-to-column connections are often subjected to axial tensile forces. This occurs when eccentric loading causes rotation of the connection and uplift in parts of the fastener group. The fasteners must therefore be verified not only for lateral resistance, but also for axial tensile resistance. According to the draft EN 1995-1-1:2025 (CEN, 2025), the axial resistance of screws is governed by the relevant failure modes for axially loaded screws, primarily withdrawal failure of the threaded part, tensile failure of the screw, and, where relevant, pull-through-related failure.

### 2.5.3 Load transfer mechanisms

Load transfer in timber connections is governed by the interaction between compressive contact stresses and mechanical fasteners. Depending on the connection configuration, the applied load may be transferred through direct bearing between members, through fasteners, or through a combination of both (CEN, 2025).

In compression-dominated connections, load transfer is primarily achieved through compression perpendicular to the grain. As described in Section 2.5.1, the load is introduced over a limited contact area and subsequently redistributed within the timber through stress spreading, resulting in an increased effective load transfer area, as illustrated in Figure 2.4.

In connections relying on mechanical fasteners, load transfer occurs through localized contact stresses between the fastener and the surrounding timber. As described in Section 2.5.2, this interaction is governed by embedment behavior and potential yielding of the fastener.

In many practical connections, load transfer is achieved through a combination of these mechanisms. The relative contribution of each mechanism depends on the connection geometry, material properties, and loading conditions.

When the load-carrying capacity governed by CPG is insufficient, reinforcement can be introduced to enhance the load transfer mechanism (CEN, 2025).

## 2.6 Literature review of concealed reinforcement strategies

Compression perpendicular to the grain may govern the resistance and deformation of bearing-type timber connections. Reinforcement can be introduced into the loaded timber region to transfer part of the contact force deeper into the member, increase the effective load-distribution area, and reduce local deformation. A range of steel- and timber-based reinforcement strategies has been investigated in previous research.

The present thesis is specifically concerned with *concealed reinforcement*. In this context, reinforcement is considered concealed when the load-transferring elements are embedded within the timber member or installed from a surface that is subsequently covered by the connection assembly. The reinforcement should therefore not interrupt the exposed timber surfaces after installation. External steel plates, surface-mounted straps, and reinforcement applied to visible side faces are outside the scope of the study. Particular consideration is also given to whether the reinforcement can be accommodated without interfering with the internal steel components of the concealed beam-to-column connection.

### 2.6.1 Mechanically installed steel reinforcement

Mechanically installed reinforcement commonly consists of fully or partially threaded self-tapping screws inserted approximately perpendicular to the loaded timber surface. Rods with wood-screw thread use a similar load-transfer principle but generally have larger diameters and may provide greater axial resistance. When these elements are installed from the bearing surface and subsequently covered by a bearing plate or another internal connection component, the complete reinforcement arrangement can remain concealed.

The reinforcing elements transfer part of the applied compressive force through axial action and distribute it into timber located farther from the loaded surface. The resistance is therefore influenced by the number and arrangement of the reinforcing elements, their diameter and penetration depth, the axial resistance of the steel, the interaction between the thread and timber, and the compression resistance of the surrounding wood.

Kanagaki et al. (2025) experimentally investigated reinforcement of column-base and beam-joint regions using partially and fully threaded screws. The study showed that both alternatives could increase the CPG-capacity and initial stiffness. Fully threaded screws generally provided a greater reinforcement effect than partially threaded screws because a larger part of their length contributed to the force transfer. The results also showed that reinforcement performance depends on the screw dimensions, penetration length, number and arrangement of screws, timber properties, and the surrounding loading configuration.

A broader assessment of screw-reinforcement models was presented by Aloisio et al. (2023). Based on a database of experimental results, the authors concluded that self-tapping screws can provide an effective method for increasing CPG-resistance. However, they also identified uncertainty in the prediction of the governing failure mode and reinforced capacity. Existing models may, for example, predict failure at the screw tip even where this mechanism was not observed experimentally. The behavior should therefore not be described solely by adding the individual axial resistances of the reinforcing elements to the unreinforced timber resistance.

A principal practical advantage of self-tapping screws and rods with wood-screw thread is that they can be installed without adhesive or curing time. The method is therefore compatible with prefabrication and can be fully concealed by locating the screw heads beneath the internal bearing component or within a subsequently closed recess. The available dimensions and installation angles also provide some flexibility when adapting the reinforcement to the available member geometry.

The method nevertheless has several limitations. Minimum spacing, edge distances, and penetration requirements restrict the number of reinforcing elements that can be accommodated within the bearing region. Long or large-diameter elements may require substantial installation torque and may interfere with the concealed connection hardware. Their resistance may also be governed by steel failure, axial withdrawal or push-in behavior, instability of the reinforcing element, or local failure of the surrounding timber. These mechanisms and their interaction are not represented with equal accuracy by the available analytical models.

### 2.6.2 Bonded-in steel reinforcement

Bonded-in steel reinforcement consists of threaded or ribbed steel rods inserted into predrilled holes and bonded to the surrounding timber using an adhesive. The applied compressive force is transferred from the loaded surface into the rods and subsequently into the timber through shear stresses along the bonded length. As the rods can be installed entirely within the member, the method is compatible with concealed reinforcement and does not require visible external hardware.

Steiger et al. (2015) reviewed the use of glued-in rods for strengthening timber structures, including applications in support and contact regions subjected to high compression perpendicular to the grain. The authors identified the high axial stiffness of steel rods and the possibility of using different rod lengths as relevant advantages. The rods can act similarly to internal piles by transferring forces away from the highly stressed contact zone and into a larger volume of timber.

Bonded-in rods can provide greater freedom in the choice of diameter and anchorage length than commercially available self-tapping screws. They may therefore be suitable where a high reinforcement resistance or a substantial penetration depth is required. Since the rods do not require screw heads or installation access after bonding, they can also be positioned beneath an internal bearing plate and remain fully concealed after assembly.

The main disadvantages are associated with fabrication and quality control. The holes must be drilled with sufficient accuracy, cleaned, and filled so that a continuous adhesive layer is obtained around the rod. The rod must be centered and maintained in the correct position during curing. Voids, incomplete bonding, inaccurate hole geometry, unsuitable adhesive properties, or insufficient curing conditions can reduce the resistance. The finished bond line is also difficult to inspect once the rod has been installed. Compared with mechanically installed screws, bonded-in reinforcement therefore requires more controlled production and introduces additional uncertainty associated with the adhesive and timber–adhesive interface.

### 2.6.3 Timber-based reinforcement

Timber-based reinforcement provides an alternative to steel elements and can include glued-in hardwood rods, densified-wood dowels, or internal plywood plates. These methods aim to increase the CPG-resistance by introducing material with greater strength and stiffness in the direction of the applied load. When the reinforcing elements are embedded within the member, they can be incorporated without changing the exposed timber appearance.

Wang et al. (2025b) investigated reinforcement using adhesively bonded birch plywood plates and glued-in birch rods. The experimental study showed that both approaches could increase the compression-perpendicular-to-the-grain resistance. The glued-in rods were particularly effective because their grain direction was aligned with the applied compressive load, allowing the rods to utilize the substantially greater strength and stiffness of timber parallel to the grain.

Not all plywood arrangements investigated by Wang et al. (2025b) are equally applicable where the reinforcement is required to remain concealed. Plywood plates bonded to the external side faces of a timber member remain visible and therefore fall outside the scope adopted in this thesis. An internal plywood plate inserted into a slot may instead be concealed within the cross-section. However, such a solution requires a continuous recess and bonded interface, which reduce the remaining timber cross-section and may restrict the space available for other concealed connection components. Glued-in timber rods offer greater geometric flexibility because they can be arranged as discrete reinforcing elements within the loaded region without requiring a continuous internal slot.

Further testing of glued-in hardwood and densified-wood rods was presented by Wang et al. (2025a). The study showed that reinforcement resistance and stiffness generally increased with greater penetration depth and a larger number of rods. However, the effectiveness depended on sufficient anchorage within the timber, and adhesive-related failures were observed in some configurations. This demonstrates that timber-based rods are governed not only by the strength of the reinforcing material but also by the quality of the bonded interface and the geometry of the surrounding timber.

Densified-wood dowels have also been investigated as reinforcement for compression perpendicular to the grain. The pilot study by Conway et al. (2021) demonstrated the potential of densified-wood dowels as an all-timber alternative to steel screw reinforcement. Their use may reduce the quantity of metal introduced into the timber member and provide greater material compatibility. However, densified timber requires additional manufacturing, and the available experimental and design basis remains more limited than that for steel screws.

Timber-based reinforcement has the architectural advantage of being fully integrated into the timber member and may provide environmental benefits where steel use can be reduced. It can also avoid some of the installation conflicts associated with steel reinforcement and concealed steel connection components. Its limitations include the need for adhesive in many arrangements, variability in timber properties, potentially lower axial stiffness than steel, and comparatively limited standardized design guidance. The ability of ordinary or densified timber dowels to provide sufficient resistance in very highly loaded support regions must therefore be established for the particular application.

Overall, the reviewed reinforcement strategies can all be arranged within the timber member and thereby remain concealed after assembly. Mechanically installed screws and threaded rods offer relatively simple installation without adhesive, whereas bonded-in steel and timber rods provide greater freedom regarding diameter and anchorage length but require more controlled fabrication. Timber-based reinforcement may reduce the use of steel, although the available design guidance and demonstrated capacity for highly loaded applications are more limited. The reinforcement strategies investigated in this thesis are selected to represent these different load-transfer mechanisms, installation requirements, and material choices.

## 2.7 Design principles and Eurocode provisions

The design of timber connections in Europe is primarily governed by Eurocode 5, which provides simplified analytical models to assess load-carrying capacity and serviceability. These models are based on limit state design principles and account for the anisotropic nature of timber through characteristic material properties and modification factors.

This study is primarily based on the recent draft revisions of Eurocode 5 (CEN, 2025). However, for certain reinforcement strategies and connection configurations, standardized design methods are not fully established. In such cases, analytical models proposed in recent research are adopted to estimate the load-carrying capacity and structural behavior. These models are used in a comparative manner and are not intended to represent validated design rules, but rather to provide insight into the relative performance of different solutions.

### 2.7.1 Design of compression perpendicular to grain

The design of CPG is based on limiting the contact stress relative to a design strength, which depends on the properties of the material and the modification factors (CEN, 2025).

$$\sigma_{c,90,d} \leq k_{mat}\, k_{c,90}\, f_{c,90,d} \tag{2.1}$$

$$\text{with} \quad \sigma_{c,90,d} = \frac{F_{c,90,d}}{A} \tag{2.2}$$

where $\sigma_{c,90,d}$ is the design compressive stress perpendicular to grain, $k_{mat}$ is a material factor accounting for compressive deformation perpendicular to grain, $k_{c,90}$ is a factor considering stress spreading, $f_{c,90,d}$ is the design compressive strength perpendicular to grain, $F_{c,90,d}$ is the design compressive force perpendicular to grain, and $A$ is the loaded contact area.

Because the size of the loaded area directly governs the concentration of compressive stresses in the beam, it plays a critical role in determining the beam's capacity. In bearing-type connections, this directly influences the design requirements of the bearing area.

### 2.7.2 Design resistance of fasteners

As discussed in Section 2.5.2, fasteners in beam-to-column connections are often subjected to combined lateral shear and axial tensile forces. The fastener design resistance is therefore evaluated according to the Eurocode 5 design model for dowel-type fasteners in lateral loading together with the provisions for axially loaded screws in tension.

The characteristic dowel-effect contribution is taken as the most critical failure mode from:

$$F_{D,k} = \left[ \begin{array}{c} \dfrac{f_{h,1,k}\, t_{h,1}\, d}{1+\beta} \\ f_{h,2,k}\, t_{h,2}\, d \\ \dfrac{f_{h,1,k}\, t_{h,1}\, d}{1+\beta} \left( \sqrt{\beta + 2\beta^2 \left[ 1 + \dfrac{t_{h,2}}{t_{h,1}} + \left( \dfrac{t_{h,2}}{t_{h,1}} \right)^2 \right] + \beta^3 \left( \dfrac{t_{h,2}}{t_{h,1}} \right)^2} - \beta \left( 1 + \dfrac{t_{h,2}}{t_{h,1}} \right) \right) \\ \dfrac{1.05\, f_{h,1,k}\, t_{h,1}\, d}{2+\beta} \left( \sqrt{2\beta(1+\beta) + \dfrac{4\beta(2+\beta) M_{y,k}}{f_{h,1,k}\, d\, t_{h,1}^2}} - \beta \right) \\ \dfrac{1.05\, f_{h,1,k}\, t_{h,2}\, d}{1+2\beta} \left( \sqrt{2\beta^2(1+\beta) + \dfrac{4\beta(1+2\beta) M_{y,k}}{f_{h,1,k}\, d\, t_{h,2}^2}} - \beta \right) \\ 1.15 \sqrt{\dfrac{2\beta}{1+\beta}} \sqrt{2 M_{y,k} f_{h,1,k} d} \end{array} \right] \tag{2.3}$$

Where the corresponding design dowel-effect resistance is obtained as

$$F_{D,d} = \frac{F_{D,k}}{\gamma_M} \tag{2.4}$$

In addition to the dowel-effect contribution, the rope-effect contribution is included in accordance with Eurocode 5. The design lateral resistance is therefore taken as

$$F_{v,d} = F_{D,d} + F_{rp,d} \tag{2.5}$$

where $F_{rp,d}$ is the design rope-effect contribution.

For the axial verification, the axial force in each screw is compared with the design axial resistance of the screw, evaluated according to the Eurocode 5 provisions for screws loaded axially:

$$F_{ax,Rd} = \min \left( \frac{k_{mod}}{\gamma_R} F_{w,k}, \frac{F_{t,k}}{\gamma_{M2}} \right) \tag{2.6}$$

where $F_{w,k}$ is the characteristic withdrawal resistance, and $F_{t,k}$ is the tensile resistance of the screw.

Since the screws are subjected to combined lateral shear and axial forces, the final verification is performed using the interaction check

$$\left( \frac{F_{v,Ed}}{F_{v,d}} \right)^2 + \left( \frac{F_{ax,Ed}}{F_{ax,Rd}} \right)^2 \leq 1 \tag{2.7}$$

where $F_{v,Ed}$ and $F_{ax,Ed}$ are obtained from the analytical force-distribution model described in Section 4.3.

### 2.7.3 Design of reinforcement

Reinforcement of members subjected to compression perpendicular to the grain can be achieved by introducing elements that enhance the load transfer within the highly stressed region. The new draft of Eurocode 5 provides design provisions for reinforcement in the compressed member with fully threaded screws, rods with wood screw thread or bonded-in rods.

As illustrated in Figure 2.6, reinforcement can be arranged in the vicinity of the support to modify the stress distribution and increase the effective load transfer area. The load introduced at the contact surface is redistributed into the member through inclined stress fields, while the reinforcement contributes by carrying part of the load and limiting local deformations (CEN, 2025). This results in a more favorable stress distribution and reduces the risk of localized crushing in the timber.

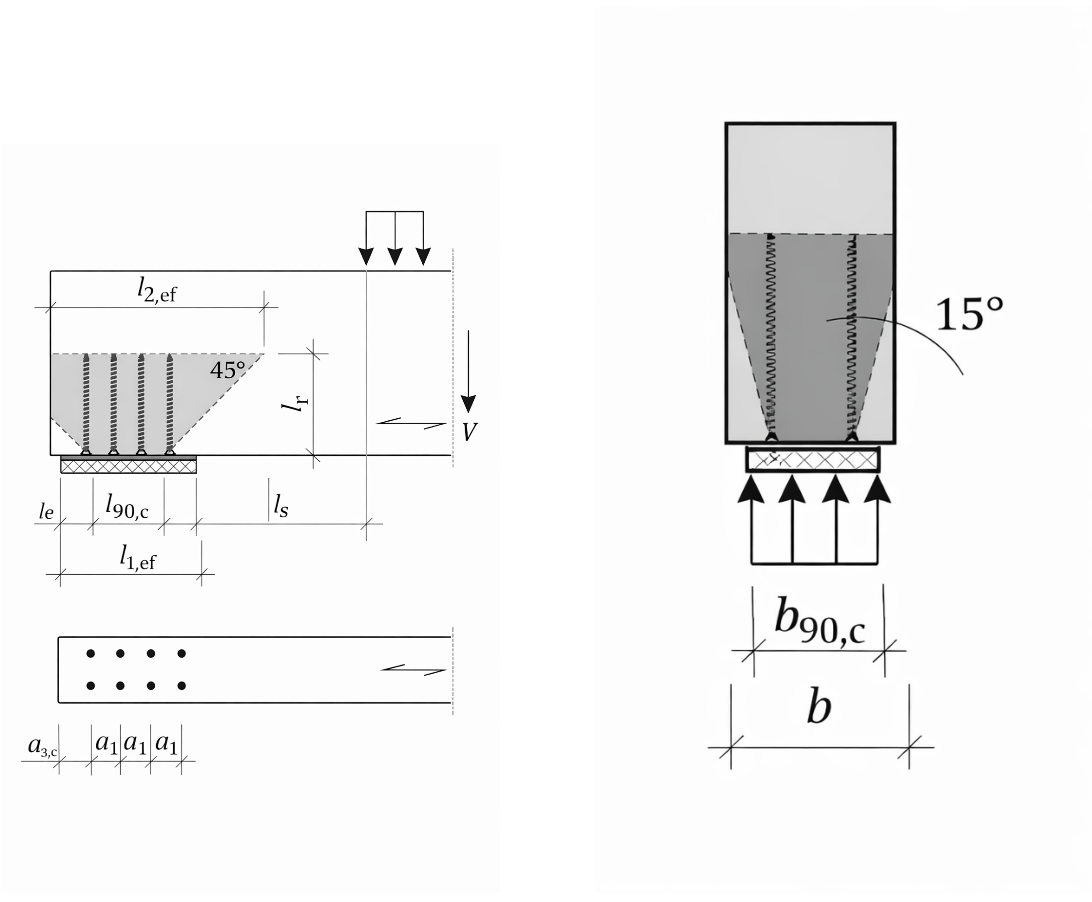


**(a)** Reinforced discrete end support. **(b)** Reinforced discrete support.

**Figure 2.6:** Reinforcement using fully threaded screws or threaded rods in zones of concentrated compression perpendicular to the grain.

According to Eurocode 5 (CEN, 2025) the design load-carrying capacity of the reinforced contact area $F_{c,90,d}$, can be determined as follows:

$$F_{c,90,d} = \min \begin{cases} k_{\text{mat}}\, b_{90,c}\, l_{1,\text{ef}}\, \dfrac{k_{\text{mod}}}{\gamma_M}\, f_{c,90,k} + n \min\left(\dfrac{k_{\text{mod}}}{\gamma_R} F_{w,k}\ ;\ \dfrac{1}{\gamma_{M1}} F_{c,k}\right) \\ b\, l_{2,\text{ef}}\, \dfrac{k_{\text{mod}}}{\gamma_M}\, f_{c,90,k} \end{cases} \tag{2.8}$$

The effective contact length $l_{1,\text{ef}}$ and load-distribution length $l_{2,\text{ef}}$ parallel to grain seen in Figure 2.6, are defined as:

$$l_{1,\text{ef}} = l_{90,c} + \min\{l_e; 30; l_s/2\} + \min\{30; l_s/2\} \tag{2.9a}$$

$$l_{2,\text{ef}} = l_r + (n_0 - 1)a_1 + \min\{l_r; a_{3,c}\}, \tag{2.9b}$$

Where the remaining influencing parameters seen in Figure 2.6 are defined as follows:

$k_{\text{mat}}$ is the factor that takes into account the material behaviour.

$b_{90,c}$ is the width of the contact area perpendicular to grain.

$f_{c,90,k}$ is the characteristic compressive strength perpendicular to grain.

$F_{w,k}$ is the reinforcing members characteristic withdrawal resistance.

$F_{c,k}$ is the reinforcing members characteristic axial compression resistance.

$b$ is the beam width.

$l_{90,c}$ is the length of the contact area.

$l_e$ is the clear spacing parallel to grain between the end of the member and the contact area.

$l_s$ is the clear spacing parallel to grain between the contact area and the nearest concentrated load.

$l_r$ is the reinforced length of the threaded part of the reinforcing member.

$n_0$ is the number of reinforcing members arranged in a row parallel to grain.

$n_{90}$ is the number of reinforcing members arranged in a row perpendicular to grain.

$n$ is the total number of reinforcing members, $n = n_0 \cdot n_{90}$.

$a_1$ is the spacing parallel to grain between reinforcing members.

$a_{3,c}$ is the distance between the reinforcing member and the unloaded end of the member.

The Eurocode 5 draft does not, however, cover wooden reinforcement methods such as bonded-in hardwood- or densified hardwood dowels. Instead these methods can be design according to Wang et al., 2025b, where the analytical compressive strength $f_{c,90,ana}$ is predicted as follows:

$$f_{c,90,ana} = \frac{k_{mat} \cdot k_{c,90} \cdot A_{GL} \cdot f_{c,90,GL} + n \cdot F_{c,r}}{A_{tot}} \tag{2.10}$$

where, $A_{GL}$ and $A_{tot}$ are the cross-sectional areas of the of the specimen without and with reinforcement. $f_{c,90,GL}$ is the compressive strength perpendicular to the grain of glulam and $F_{c,r}$ is the compressive capacity of each reinforcement element governed by its compressive strength or buckling capacity.

# 3 Methodology

Following the concept selection in Chapter 2, this chapter presents the methodology used to develop and assess the selected concealed beam-to-column connection concept. First, the connection geometry and the structural behavior are defined. The numerical model developed in Abaqus is then presented, followed by the analytical validation of selected numerical response quantities. Finally, the beam-side compression-perpendicular-to-grain response and the reinforcement optimization procedure are described.

## 3.1 Methodological framework

The methodology follows a sequential process beginning with the qualitative screening of the concealed connection families identified in the literature review. Based on this screening, one connection family is selected as the basis for concept development. The selected concept is subsequently investigated through numerical modeling and analytical validation, while the beam-side CPG-response is evaluated separately using analytical design models. Finally, reinforcement alternatives are assessed through optimization and parameter analyses. The overall methodological workflow is presented in Figure 3.1.

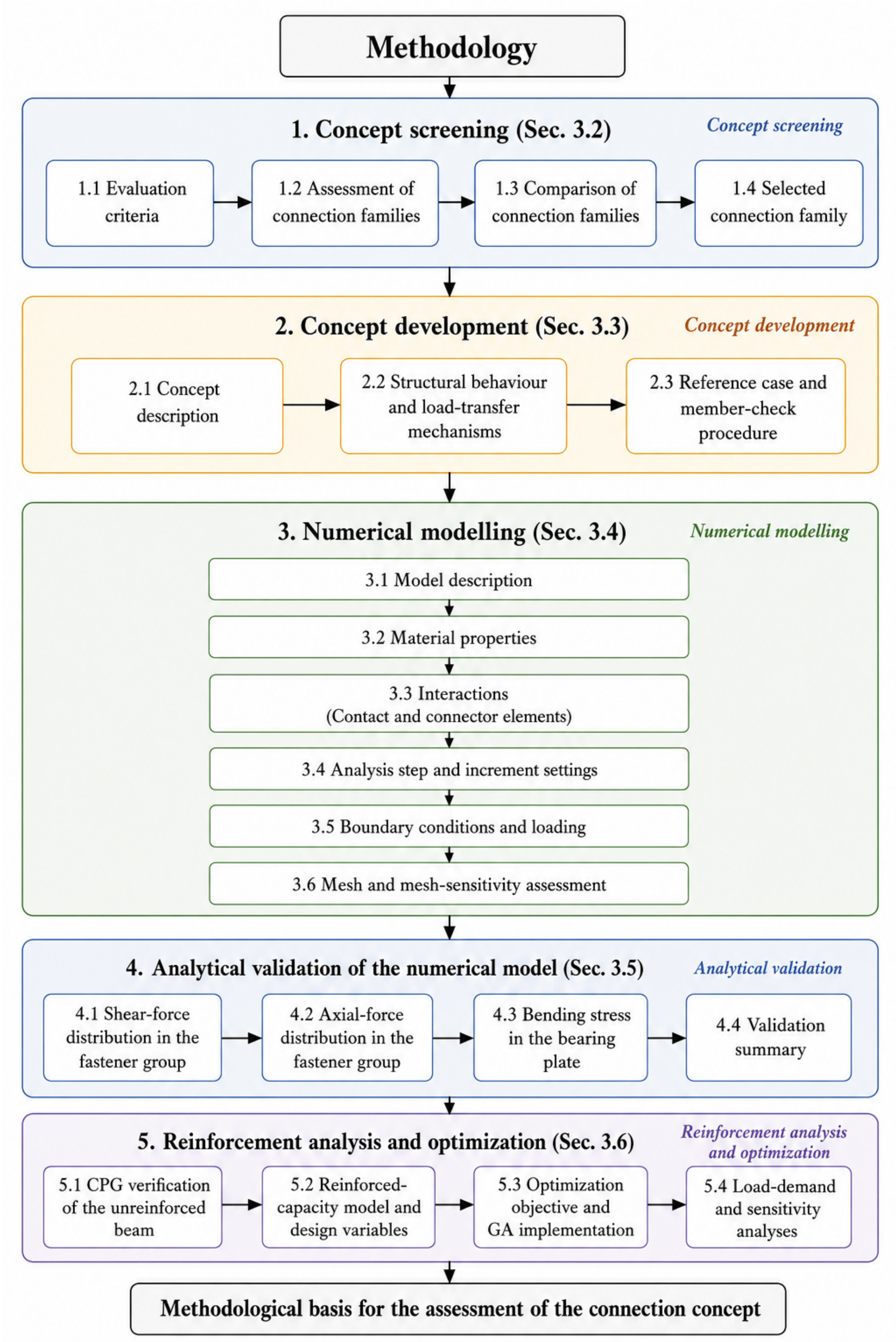


**Figure 3.1:** Flow chart of the methodology used to develop and assess the concealed beam-to-column connection concept.

## 3.2 Concept screening

This section presents a qualitative screening of different connection families for concealed beam-to-column connections. Based on the literature review in Chapter 2, moment-resisting, hanger-type, and bearing-type connections are evaluated with respect to their structural performance, constructability, and suitability for the intended application. The aim is to identify a connection family for further detailed investigation.

The comparison concerns the general characteristics of each connection family rather than the resistance of a particular connection geometry. The qualitative ratings should therefore not be interpreted as generally applicable rankings or as equally weighted numerical scores.

### 3.2.1 Evaluation criteria

The connection families are evaluated based on the following criteria:

- load-transfer efficiency,
- structural behavior and deformation capacity,
- constructability and tolerance sensitivity, and
- degree of concealment.

#### 3.2.1.1 Load-transfer efficiency

Load-transfer efficiency refers to the ability of the connection to transmit forces between structural members through a direct and predictable load path. High load-transfer efficiency is associated with a clear force flow, limited load-path complexity, and reduced reliance on unnecessary intermediate mechanisms.

The criterion concerns the general load-transfer mechanism of the connection family rather than the verified resistance of a particular connection design.

#### 3.2.1.2 Structural behavior and deformation capacity

Structural behavior and deformation capacity refer to the stiffness, rotational response, deformation characteristics, and potential failure modes of the connection. Particular consideration is given to whether the connection can maintain load transfer while undergoing deformation and whether failure is expected to develop gradually or through brittle timber failure.

The response depends on the geometry, detailing, and relative resistance of the individual connection components. The assessment therefore represents the general opportunities and limitations identified in the literature rather than guaranteed behavior for every connection within a family.

#### 3.2.1.3 Constructability and tolerance sensitivity

Constructability refers to the ease with which a beam-to-column connection can be manufactured, assembled, and integrated into the structural system. Tolerance sensitivity describes the extent to which geometric and material variations arising during fabrication and erection may influence the intended load transfer.

In concealed beam-to-column connections, limited accessibility and stricter geometric constraints increase the importance of both constructability and tolerance control. Since the requirements may differ between individual concepts, this criterion is assessed at the connection-family level.

#### 3.2.1.4 Degree of concealment

Degree of concealment refers to the extent to which a connection can be integrated within the timber members without visible or externally exposed components. A high degree of concealment is associated with limited interference with the architectural expression of the structure.

The assessment also considers whether the load-transferring components and anchorage regions can be accommodated within the available member cross-sections while maintaining sufficient structural performance.

### 3.2.2 Assessment of connection families

As discussed in Section 2.4.1, moment-resisting connections can provide substantial rotational stiffness, moment capacity, and deformation capacity. Concealed solutions using glued-in rods, slotted-in plates, inclined threaded rods, or integrated timber components have been demonstrated in previous research. However, their load transfer generally relies on tension–compression force couples and highly loaded anchorage regions. This results in comparatively complex detailing and may lead to brittle timber failure, such as splitting around rods or fastener groups, if the components are not appropriately proportioned.

As discussed in Section 2.4.2, hanger-type connections provide efficient vertical-load transfer through connector components and mechanical fasteners. Proprietary systems can offer rapid assembly and a high degree of concealment when recessed into the timber. Experimental studies also demonstrate that some systems can accommodate considerable rotation while maintaining gravity-load resistance. However, their response may be semi-rigid and connector-specific. Accurate alignment and engagement are required, and interface gaps may influence the structural and fire performance of the connection.

As discussed in Section 2.4.3, bearing-type connections transfer the vertical beam reaction primarily through compressive contact. This provides a direct and clearly defined load path. Local compression may develop gradually without immediately causing a complete loss of load-carrying capacity. However, the response is governed by the relatively low strength and stiffness of timber perpendicular to the grain. The resistance and deformation are also influenced by contact geometry, stress spreading, and the quality of contact between the connected components.

Bearing-type connections can be developed using different bearing surfaces and internal components, allowing the geometry to be adapted to the available member dimensions and required load. Their constructability and tolerance sensitivity nevertheless depend on the selected concept, since uneven contact or unintended gaps may concentrate the applied reaction over a smaller area than assumed.

### 3.2.3 Comparison of connection families

The connection families are compared qualitatively based on the evaluation criteria defined in Section 3.2.1. The results are summarized in Table 3.1.

**Table 3.1:** Qualitative comparison of concealed connection families.

| Criterion | Moment-resisting | Hanger-type | Bearing-type |
|---|---|---|---|
| **Load-transfer efficiency** | **Moderate** — Combined mechanisms. | **High** — Direct shear transfer. | **High** — Direct bearing transfer. |
| **Structural behaviour and deformation capacity** | **Moderate** — Ductility possible; splitting risk. | **Moderate** — Rotation capacity; connector-specific. | **Moderate** — Gradual response; bearing deformation. |
| **Constructability and tolerance sensitivity** | **Low** — Complex anchorage and detailing. | **Moderate** — Rapid assembly; alignment-sensitive. | **Moderate** — Concept-dependent; contact control required. |
| **Degree of concealment** | **Moderate** — Concealed systems are possible. | **High** — Recessed compact components. | **High** — Components can be integrated. |

The comparison indicates that all three connection families can provide effective structural performance when appropriately designed. However, their suitability depends on how their load-transfer mechanisms and practical characteristics correspond to the intended application.

Moment-resisting connections can provide high stiffness, moment resistance, and architectural concealment. However, their force-couple mechanisms and anchorage requirements introduce comparatively complex detailing. The possibility of brittle timber splitting must also be considered when designing the anchorage regions.

Hanger-type connections provide efficient vertical-load transfer, favorable concealment, and potentially rapid assembly. However, the reviewed systems are generally proprietary and have predefined geometries, fastener arrangements, and documented capacities. Their rotational response and sensitivity to alignment are also dependent on the selected connector.

Bearing-type connections provide an equally direct vertical-load path through compressive contact. Unlike proprietary hanger systems, the bearing geometry and any associated internal components can be developed specifically for the required load and available member dimensions. This flexibility is particularly relevant to the project-specific high-load application considered in this thesis.

The bearing-type family does not receive a higher rating in every criterion. In particular, hanger-type systems may provide more efficient standardized assembly when a suitable connector with sufficient documented resistance is available. For the present application, however, the combination of direct load transfer, geometric adaptability, and a high degree of concealment makes the bearing-type family the most suitable basis for further concept development.

### 3.2.4 Selected connection family

Based on the qualitative comparison presented in Table 3.1, the bearing-type connection family is selected for further investigation.

The selection does not imply that bearing-type connections are generally superior to moment-resisting or hanger-type connections. Hanger-type systems may represent an effective solution where a proprietary connector satisfies the required resistance and geometric constraints. Moment-resisting connections may similarly be preferable where rotational stiffness and moment transfer are required from the structural frame.

For the application considered in this thesis, the principal advantages of the bearing-type family are that the vertical beam reaction can be introduced through bearing at the beam-side interface and that the bearing geometry and associated internal components can be adapted to the required load and available timber-member dimensions. The subsequent transfer of the reaction into the supporting column may involve steel-plate bending, contact, and mechanical fasteners. These characteristics provide a suitable basis for developing a project-specific concealed connection while allowing the different load-transfer mechanisms to be assessed separately.

The literature review also identifies important limitations that must be considered during concept development. These include compression perpendicular to the grain in the beam, deformation at the bearing interface, resistance and deformation of the internal steel components, fabrication and assembly tolerances, and the transfer of forces from the steel components into the supporting column.

## 3.3 Concept development

This section presents the development of the selected connection concept. First, the structural behavior of the concept is described in order to establish the principal load transfer within the connection. Thereafter, the force distribution in the fastener group is evaluated analytically. Based on these assumptions, selected structural response quantities in the connection are evaluated analytically for later comparison with the numerical model. Finally, the corresponding design resistances are assessed using applicable Eurocode provisions in order to evaluate the feasibility of the concept.

### 3.3.1 Concept description

The selected connection concept is based on a bearing-type load transfer mechanism, implemented as an internal beam shoe integrated within the beam cross-section. The connection comprises steel components, including a bearing plate (flange), stiffener (web), backplate, fasteners and a filler block. Load is transferred from the beam to the column through the internal beam shoe. A schematic representation of the connection is shown in Figure 3.2 and the geometry of the internal beam shoe is presented in Figure 3.3.

The compact geometry of the connection allows it to be fully concealed within the structural members. The steel components are embedded within the timber beam with a minimum cover depth of 58.5 mm. This dimension is governed by the required charring depth for a fire exposure duration of 90 minutes, in accordance with applicable fire design provisions (CEN, 2004).

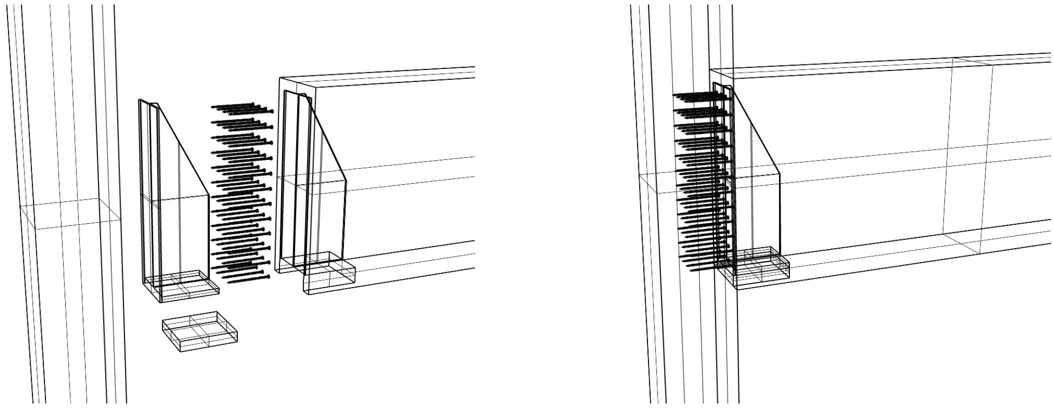

**Figure 3.2:** Schematic illustration of the exploded assembly of the beam–column connection showing the internal beam shoe, screw arrangement, timber beam, column, and filler block prior to installation.

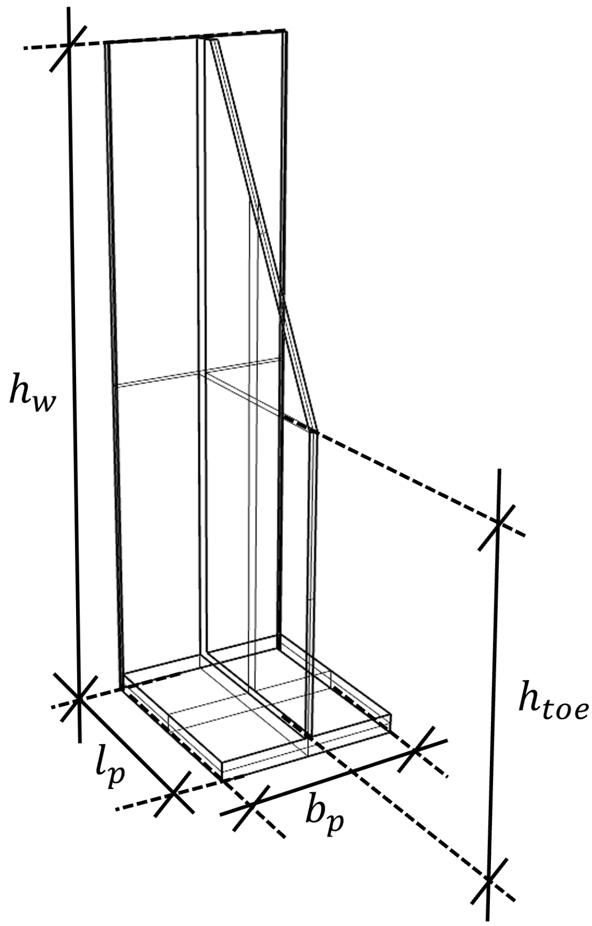


**Figure 3.3:** Geometry of internal beam shoe.

The principal geometric dimensions of the internal beam shoe and the adopted fastener configuration are summarized in Tables 3.2 and 3.3. These dimensions define the connection geometry used in the subsequent analytical and numerical analyses.

**Table 3.2:** Geometric dimensions of the internal beam shoe.

| **Component** | **Parameter** | **Symbol** | **Value [mm]** |
|---|---|---|---|
| Backplate | Height | $h_w$ | 953 |
| Backplate | Thickness | $t_w$ | 15 |
| Backplate | Width | $b_w$ | 283 |
| Stiffener | Height | $h_s$ | 923 |
| Stiffener | Toe height | $h_{toe}$ | 461.5 |
| Stiffener | Thickness | $t_s$ | 15 |
| Stiffener | Bottom width / toe length | $b_{s,b}$ | 320 |
| Stiffener | Top width | $b_{s,t}$ | 50 |
| Bearing plate | Length | $l_p$ | 320 |
| Bearing plate | Width | $b_p$ | 283 |
| Bearing plate | Thickness | $t_p$ | 30 |

**Table 3.3:** Fastener dimensions and configuration adopted for the internal beam shoe.

| **Parameter** | **Value** |
|---|---|
| Fastener type | Screw |
| Fastener diameter, $d$ [mm] | 10 |
| Fastener length, $l$ [mm] | 200 |
| Number of rows, $n_0$ [-] | 13 |
| Number of screws per row, $n_{90}$ [-] | 4 |
| Total number of screws, $n$ [-] | 52 |
| Spacing parallel to grain, $a_1$ [mm] | 76.1 |
| Spacing perpendicular to grain, $a_2$ [mm] | 67.7 |
| End distance parallel to grain, $a_3$ [mm] | 20 |
| Edge distance perpendicular to grain, $a_4$ [mm] | 40 |

### 3.3.2 Structural behavior

The structural behavior of the connection is governed by the transfer of forces through the internal beam shoe and its interaction with the surrounding timber. The applied beam reaction from the supported member is introduced into the bearing plate, where it is redistributed within the internal beam shoe before being transferred to the backplate and further into the column through the fastener group.

At the bearing plate, the load is transferred from the timber into the steel through compressive contact. This produces localized compressive stresses in the timber and in the bearing plate. From the bearing plate, the load is redistributed within the steel assembly through a combination of plate bending, membrane action, and shear transfer. The structural response is therefore governed by the interaction between the bearing plate, the stiffener, the backplate, and the welds connecting these parts.

The stiffener contributes significantly to the internal redistribution of forces within the internal beam shoe. In the overall load path, the stiffener may be regarded as primarily tension-carrying, since it transfers load from the seat region toward the backplate through diagonal axial action. At the same time, the transfer of force into the backplate also gives rise to local compressive and bending effects in the lower vertical part of the stiffener. The stiffener should therefore not be viewed as a purely tension-carrying component, but rather as a plate component participating in combined tension, compression, bending, and shear.

The backplate transfers the forces from the internal beam shoe to the column through a group of mechanical fasteners. Because the applied load is eccentric relative to the fastener group, the fasteners are subjected to a non-uniform force distribution. The highest demands occur in the fasteners with the largest lever arms relative to the rotation center, and within the most critical rows the screws closest to the stiffener are the most highly loaded. The detailed force distribution is described in Sections 3.5.1 and 3.5.2.

Within the beam, the load is transferred from the bearing plate into the surrounding timber through a confined contact area. This leads to localized compressive stresses and a non-uniform stress distribution, with higher stresses occurring near the edges of the contact zone. As described in Section 2.5.1, increasing load leads to local deformation, partial stress redistribution, and an increase in the effective contact area.

Overall, the structural behavior of the internal beam shoe is governed by the combined action of bearing-plate bending, stiffener plate action, backplate force transfer, weld resistance, and non-uniform fastener loading. The connection should therefore be understood as a steel-timber interaction problem in which no single component acts in isolation, and where the overall behavior is controlled by the interaction between local plate action, axial force transfer, shear transfer, and contact stresses.

### 3.3.3 Reference case and member checks

As mentioned in Chapter 1, the selected connection concept is evaluated using a reference case that represents the project context considered in this thesis. The reference case is defined by a beam span of $L_b = 10\,\mathrm{m}$ with an assumed uniformly distributed design load of $f_{Ed,b} = 100\,\mathrm{kN/m}$, a column length of $L_c = 3\,\mathrm{m}$, and a design normal force in the column of $N_{Ed} = 3\,\mathrm{MN}$. The distributed load represents the combined effect of self-weight and additional imposed loads. Furthermore, the member dimensions were selected as $400 \times 1100\,\mathrm{mm}$ for the glulam beam and $400 \times 400\,\mathrm{mm}$ for the glulam column.

The beam and the column are then checked at member level in order to validate the feasibility of the selected dimensions. The beam is verified with respect to bending and shear, while the column is verified with respect to compression parallel to the grain.

For the simply supported beam, the governing design actions are taken as

$$V_{Ed} = \frac{f_{Ed,b} L_b}{2} \tag{3.1}$$

$$M_{Ed} = \frac{f_{Ed,b} L_b^2}{8} \tag{3.2}$$

These actions are used in the beam bending and shear checks. The corresponding beam resistances are evaluated using the applicable Eurocode expressions for bending and shear in glulam members (CEN, 2004).

The shear check is introduced at the critical section in the slotted beam in the connection. This section is selected because the beam cross-section is locally reduced by the embedded connection geometry. The reduced section is represented by subtracting the material removed by the bearing plate and filler block, together with the stiffener slit, from the gross beam area. The resulting effective shear area is then used to evaluate the reduced local shear resistance as

$$V_{Rd} = \frac{A_{eff} f_{v,d}}{1.5} \tag{3.3}$$

where $A_{eff}$ is the effective reduced shear area and $f_{v,d}$ is the design shear strength of the timber.

For the column, the applied design normal force $N_{Ed}$ is checked against the compression resistance parallel to the grain. This verification is carried out using the corresponding Eurocode provisions for timber columns (CEN, 2004).

## 3.4 Numerical modelling

This section presents the numerical model of the connection developed in Abaqus, including the essential modeling assumptions, material properties, interactions, boundary conditions, loading, and mesh configuration.

### 3.4.1 Model description

The model consists of a column part and an internal beam shoe part, see Figure 3.4 for a representation of the whole model. Both parts are created as 3D deformable bodies in which the stress is represented by a symmetric tensor:

$$\boldsymbol{\sigma} = \begin{bmatrix} \sigma_{xx} & \sigma_{xy} & \sigma_{xz} \\ \sigma_{xy} & \sigma_{yy} & \sigma_{yz} \\ \sigma_{xz} & \sigma_{yz} & \sigma_{zz} \end{bmatrix}, \tag{3.4}$$

where the diagonal components are normal stresses and the off-diagonal components are shear stresses.

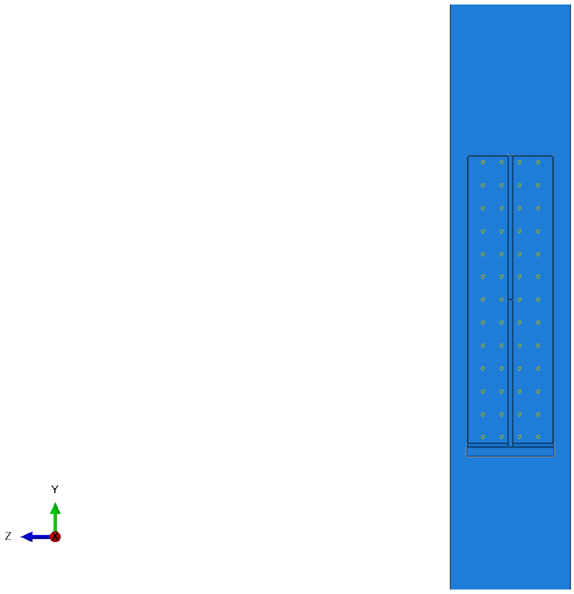


**Figure 3.4:** Illustration of the FE-model used in the analysis.

### 3.4.2 Material properties

The column and internal beam shoe are both assigned linear elastic material properties with some distinctions. For the column part, a local coordinate system is created to account for orientation-dependent orthotropic material properties in timber, which are applied through engineering constants. The orientation specific assigned material properties are shown in Table 3.4, and the isotropic material properties for the steel components are shown in Table 3.5.

**Table 3.4:** Orthotropic Material Properties For GL32h (x=L, y=R, z=T).

| **Grade** | $E_x$ | $E_y$ | $E_z$ | $G_{xy}$ | $G_{xz}$ | $G_{yz}$ | $\nu_{xy}$ | $\nu_{xz}$ | $\nu_{yz}$ |
|---|---|---|---|---|---|---|---|---|---|
| GL32h | 13 500 | 300 | 300 | 650 | 650 | 65 | 0.04 | 0.04 | 0.35 |

*Note:* $E$ and $G$ in MPa.

**Table 3.5:** Isotropic Steel Material Properties For Internal Beam Shoe.

| **Material** | $E$ [MPa] | $\nu$ [-] |
|---|---|---|
| Steel | 210 000 | 0.3 |

### 3.4.3 Interactions

In this section the modeling of the interaction between the backplate and the column, including contact and connector elements is described.

#### 3.4.3.1 Contact

A surface-to-surface contact is defined between the timber column and back plate of the internal beam shoe, see Figure 3.5. In addition, behaviors in the normal and tangential direction are added as follows:

- **Normal behavior:** Hard contact and no penetration.
- **Tangential behavior:** Frictionless and allowing separation after initiated contact.

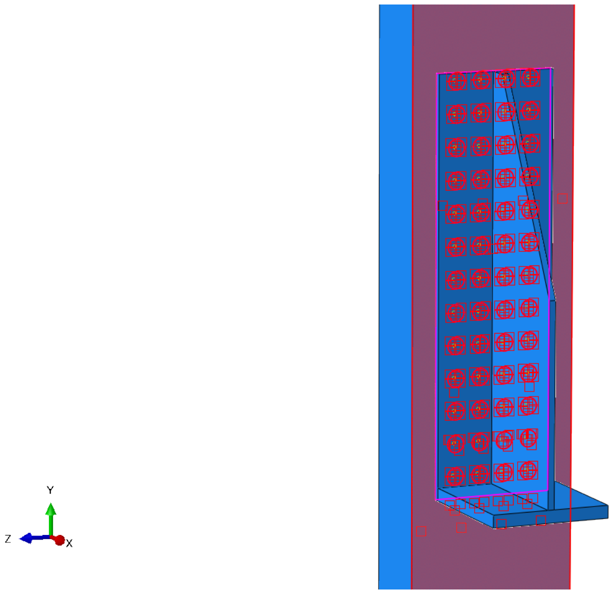


**Figure 3.5:** Highlighted contact surfaces between the column and back plate of the internal beam shoe.

#### 3.4.3.2 Connector elements

To represent the screws, Cartesian connector elements are introduced between the steel backplate and the timber column at the screw locations. A Cartesian connector is a two-node element with local directions in the $x$-, $y$-, and $z$-directions, which measures the relative displacement between the connected steel node and timber node. In the present model, the connector elements are used to represent the axial and lateral stiffness contribution of the screws without explicitly modeling their detailed geometry.

The assigned connector stiffness's are based on the draft EN 1995-1-1:2025 (CEN, 2025) provisions for screw stiffness. The axial slip modulus is taken as

$$K_{ULS} = \frac{2d^{0.6} l_w^{0.6} \rho_{mean}^{0.9}}{1.5}$$

and the lateral slip modulus is taken as

$$K_{ULS,lat} = 2\frac{60d^{1.7} l_w^{0.6} \left(\frac{\rho_{mean}}{420}\right)^{1.1}}{1.5}$$

where $d$ is the screw diameter, $l_w$ is the penetration length, and $\rho_{mean}$ is the mean timber density.

The connector response is defined through linear force–displacement relationships in the relevant local directions. In the axial direction, the connector force is expressed as

$$F_x = K_{ULS} u_x$$

and in the lateral direction as

$$F_y = K_{ULS,lat} u_y$$

where $u_x$ and $u_y$ are the relative displacements in the axial and lateral directions, respectively.

In the axial direction, only the screws located above the compression-dominated contact region are intended to carry tensile axial forces, while the lower part of the connection transfers load primarily through contact between the backplate and the timber column. To reflect this behavior, the axial connector response is defined such that the screws carry load only in tension and remain inactive in compression. In this way, the connector formulation allows the model to represent the combined action of withdrawal in the upper screw rows and compressive contact in the lower part of the connection.

The connector elements therefore do not explicitly model the detailed local behavior of the screws, such as embedment deformation, screw bending, or local yielding. Instead, they provide an equivalent stiffness-based representation of the screw response, which is suitable for evaluating the force distribution in the fastener group within the present numerical model. An illustration of the connector elements on the back of the plate of the internal been shoe is shown in Figure 3.6.

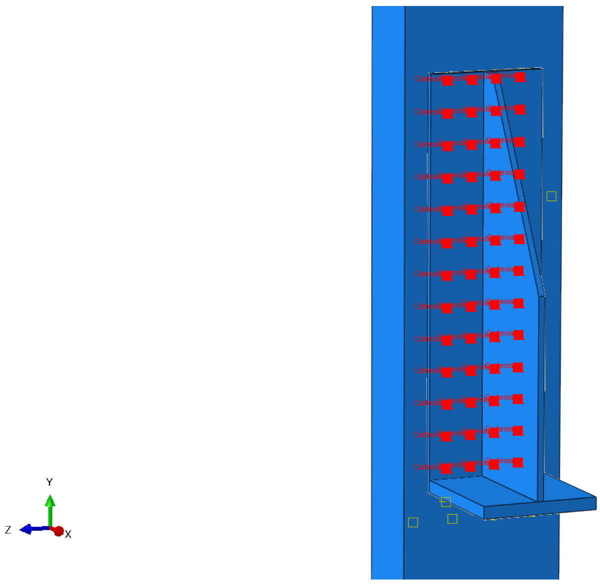

**Figure 3.6:** Highlighted Cartesian connector elements placed at screw locations.

### 3.4.4 Step module

In a contact-driven analysis, applying the full load in a single increment can lead to poor convergence because the contact constraint is not yet established. Instead, the load is applied incrementally so that contact can settle and redistribute some of the load from the contact faces, through the internal beam shoe and screws before larger loads are imposed. Therefore, the step settings shown in Table 3.6 with prescribed minimum, maximum and initial increment sizes are chosen.

**Table 3.6:** Increment Size Settings for Contact-Driven Analysis

| Step Setting | Initial Increment | Min. Increment | Max. Increment |
|---|---|---|---|
| Static General Step | 0.1 | 1e-6 | 0.1 |

### 3.4.5 Boundary conditions and load

The boundary conditions and load application in the model are defined as follows:

- **Bottom of the column:** $U_1 = U_2 = U_3 = 0$. This BC fully restrains translation at the column base in all directions.
- **Top of the column:** $U_1 = U_3 = 0$. This BC only restrains horizontal translations.
- **Middle of the column:** $U_1 = U_{R2} = U_{R3} = 0$. Symmetry BC about the Y-Z plane to represent an interior span.
- **Load application:** The load is applied on the contact areas at each side of the stiffener as uniform pressure, see Figure 3.7.

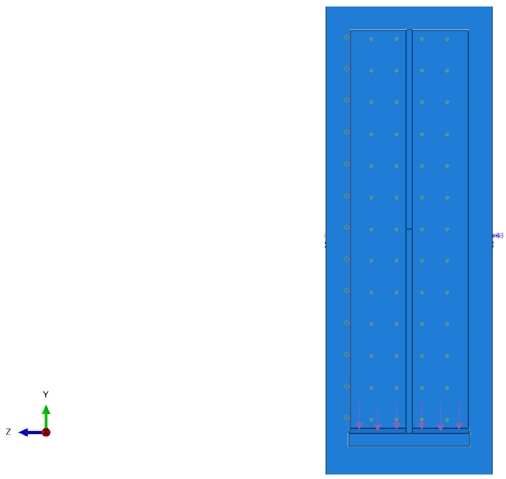


**Figure 3.7:** Illustration of load applied as uniform pressure on the bearing plate.

### 3.4.6 Mesh

Since the analysis contains both contact interactions and connector elements, mesh size and local refinement are critical to accurately capture the mechanical response. In Table 3.7, the mesh sizes and local refinements used for a converged result are presented. Local mesh refinement is applied in close surroundings of the screw locations. In Figure 3.8 an illustration of the mesh surrounding the contact and fastener group is shown.

**Table 3.7:** Mesh Parameters for Column and Internal Beam Shoe

| Part | Mesh Size [mm] | Element Type | Refinement [mm] |
|---|---|---|---|
| Column | 75 | C3D10 tetrahedral | 20 |
| Internal Beam Shoe | 30 | C3D10 tetrahedral | 18 |

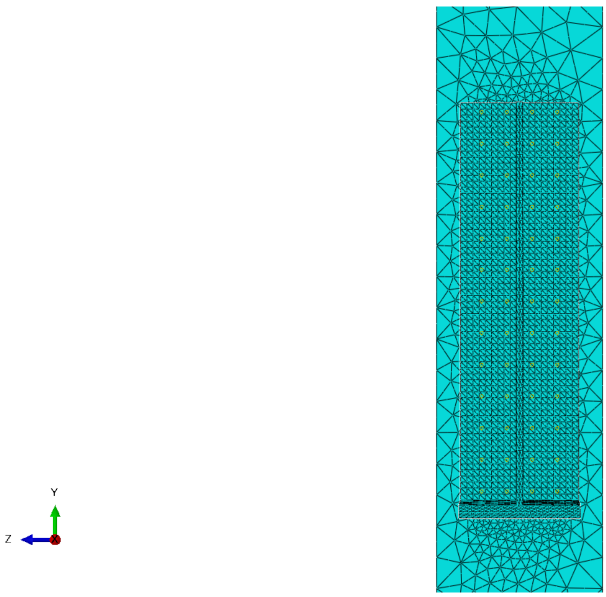


**Figure 3.8:** Mesh setup illustration for the full assembly with local refinement in contact region and at screw locations.

## 3.5 Analytical validation of the numerical model

In this section, the analytical methods used to verify the numerical model are presented. The shear and axial forces in the screws, as well as bending stresses in the bearing plate are evaluated analytically to later be compared with numerical results. All hand calculations used in the validation process are shown in Appendix A.

### 3.5.1 Validation of shear force distribution in the fastener group

The lateral shear forces in the fastener group is expected to be equally distributed:

$$F_{v,i} = \frac{V_{Ed}}{n} \tag{3.5}$$

where $V_{Ed}$ is the applied shear force and $n$ is the number of fasteners transferring shear forces into the column. See Figure 3.9 for a schematic illustration of the shear force distribution in the fastener group.

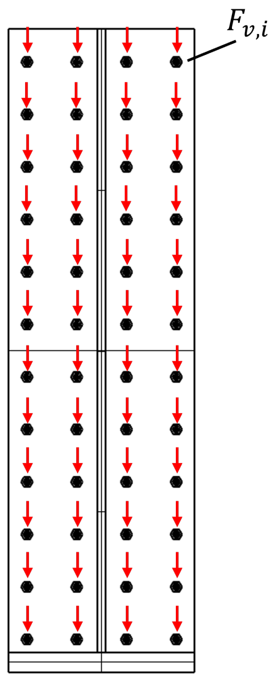


**Figure 3.9:** Schematic illustration of the shear force distribution in the fastener group, with shear force for screw $i$ is $F_{v,i}$.

### 3.5.2 Validation of axial force distribution in the fastener group

Due to complex structural behavior explained in Section 3.3.2, the axial force distribution is difficult to capture analytically. To validate the connector elements used in the numerical model, a global rotational model of the internal beam shoe is used with the assumption that it can rotate as a rigid body about its toe, see Figure 3.10. The screw axial displacement follows from small-rotation kinematics:

$$\delta_r = \sin\theta\, y_r \approx \theta\, y_r \tag{3.6}$$

The screw row force can be expressed as:

$$F_r = K_{\text{row}}\, \delta_r = K_{\text{row}}\, \theta\, y_r \tag{3.7}$$

Moment equilibrium about the toe gives:

$$M_z = \sum_{r=1}^{n_0} F_r\, y_r = \sum_{r=1}^{n_0} (K_{\text{row}}\, \theta\, y_r)\, y_r \tag{3.8}$$

Factoring out the rotation angle gives:

$$M_z = \theta \sum_{r=1}^{n_0} K_{\text{row}}\, y_r^2 \tag{3.9}$$

The rotation angle is then:

$$\theta = \frac{M_z}{\sum_{r=1}^{n_0} K_{\text{row}}\, y_r^2}. \tag{3.10}$$

With the rotation angle determined, the screw row forces $F_r$ can be obtained through Equation 3.7.

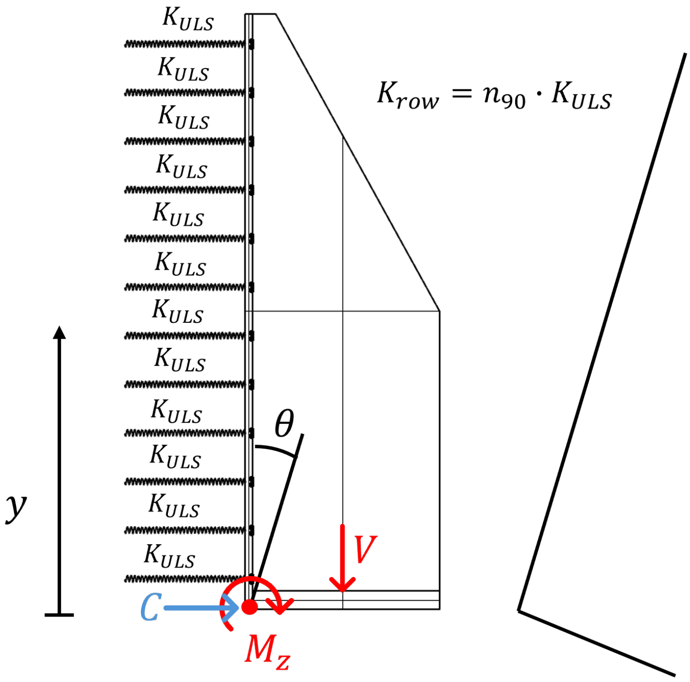


**Figure 3.10:** Schematic illustration of the rigid body axial force mechanism. The figure shows the applied load $V_{Ed}$, contact reaction force $C$, external moment $M_z$, rotation angle $\theta$ and axial stiffness for each screw $K_{ULS}$.

### 3.5.3 Validation of bending stresses in bearing plate

The bearing plate will transfer forces from contact with the beam and distribute it through the internal beam shoe. It is supported by both the stiffener and the back plate where the load acting on one side of the bearing plate is represented by an equivalent unit load:

$$q = \frac{V_{Ed}}{2\, l_p\, a} \tag{3.11}$$

where $\frac{V_{Ed}}{2}$ is the applied design load on one side of the bearing plate, $l_p$ is the length of the bearing plate, and $a$ is the cantilever length measured from the stiffener line to the free edge. To validate the numerical model, bending stresses in an outmost cantilever strip with width $b$ is evaluated as shown in Figure 3.11, where the support moment is given as:

$$M = \frac{qa^2}{2}\, b \tag{3.12}$$

And the maximum bending stress:

$$\sigma = \frac{M}{W_{el}} \tag{3.13}$$

where $W_{el}$ is the elastic section modulus for the evaluated strip.

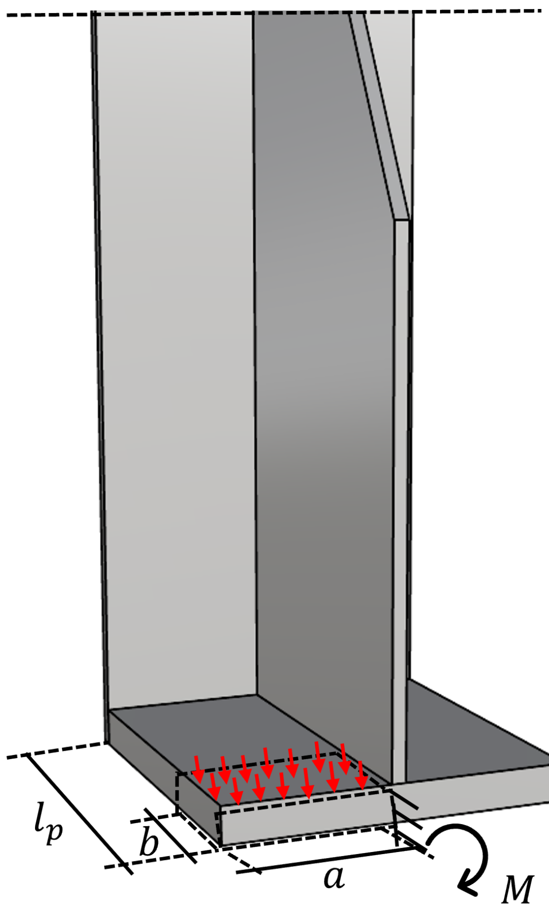


**Figure 3.11:** Schematic illustration of the outmost cantilever strip, with strip width $b$ and strip length $a$ and support moment $M$.

### 3.5.4 Results of the analytical validation

In this section the results from the analytical validation of the numerical model is presented.

#### 3.5.4.1 Shear force distribution in the fastener group

The lateral shear forces, calculated as described in Section 3.5.1, give the equal distribution of $9.62\,\mathrm{kN}$ per screw. The corresponding numerical results are summarized in Table 3.8, showing a nearly equal distribution of shear forces, ranging from $10.06\,\mathrm{kN}$ to $9.40\,\mathrm{kN}$.

**Table 3.8:** Numerical shear forces $F_v$ [kN] for each screw, where the first row corresponds to the top row in the connection. The highest loaded fasteners are highlighted.

| Outer | Inner | Inner | Outer |
|---|---|---|---|
| 9.73 | 9.70 | 9.70 | 9.73 |
| 9.61 | 9.54 | 9.54 | 9.61 |
| 9.55 | 9.45 | 9.46 | 9.55 |
| 9.53 | 9.41 | 9.41 | 9.52 |
| 9.52 | 9.40 | 9.40 | 9.52 |
| 9.53 | 9.41 | 9.40 | 9.53 |
| 9.56 | 9.43 | 9.43 | 9.56 |
| 9.60 | 9.47 | 9.47 | 9.60 |
| 9.66 | 9.53 | 9.53 | 9.66 |
| 9.73 | 9.61 | 9.61 | 9.73 |
| 9.82 | 9.71 | 9.72 | 9.82 |
| 9.92 | 9.85 | 9.85 | 9.92 |
| **10.06** | 10.05 | 10.05 | **10.06** |

Comparing the average shear force per fastener from the numerical model with the analytical assumption of equal force distribution shows good agreement between the two approaches, see Table 3.9. The differences are small, indicating that the numerical model reproduces the assumed shear distribution in the fastener group with reasonable accuracy.

**Table 3.9:** Difference between analytical and numerical fastener shear force distribution

| $F_{v,i}$ **[kN]** | $F_{v,avg,FEM}$ **[kN]** | **Difference [%]** |
|---|---|---|
| 9.62 | 9.63 | 0.15 |

#### 3.5.4.2 Axial force distribution in the fastener group

Under the rigid body assumption described in Section 3.5.2, the withdrawal forces increase linearly with the height of the backplate, as expected. The analytical and numerical results are closely aligned, validating the numerical model with regard to axial force distribution in the fasteners, see Figure 3.12.

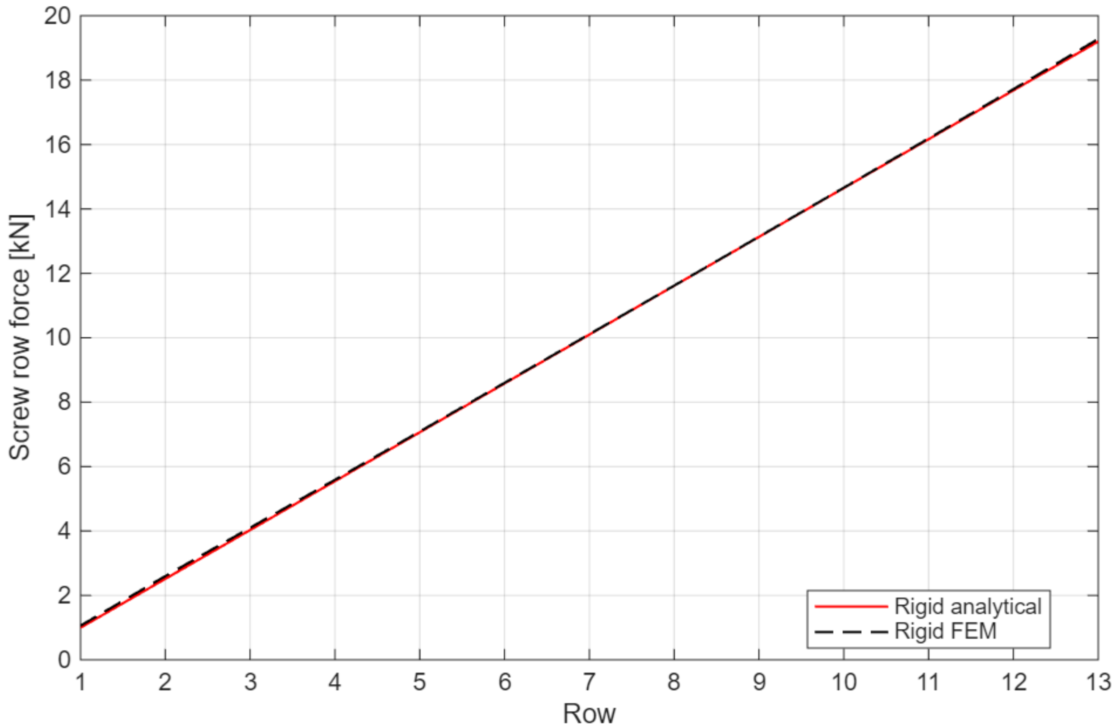


**Figure 3.12:** Validation using the rigid body assumption, comparing analytical with Abaqus results. Summarized screw row forces plotted against row number along the screw group.

#### 3.5.4.3 Bending stress in the bearing plate

The bearing plate was analytically evaluated using the cantilever-strip analogy described in Section 3.5.3. The bending stress was shown to be slightly higher than the result from the numerical model, as shown in Table 3.10. The comparison shows a relatively good

**Table 3.10:** Comparison between analytical and numerical bending stresses in bearing plate.

| $\sigma_z$ **[MPa]** | $\sigma_{z,FEM}$ **[MPa]** | **Difference [%]** |
|---|---|---|
| 349.0 | 340.2 | 2.6 |

agreement between the models with a difference of approximately $2.6\%$, finalizing the validation of the numerical model.

## 3.6 Reinforcement analysis and optimization

In this section, the design challenge of beam crushing caused by CPG is addressed by reinforcing the beam using the analytical equations provided in the new draft of Eurocode 5 explained in section 2.7.3 (CEN, 2025). Additionally, a parametric study is performed by applying this analytical model within a genetic algorithm optimization, evaluating screws, rods with wood screw thread and bonded-in rods to identify the most structurally and material efficient reinforcement solution.

### 3.6.1 CPG-verification of the unreinforced beam

As a starting point for the reinforcement analysis, the timber beam is first verified without reinforcement with respect to CPG. This verification is used to assess whether the bearing stresses introduced by the bearing plate can be carried by the unreinforced timber, and thereby to determine whether reinforcement is required.

The verification is carried out directly according to the Eurocode formulation introduced in Section 2.7.1, using the loaded bearing area and the corresponding stress-spreading provisions. The assumed stress spreading is consistent with the load-spreading concept illustrated in Figure 2.4.

The design compressive stress perpendicular to the grain is calculated by Equation (2.2) and evaluated against the design resistance as shown in expression (2.1).

### 3.6.2 Analytical model and design variables for reinforced capacity

The analytical model is based on Equation (2.8). It is evident that numerous variables related to timber and steel properties, spacing demands and overall geometry affect the reinforced capacity of the contact area $F_{c,90,d}$, as well as each other. Consequently, identifying the most influential variables can be challenging. The effective stress-distribution length $l_{2,\mathrm{ef}}$ alone, is directly influenced by the penetration length inside the timber $l_w$, the number of reinforcing members and corresponding spacing parallel to grain $n_0, a_1$ and $a_{3,c}$, see Equation (2.9b) and Figure 2.6.

The characteristic compressive strength perpendicular to grain $f_{c,90,k}$ corresponding to a GL32h-member is taken as 2.5 MPa (Swedish Wood, 2022). Since spacing variables is a function of the reinforcing members diameter and the steel material properties are chosen in accordance with the new draft of EC5 (CEN, 2025), the remaining set of free variables and can be seen in Table 3.11.

### 3.6.3 Genetic algorithm (GA)

In this section the basis of the GA-optimization is described and its implementation is presented.

#### 3.6.3.1 Most material-efficient configuration

A genetic algorithm (GA) is a population-based stochastic optimization method, meaning it searches for optimal solutions iteratively within that population of candidate solutions (MathWorks, 2025). Each candidate solution is evaluated using an objective function that determines how well that design meets the chosen objective, within a frame of constraints. The chosen objective is minimizing steel-related $CO_2$ emissions (and glue if bonded reinforcing members) while satisfying both structural utilization and spacing constraints as follows:

- **Design variables:** diameter ($d$), penetration depth ($l_w$), number of reinforcing members parallel ($n_0$) and perpendicular ($n_{90}$) to grain. These variables are free with intervals shown in Table 3.11. The spacing between reinforcing members along ($a_1$) and perpendicular ($a_2$) to the grain is computed based on the number of fasteners and minimum end/edge distances, and naturally pushes towards maximum spacing within the available space, such that:

$$a_1 = \frac{l_{\text{plate}} - 2a_3}{n_0 - 1}, \qquad a_2 = \frac{b_{\text{plate}} - 2a_4}{n_{90} - 1}.$$

- **Objective function:** computes the mass of steel and multiplies it with the steel emission factor $\text{EF}_{\text{steel}}$:

$$f_{\text{CO2}} = \text{Volume} \cdot \rho_{\text{steel}} \cdot \text{EF}_{\text{steel}} = n_0 \cdot n_{90} \cdot \frac{\pi d^2}{4} \cdot l_w \cdot \rho_{\text{steel}} \cdot \text{EF}_{\text{steel}}.$$

- **Constraints:** ensures the design is safe. Using the utilization ratio (UR) between the load $V_{Ed}$ and the reinforced capacity $F_{c,90,d}$ the analytical model:

$$\text{UR} = \frac{V_{Ed}}{F_{c,90,d}} < 1,$$

  while enforcing minimum spacing requirements for the reinforcing members as well as ensuring the physical dimensions of the plate are not exceeded:

$$\begin{aligned} a_1 &\geq a_{1,\min}, & a_2 &\geq a_{2,\min}, \\ a_3 &\geq a_{3,\min}, & a_4 &\geq a_{4,\min}, \\ (n_0 - 1) \cdot a_1 + 2a_3 &\leq l_{\text{p}}, & (n_{90} - 1) \cdot a_2 + 2a_4 &\leq b_{\text{p}}. \end{aligned}$$

Hence, the GA searches within the space of free variables to find possible candidates, rejecting infeasible design solutions while minimizing the $CO_2$ objective.

**Table 3.11:** Definition of free variables in the reinforcement optimization for different reinforcement types.

| **Screws** | | |
|---|---|---|
| **Variable** | **Unit** | **Interval** |
| Diameter, $d$ | [mm] | [7, 8, ..., 14] |
| Penetration depth, $l_w$ | [mm] | [50, 100, ..., $h_b$] |
| Number of fasteners parallel to grain, $n_0$ | [-] | [1, 2, ..., 10] |
| Number of fasteners perpendicular to grain, $n_{90}$ | [-] | [2, 4, ..., 10] |
| **Rods with wood screw thread** | | |
| **Variable** | **Unit** | **Interval** |
| Diameter, $d$ | [mm] | [12, 13, ..., 20] |
| Penetration depth, $l_w$ | [mm] | [50, 100, ..., $h_b$] |
| Number of fasteners parallel to grain, $n_0$ | [-] | [1, 2, ..., 10] |
| Number of fasteners perpendicular to grain, $n_{90}$ | [-] | [2, 4, ..., 10] |
| **Bonded-in rods** | | |
| **Variable** | **Unit** | **Interval** |
| Diameter, $d$ | [mm] | [12, 13, ..., 20] |
| Penetration depth, $l_w$ | [mm] | [50, 100, ..., $h_b$] |
| Number of fasteners parallel to grain, $n_0$ | [-] | [1, 2, ..., 10] |
| Number of fasteners perpendicular to grain, $n_{90}$ | [-] | [2, 4, ..., 10] |
| **Wooden dowels** | | |
| **Variable** | **Unit** | **Interval** |
| Diameter, $d$ | [mm] | [12, 13, ..., 20] |
| Penetration depth, $l_w$ | [mm] | [50, 100, ..., $h_b$] |
| Number of fasteners parallel to grain, $n_0$ | [-] | [1, 2, ..., 10] |
| Number of fasteners perpendicular to grain, $n_{90}$ | [-] | [2, 4, ..., 10] |

#### 3.6.3.2 Most influencing parameters

To explain the GA results and capture potential trends and/or limitaations, two additional analyses were performed:

- **Load-path analysis:** The GA-optimization with the same objective was repeated for increasing target loads, where the selected parameters were recorded to see what the optimizer chose to increase as demand grew.
- **Sensitivity analysis:** One parameter was varied at a time around the GA-optimum, while the others were kept fixed. Capacity was then recalculated to see which parameters gave useful capacity increase and where the the response reached potential plateaus.

# 4 Results and Discussion

This chapter presents the results of the member design checks, the numerical modeling of the connection, and the beam-side reinforcement optimization, together with the corresponding discussions of each result. The validation of the numerical model against analytical hand calculations is presented in Section 3 and is not repeated here. Hand calculations providing design resistance for the members and fasteners is presented in Appendix A.

These results are structured to address the research questions introduced in Section 1.2. Section 4.1 first verifies the reference-case member dimensions on which the subsequent connection-level checks are based. Sections 4.2 and 4.3 address how the connection distributes shear and axial forces to the column and what factors influence that distribution. Sections 4.2, 4.3, 4.4, 4.5 and 4.6 together address which components are most critical and to what extent the concept provides sufficient load transfer and resistance, considering both column-side force transfer through the steel components and fasteners as well as both column-side and beam-side compression perpendicular to grain. Section 4.7 addresses which reinforcement strategy is most material-efficient and which design parameters are most influential in achieving that efficiency.

## 4.1 Member design checks

The member checks were evaluated using the procedure described in Section 3.3.3. For the simply supported beam, the governing design actions were obtained as $V_{Ed} = 500\,\mathrm{kN}$ and $M_{Ed} = 1250\,\mathrm{kNm}$, see Equations (3.1) and (3.2). Table 4.1 summarizes the bending check, Table 4.2 the shear check at the slotted beam section, and Table 4.3 the column compression check.

**Table 4.1:** Bending check results in beam member check.

| Check | Value | UR [-] |
|---|---|---|
| $M_{Ed}$ [kNm] | 1250 | – |
| $M_{Rd}$ [kNm] | 1652 | 0.76 |

**Table 4.2:** Shear check at the slotted beam section.

| Check | Value | UR [-] |
|---|---|---|
| $V_{Ed}$ [kN] | 500 | – |
| $V_{Rd}$ [kN] | 513.4 | 0.97 |

**Table 4.3:** Column compression check results.

| Check | Value | UR [-] |
|---|---|---|
| $N_{Ed}$ [kN] | 3000 | – |
| $N_{c,0,Rd}$ [kN] | 3276.8 | 0.92 |

The beam is governed by shear rather than bending, with the slotted section reaching a utilization of 0.97 against 0.76 for bending, most likely since the effective cross-sectional area is reduced to be able to slot in the internal beam shoe. The column reaches a utilization of 0.92 in compression parallel to grain, leaving a small margin. Since none of the three checks exceed in capacity, the chosen member dimensions are adequate for the reference load case, but the beam shear check and the column compression check both operate close to their design limit, hence offering little room for load increases without resizing the members.

## 4.2 Fastener shear resistance

The lateral shear design resistance $F_{v,Rd}$ was evaluated against the governing screw force obtained from the numerical model, following the procedure in Section 2.7.2. Table 4.4 gives the full distribution of shear forces across the fastener group, and Table 4.5 the resulting design check.

**Table 4.4:** Numerical shear forces $F_v$ [kN] for each screw, where the first row corresponds to the top row in the connection. The highest loaded fasteners are highlighted.

| **Outer** | **Inner** | **Inner** | **Outer** |
|---|---|---|---|
| 9.73 | 9.70 | 9.70 | 9.73 |
| 9.61 | 9.54 | 9.54 | 9.61 |
| 9.55 | 9.45 | 9.46 | 9.55 |
| 9.53 | 9.41 | 9.41 | 9.52 |
| 9.52 | 9.40 | 9.40 | 9.52 |
| 9.53 | 9.41 | 9.40 | 9.53 |
| 9.56 | 9.43 | 9.43 | 9.56 |
| 9.60 | 9.47 | 9.47 | 9.60 |
| 9.66 | 9.53 | 9.53 | 9.66 |
| 9.73 | 9.61 | 9.61 | 9.73 |
| 9.82 | 9.71 | 9.72 | 9.82 |
| 9.92 | 9.85 | 9.85 | 9.92 |
| **10.06** | 10.05 | 10.05 | **10.06** |

**Table 4.5:** Lateral shear resistance and utilization ratio for the governing screw.

| $F_{v,Rd}$ **[kN]** | $F_{v,FEM,\max}$ **[kN]** | $UR = F_{v,FEM,\max}/F_{v,Rd}$ **[-]** |
|---|---|---|
| 11.04 | 10.06 | 0.91 |

The governing fastener reaches a utilization of $0.91$, indicating that the fasteners resist the applied lateral shear force with a limited but sufficient margin. It should be noted that the numerical model does not explicitly capture the physical shear failure mechanisms of the screws such as embedment deformation, screw bending, or rope-effect interaction. Instead, the screws are modelled as connector elements with axial and lateral stiffness directly affected by timber density, screw diameter and screw penetration depth, as described in Section 3.4.3.2. The model is therefore used only to determine the force distribution within the fastener group, while the design resistance itself is evaluated separately using the approach provided by Eurocode 5.

Since the governing utilization remains below the design limit, the fastener configuration is considered feasible with respect to shear, though it remains among the more highly utilized components in the connection.

## 4.3 Fastener withdrawal and tensile resistance

The axial design resistance $F_{ax,t,d}$ was evaluated against the governing axial force in the fastener group, following Section 2.7.2. The numerical result shows that the bottom fasteners are not engaged in carrying axial forces, while the force increases sharply toward the top rows, in a non-linear manner. The full axial force distribution for a backplate thickness of $t_p = 15$ mm is given in Table 4.6, and the resulting design check in Table 4.7.

**Table 4.6:** Numerical axial forces $F_{ax}$ [kN] for each screw, where the first row corresponds to the top row in the connection. The highest loaded fastener is highlighted.

| Outer | Inner | Inner | Outer |
|---|---|---|---|
| 6.89 | 9.02 | **9.03** | 6.88 |
| 4.98 | 6.34 | 6.31 | 4.98 |
| 4.11 | 5.04 | 5.06 | 4.11 |
| 3.38 | 4.10 | 4.07 | 3.39 |
| 2.66 | 3.20 | 3.20 | 2.67 |
| 1.97 | 2.37 | 2.36 | 1.97 |
| 1.30 | 1.55 | 1.56 | 1.31 |
| 0.68 | 0.80 | 0.81 | 0.67 |
| 0.23 | 0.23 | 0.24 | 0.25 |
| 0.11 | 0.05 | 0.02 | 0.12 |
| 0.03 | 0.00 | 0.00 | 0.07 |
| 0.00 | 0.00 | 0.00 | 0.00 |
| 0.00 | 0.00 | 0.00 | 0.00 |

**Table 4.7:** Axial design resistance and utilization ratio for the governing screw.

| $F_{ax,\max}$ **[kN]** | $F_{ax,t,d}$ **[kN]** | $UR = F_{ax,\max}/F_{ax,t,d}$ **[-]** |
|---|---|---|
| 9.03 | 21.45 | 0.42 |

The combined shear-axial verification of the governing top inner screw was carried out using the interaction expression:

$$UR = \left(\frac{F_{v,\mathrm{FEM}}}{F_{v,Rd}}\right)^2 + \left(\frac{F_{ax,\mathrm{FEM}}}{F_{ax,t,d}}\right)^2 = 0.95 < 1$$

.

The pronounced non-linearity in the axial distribution reflects the global rotational behaviour of the internal beam shoe under eccentric loading: within the most highly loaded rows, the inner screws closest to the stiffener carry the largest axial forces, showing that the axial response is governed both by the vertical row position and by the local stiffness distribution within the steel assembly. Three interacting effects can explain this pattern. First, the finite stiffness of the backplate affects how rotational deformation is distributed over the fastener group and within each row. Second, the varying geometry of the stiffener produces a non uniform stiffness along the height of the connection. Third, contact between the backplate and the timber column introduces local compression in the lower part of the connection, reducing the axial demand in the adjacent lower rows, while also inducing local timber deformation that further affects the force distribution. Because the governing axial force (9.03 kN) remains well below the axial design resistance (21.45 kN), and the combined interaction ratio remains below the design limit, the fasteners satisfy the design requirements for axial loading, and the connection is feasible from this perspective.

This rotation-driven, non-uniform axial distribution is consistent with the general behaviour of bracketed steel-bearing connections discussed in Section 2.4.3.1, where force transfer through an internal steel component was shown to depend on the combined response of the bracket, its fasteners and the surrounding timber rather than on fastener action alone (Madland et al., 2023b). The present result can therefore be seen as a more detailed, component-level, account of a behaviour that previous bearing-type connection studies only observed at the level of deformation compatibility.

### 4.3.1 Influence of thicker back plate

Since the axial force distribution above is governed partly by backplate stiffness, the effect of backplate thickness $t_p$ on the force distribution in the top, most-loaded row was investigated. Figure 4.1 shows the result.

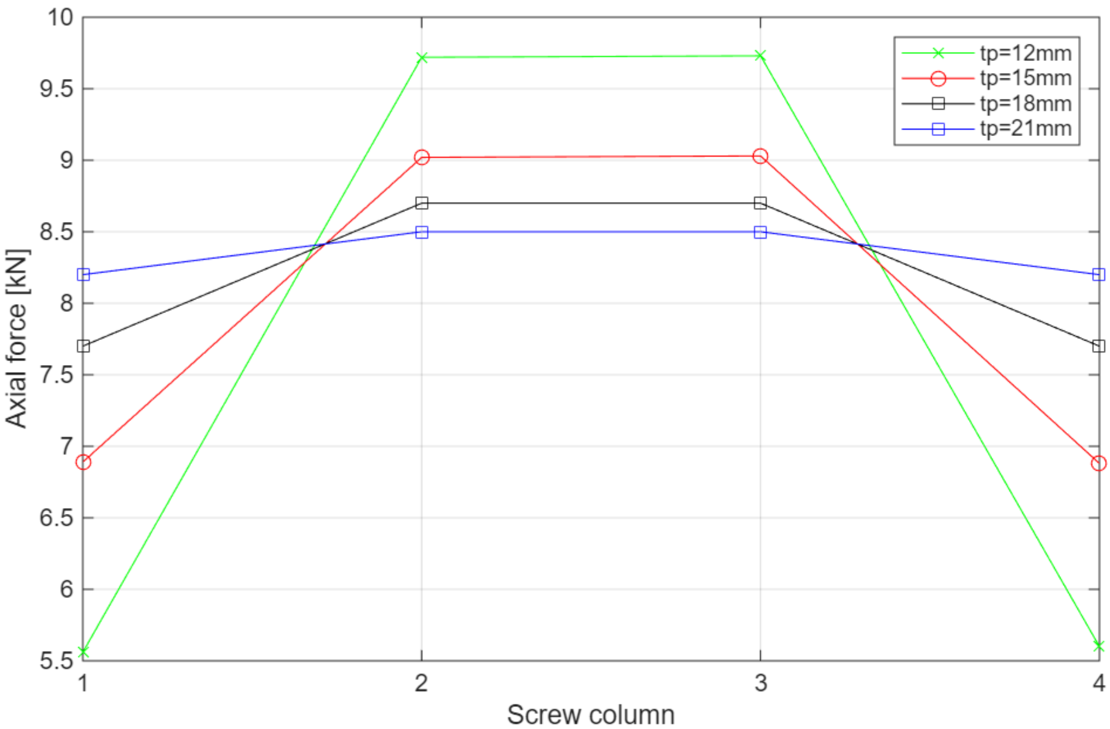


**Figure 4.1:** Axial force distribution in the top and most loaded row, for increasing thickness of the backplate $t_p$.

A back plate thickness of $t_p = 12$ mm produces a markedly non-uniform distribution, attracting more load to the inner rows, reaching a maximum of approximately 9.75 kN, whereas increasing the thickness to $t_p = 21$ mm distributes the force more evenly, reducing the maximum to approximately 8.6 kN. This confirms that backplate stiffness has a direct influence on the local axial force pattern, particularly in the upper rows where axial forces are highest; a more flexible plate deforms locally around the stiffest load paths (i.e. near the stiffener), while a stiffer plate spreads the rotational demand more evenly across all screws in the row. At the same time, the continued dominance of the inner screws even at $t_p = 21$ mm shows that the stiffener geometry remains an influential local driving force regardless of backplate thickness investigated.

## 4.4 Critical steel component: Bearing plate

The most critical stresses in the internal beam shoe occur in the bearing plate, where the maximum normal stress reaches $\sigma_z = 340.2$ MPa, as summarized in Table 4.8 and Figure 4.2.

**Table 4.8:** Utilization of the most critical component in the internal beam shoe.

| $\sigma_z$ **[MPa]** | $f_y$ **[MPa]** | $UR = \frac{\sigma_z}{f_y}$ **[-]** |
|---|---|---|
| 340.2 | 355 | 0.96 |

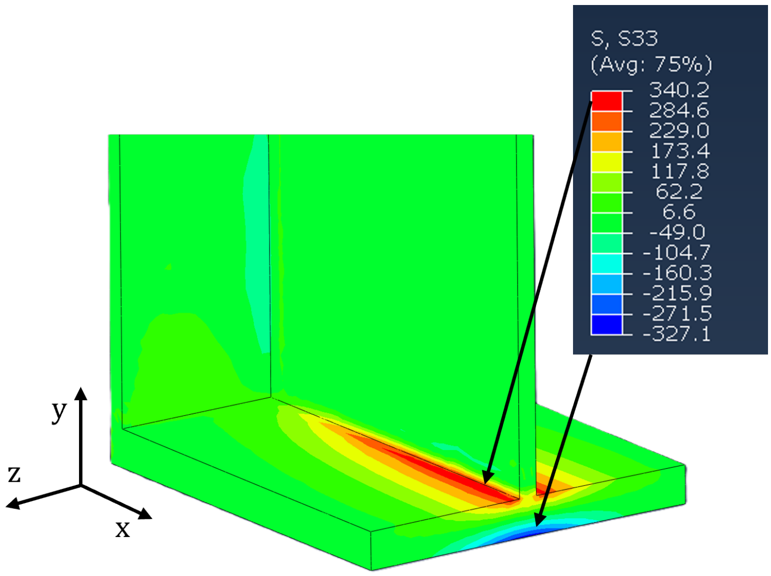


**Figure 4.2:** Normal stress distribution $\sigma_z$ in the internal beam shoe.

With a utilization ratio of 0.96, the bearing plate is the governing steel component in the connection. The stress distribution shows that the critical stresses concentrate near the free edge of the plate, close to the stiffener connection, indicating that the governing response is local plate bending in the cantilevered part of the plate. This result is also sensitive to the modelling assumption of a uniformly distributed contact load; if the beam is allowed to rotate under load, the true contact pressure would rather concentrate toward the outer part of the plate, increasing the local cantilever action and producing higher bending stresses than obtained here. Since the utilization ratio is already close to the design limit even under the more favorable uniform-load assumption, the bearing plate should be regarded as operating close to its design limit rather than with comfortable spare capacity. For this reason, the steel-side feasibility of the connection is considered governed by the bending response of the bearing plate rather than by fasteners or any other steel component, which is the component to prioritize if further optimization of the connection is pursued, especially if rotation of the beam is not prohibited.

This result cannot be directly benchmarked against previous studies: as noted in Section 2.4.3.4, existing studies of concealed bearing type connections, including the similar knife-plate system tested by Madland et al. (2023b), have focused on deformation compatibility under prescribed loading rather than investigating the connection on component level. The bearing plate utilization obtained here therefore represents new findings rather than a confirmation of established results, and supports the research gap identified in Section 2.4.3.4 regarding the need for component-level assessment of bearing type connections.

## 4.5 Column-side compression perpendicular to grain

The numerical model was used to evaluate the contact stresses between the internal beam shoe and the timber column, shown in Figure 4.3.

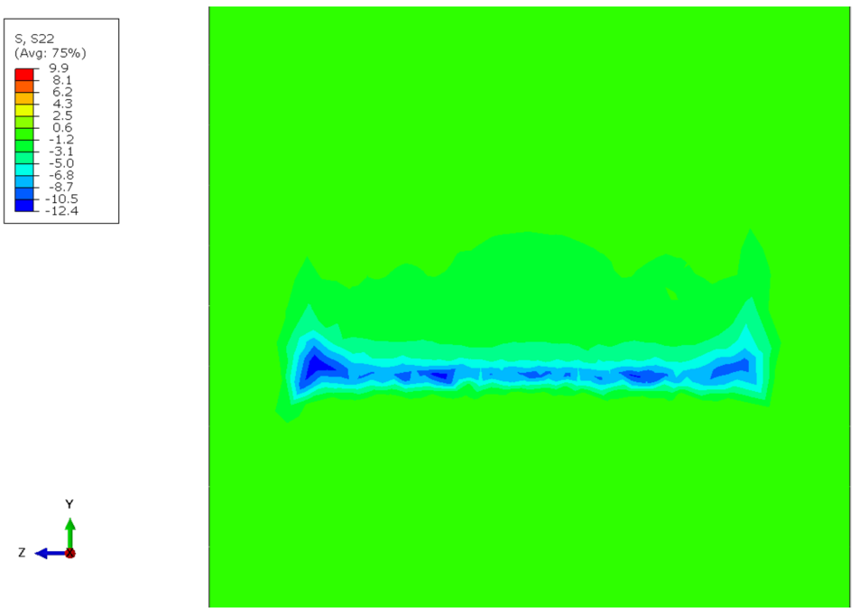


**Figure 4.3:** Compressive stresses at the contact between the internal beam shoe and the timber column.

The model indicates highly localized compressive stresses concentrated in a narrow region near the lower contact zone, with a peak value of $\sigma_{c,90,\max} = 12.4$ MPa, considerably higher than the characteristic CPG strength of the timber, $f_{c,90,k} = 2.5$ MPa. This result would suggest the column-side contact region is critical with respect to CPG. However, the result must be interpreted with care: the present model uses a linear elastic representation of the timber, which does not capture the local crushing and stress redistribution that occurs in practice under perpendicular-to-grain loading. The numerical peak stress should therefore be read as an indication that the current detailing produces an unfavourable local contact condition, with further investigation needed for the identified critical area of the connection, and not as a formal design verification.

This localization is consistent with the general behaviour described in Section 2.5.1, where non-uniform contact conditions were shown to produce pronounced stress concentrations near edges and geometric discontinuities (Jockwer & Dietsch, 2018). This reinforces that the observed peak in the column is a consequence of the non-uniform contact conditions in the numerical model, and that the region needs closer investigation rather than being dismissed on the basis of the simplified material model alone.

Since the steel geometry can be considered almost fully utilized (see Section 4.4), increasing the contact area through bracket redesign is not the most practical option, also considering the contact area is heavily influenced by the rotational deformation of the backplate. Instead, the more promising routes are measures that improve the local stress distribution within the timber itself, such as introducing a stress-spreading interlayer (e.g. plywood or hardwood) or locally reinforcing the column-side contact zone. Because the result suggests that local crushing will occur in the column, a non-linear analysis allowing plastic redistribution would be needed to properly assess this behaviour, which is carried forward as a recommendation for future work in Section 4.8.

Taken together with Sections 4.1–4.5, these results indicate that the connection concept satisfies the governing steel and fastener checks on the column side, while the column-side contact condition remains as the most critical in terms of overall resistance. This directly addresses the third research question in Section 1.2: the fasteners and steel components are sufficiently resistant under the studied load case and load application assumptions, but the column-side CPG response should be regarded as the connection's most uncertain and critical aspect to prioritize for further investigation.

## 4.6 Beam-side compression perpendicular to grain: unreinforced capacity

The CPG verification for the unreinforced beam was carried out according to the analytical procedure in Section 3.6.1. Using the bearing plate dimensions and the applied design load, the design compressive stress was obtained as $\sigma_{c,90,d} = 4.952$ MPa against a design resistance of $\sigma_{c,90,Rd} = 1.573$ MPa, summarized in Table 4.9.

**Table 4.9:** Compression-perpendicular-to-grain verification of the unreinforced beam.

| $\sigma_{c,90,d}$ **[MPa]** | $\sigma_{c,90,Rd}$ **[MPa]** | $UR = \sigma_{c,90,d}/\sigma_{c,90,Rd}$ **[-]** |
|---|---|---|
| 4.952 | 1.573 | 3.148 |

The resulting utilization ratio of 3.148 shows the unreinforced beam is roughly three times over its CPG capacity at the design load, confirming that reinforcement of the beam-side contact zone is not optional but a necessary design measure for this connection.

This magnitude of stress is consistent with the literature reviewed in Section 2.4.3, which identifies compression perpendicular to grain as the principal limiting factor in bearing-type timber connections, and shows that bearing capacity depends strongly on contact geometry and stress-spreading behaviour rather than on the contact area alone (Blass & Görlacher, 2004), (Pasca et al., 2024). The present result confirms that this general limitation applies in full to the high-load application studied here, which motivates the reinforcement optimization presented in the following section.

## 4.7 Beam-side reinforcement: strategy comparison and optimization

Four reinforcement types were assessed using a genetic algorithm (GA) to identify, for each type, the most material-efficient configuration capable of meeting the required capacity: fully threaded screws, rods with wood screw thread, bonded-in rods and wooden dowels. Table 4.10 lists the five best configurations found for each type, and Figure 4.4 compares their associated $CO_2$-equivalent emissions.

**Table 4.10:** Best reinforcement configurations for different reinforcement types.

| **Screws** | | | | | | | | |
|---|---|---|---|---|---|---|---|---|
| $d$ | $l_w$ | $a_1$ | $a_2$ | $n_0$ | $n_{90}$ | $F_{c,Rd}$ | UR | $CO_2$-eq. |
| **14** | **550** | **208** | **75.67** | **2** | **4** | **520.96** | **0.9598** | **8.5072** |
| 14 | 600 | 208 | 75.67 | 2 | 4 | 527.36 | 0.9481 | 9.2806 |
| 14 | 650 | 208 | 75.67 | 2 | 4 | 527.36 | 0.9481 | 10.0540 |
| 14 | 700 | 208 | 75.67 | 2 | 4 | 527.36 | 0.9481 | 10.8274 |
| 14 | 750 | 208 | 75.67 | 2 | 4 | 527.36 | 0.9481 | 11.6008 |
| **Rods with wood screw thread** | | | | | | | | |
| $d$ | $l_w$ | $a_1$ | $a_2$ | $n_0$ | $n_{90}$ | $F_{c,Rd}$ | UR | $CO_2$-eq. |
| 17 | 550 | 184 | 71.67 | 2 | 4 | 513.28 | 0.9741 | 12.5438 |
| 17 | 600 | 184 | 71.67 | 2 | 4 | 545.28 | 0.9170 | 13.6842 |
| 18 | 550 | 176 | 70.33 | 2 | 4 | 510.72 | 0.9790 | 14.0630 |
| 15 | 550 | 200 | 44.60 | 2 | 6 | 518.40 | 0.9645 | 14.6489 |
| 15 | 550 | 100 | 74.33 | 3 | 4 | 518.40 | 0.9645 | 14.6489 |
| **Bonded-in rods** | | | | | | | | |
| $d$ | $l_w$ | $a_1$ | $a_2$ | $n_0$ | $n_{90}$ | $F_{c,Rd}$ | UR | $CO_2$-eq. |
| 16 | 550 | 120 | 203 | 3 | 2 | 531.20 | 0.9413 | 9.0738 |
| 14 | 550 | 250 | 71 | 2 | 4 | 534.40 | 0.9356 | 9.3781 |
| 14 | 550 | 83.33 | 213 | 4 | 2 | 534.40 | 0.9356 | 9.3781 |
| 16 | 600 | 120 | 203 | 3 | 2 | 547.05 | 0.9140 | 9.8987 |
| 19 | 650 | 225 | 188 | 2 | 2 | 526.91 | 0.9489 | 9.9450 |

*Note:* $d$, $l_w$, $a_1$, and $a_2$ are given in mm; $F_{c,Rd}$ is given in kN; $CO_2$-eq. is given in kg $CO_2$-eq.; UR is dimensionless.

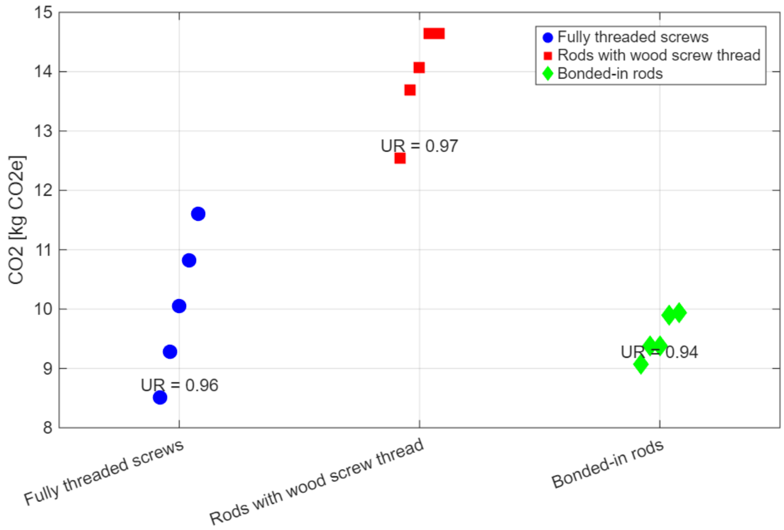


**Figure 4.4:** CO2 comparison of the five best configurations for each reinforcement type.

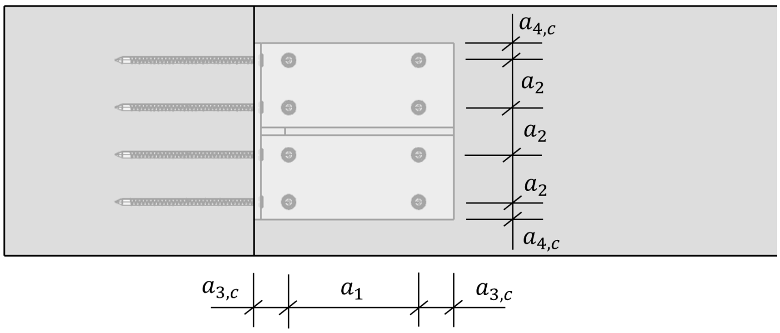


**Figure 4.5:** A schematic illustration of resulting most material-efficient configuration using screw reinforcement.

Fully threaded screws provide the most material-efficient reinforcement for the applied load with the best configuration reaching a reinforced capacity of $F_{c,Rd} = 520.96$ kN (UR 0.96) at only 8.51 kg $CO_2$-eq., against 12.5 and 9.1 kg $CO_2$-eq for the best wood-screw thread and bonded-in rod solutions, whereas no configuration of wooden dowels had sufficient capacity to carry the load. Screw reinforcement is therefore recommended for the studied load case. However, this ranking is load-dependent rather than universal, as discussed below.

The GA's consistent preference for larger diameter over additional fastener count is in line with Kanagaki et al. (2025), who found that the proportion of engaged length, rather than simply the number of fasteners, governs the reinforcement effect in screw-reinforced contact regions. At the same time, Aloisio et al. (2023) stated that existing capacity models for screw reinforcement carry some uncertainty regarding the governing failure mode, and may not always predict the mechanism observed experimentally. Since the optimization is build on the same Eurocode-provided analytical model described in Section 2.7.3, this uncertainty is inherited by the optimization result. The ranking between reinforcement types obtained here should therefore be interpreted as a relative comparison under a consistent analytical mode, rather than as an absolute prediction of capacity.

### 4.7.1 Parameter load-path analysis

To understand how the GA reaches these configurations as capacity demand increases, the evolution of each parameter was tracked across increasing load levels for all reinforcement types excluding the worst performing wooden dowels (Figures 4.6, 4.7 and 4.8).

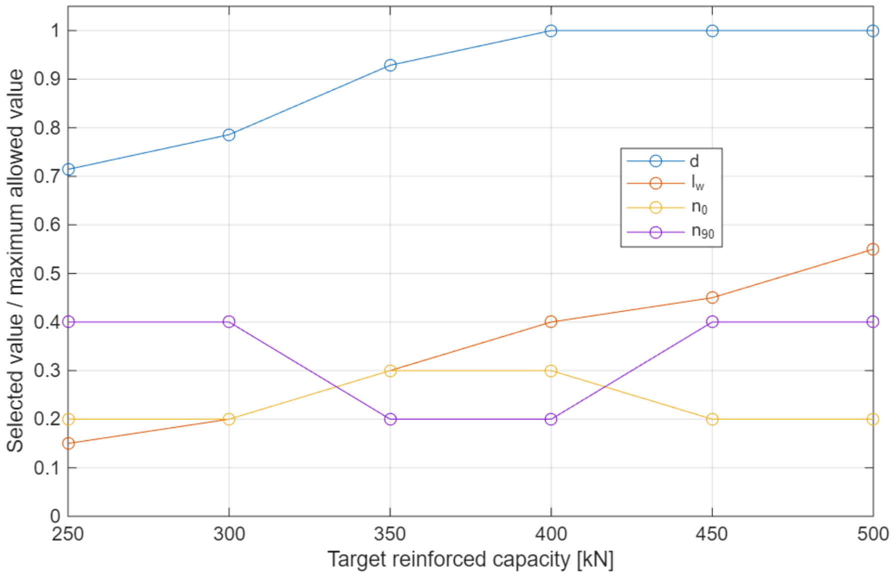


**Figure 4.6:** Normalized GA-optimized screw parameters as capacity demand increases.

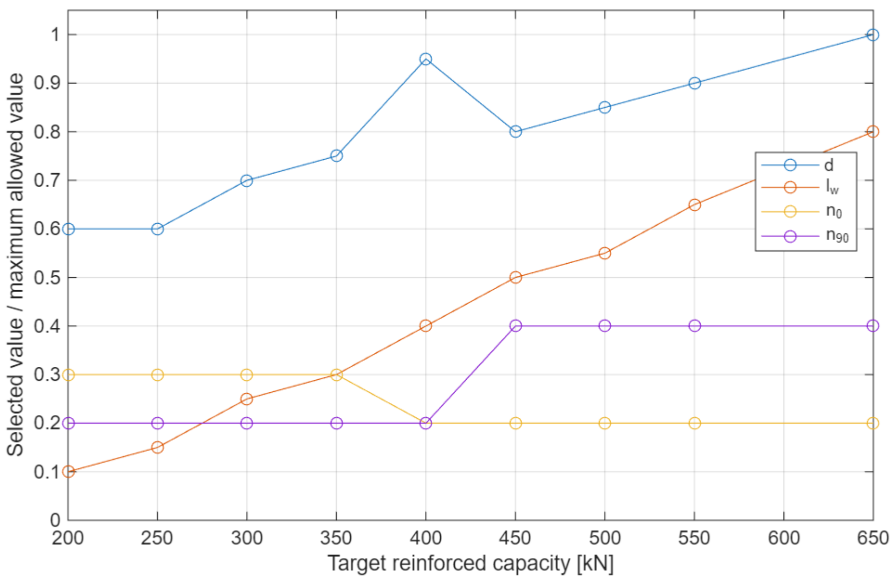


**Figure 4.7:** Normalized GA-optimized rods with wood screw thread parameters as capacity demand increases.

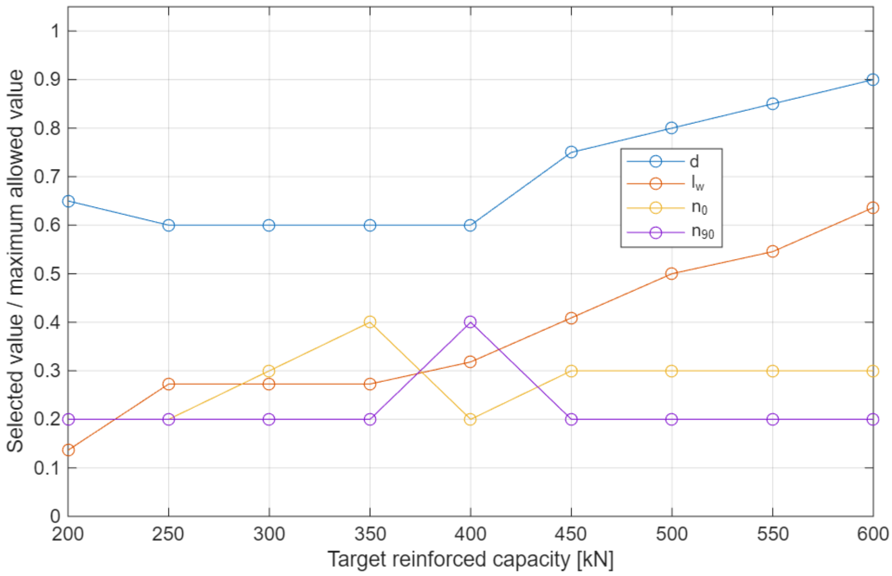


**Figure 4.8:** Normalized GA-optimized bonded-in rod parameters as capacity demand increases.

The GA does not increase all parameters uniformly as capacity demand grows. Instead, diameter $d$ is pushed high already at low load levels, while further capacity gains are achieved mainly by increasing the penetration depth $l_w$, whereas the number of fasteners remains comparatively low across all load levels. This is notable because, per the objective function in Section 3.6.3.1, increasing $d$ is penalized quadratically in the $CO_2$ cost calculation - yet the GA still prefers it consistently across all three reinforcement types, which indicates that $d$ has disproportionately strong effect on capacity relative to its material cost, outweighing the penalty. Furthermore, a clear practical limit emerges from this analysis: the screw reinforcement configurations cannot reach capacities beyond approximately 550 kN, whereas rods with wood screw thread and bonded-in rods can be scaled to higher capacities if required. This means the most material efficient reinforcement type selected as in Section 4.7 is only optimal within the load range studied here, where for applications with higher demand, one of the rod solutions would be a necessary choice regardless of $CO_2$ penalty.

### 4.7.2 Parameter sensitivity analysis

The two most influential parameters identified above, $d$ and $l_w$, were investigated further using a one-at-a-time sensitivity analysis, presented in Figures 4.9 and 4.10.

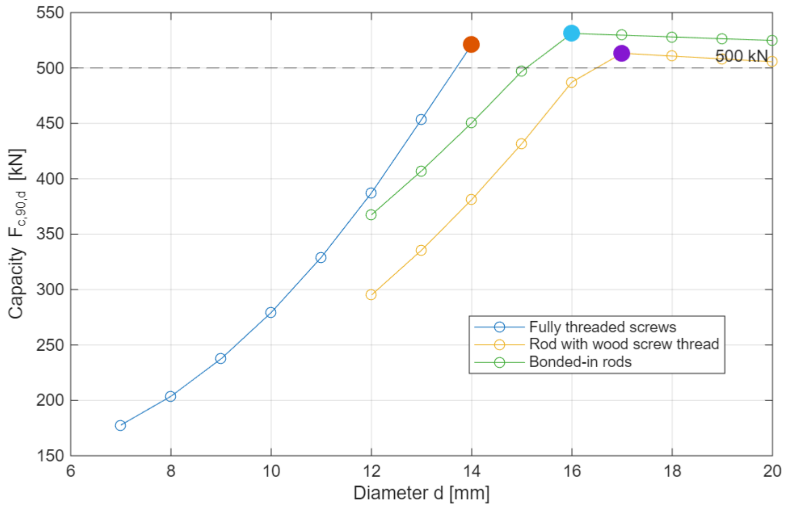


**Figure 4.9:** One-at-a-time sensitivity analysis of diameter $d$. Highlighted dots is the corresponding GA-optimal choice of parameter, for all feasible reinforcement types.

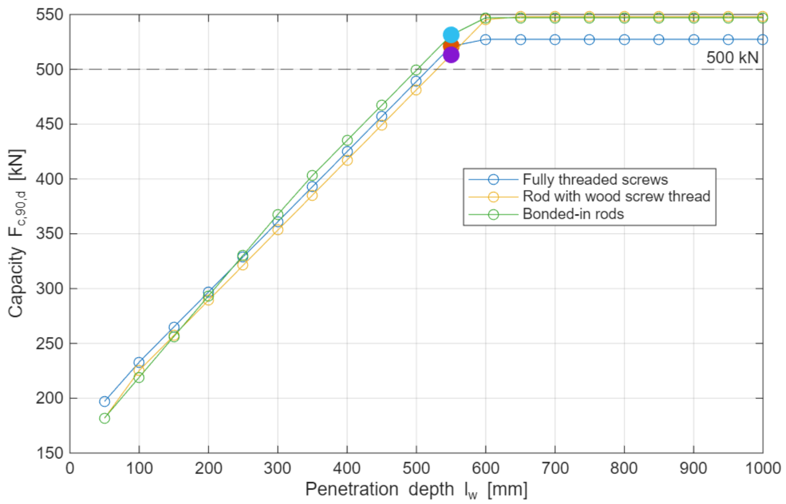


**Figure 4.10:** One-at-a-time sensitivity analysis of penetration depth $l_w$. Highlighted dots is the corresponding GA-optimal choice of parameter, for all feasible reinforcement types.

Both parameters give a clear capacity increase up to a point, after which the response plateaus. For fully threaded screws, increasing $d$ gives an almost linear capacity increase up to the maximum available diameter, while $l_w$ plateaus beyond the GA-optimum of 550 mm. The screw plateau has a specific physical cause: the best configuration uses $d = 14$ mm, and through the characteristic withdrawal strength $F_{w,k}$ used in Equation 2.8, this diameter limits the effective penetration depth to $40d$ - so beyond that point additional $l_w$ simply won't give further capacity. The other two reinforcement types plateau for different reasons - for rods with wood screw thread, a decrease in capacity is even recorded at larger $d$, most likely because the governing failure mode changes and spacing requirements become less favourable at that diameter. This confirms that no single parameter can be tuned in isolation, but instead highlights the complexity embedded in Equation 2.8, where the interaction between diameter, penetration depth, characteristic strength and governing failure mode determines where each reinforcement type's capacity ceiling lies. And this ceiling must be checked explicitly whenever the reinforcement type, configuration or load level changes.

Taken together, the load-path and sensitivity analyses identify diameter and penetration depth as the most influential design parameters for beam-side reinforcement, with fully threaded screws providing the most material-efficient solution within the load-range studied here. This directly answers the fourth research question posed in Section 1.2, while also clarifying its limits: the ranking of reinforcement strategies is specific to the studied load range and would need to be re-evaluated for substantially higher or lower demand.

## 4.8 Recommendations for future work

The results of this thesis indicate several directions for future work. First, experimental testing of the selected connection concept would be valuable in order to validate both the analytical and numerical models against physical behavior. Such testing could improve the understanding of local stress redistribution, deformation patterns, and the actual force transfer within the connection. In the longer term, a stronger experimental basis could also support the development of applicable design standards for concealed timber connections of this type.

Second, the numerical modeling could be extended to include the timber beam in greater detail. In the present study, the numerical model is limited to the internal beam shoe and the column side of the connection, while both the beam-side CPG-response and the contribution of the reinforcement are assessed analytically. A more comprehensive numerical model could provide additional insight into the local interaction between the steel components and the surrounding timber. It could further clarify the structural contribution of the reinforcement and thereby support validation of the analytical representation of the reinforcement effect.

Third, the loading conditions considered in this thesis are limited to the lateral beam load. Future studies could therefore investigate the influence of transverse loading, eccentric loading, and torsional effects in order to assess the robustness of the concept under a wider range of practical design situations. In addition, long-term effects such as moisture variations, creep, and shrinkage could be considered in order to better understand the long-term performance of the connection.

Moreover, the reinforcement study could be extended by considering additional reinforcement methods, broader parameter ranges, and alternative optimization objectives. In particular, future work could include a more detailed assessment of constructability, cost, and long-term performance, in addition to the structural response and associated $CO_2$-emissions considered in this thesis.

Finally, the present study focuses on applications with high load-carrying demands, which places strong requirements on the reinforcement capacity. Within this context, steel-based reinforcement strategies are expected to be more competitive than wooden alternatives. Future studies could therefore investigate the selected connection concept and associated reinforcement strategies for applications with lower load demands, where timber-based reinforcement solutions may become more relevant from both structural and environmental perspectives.

# 5 Conclusion

This thesis investigated concealed beam-to-column connections in timber structures for high-load applications requiring a seamless architectural expression. Based on a qualitative screening of connection families, bearing-type connections were identified as the most suitable direction for further study due to their direct load path, simple detailing, and high degree of concealment.

A concealed bearing-type concept was then developed in the form of an internal beam shoe. The analytical and numerical investigations showed that the steel-side of the connection provides sufficient resistance under the studied load case. The axial force distribution in the fastener group was shown to be non-uniform, with the highest withdrawal forces occurring in the top inner rows, while the fasteners still satisfied the governing axial, shear, and combined interaction checks. The bearing plate was identified as the critical steel component, governed by local bending in the cantilevered part of the plate. The numerical model also indicated highly localized compressive stresses at the column-side contact, suggesting that this region may be critical with respect to compression perpendicular to the grain, although this response was not formally verified and would require further nonlinear investigation.

On the beam side, the unreinforced timber did not provide sufficient resistance against compression perpendicular to the grain. This shows that the beam-side support response is a governing part of the connection behavior and that the connection cannot be assessed from the steel side alone.

The reinforcement study showed that fully threaded screws, rods with wood screw thread, and bonded-in rods can increase the beam-side compression-perpendicular-to-grain capacity sufficiently to carry the applied load, whereas wooden dowels could not. Among the feasible alternatives, screw reinforcement was found to be the most efficient solution in terms of capacity increase and associated $CO_2$-emissions. The optimization further showed that increased diameter and penetration depth are the most effective ways of increasing capacity, while the benefit of increasing penetration depth tends to plateau at withdrawal lengths of approximately 500–600 mm.

Overall, the study shows that the selected concealed connection concept is feasible on the steel side, but requires beam-side reinforcement in order to become feasible as a whole connection. The results therefore highlight that concealed high-capacity timber connections of the investigated type must be treated as a combined steel-side and beam-side design problem.

# 6 References


Aloisio, A., Ussher, E., Fragiacomo, M., & Tomasi, R. (2023). Capacity models for timber under compression perpendicular to grain with screw reinforcement. *European Journal of Wood and Wood Products*, *81*, 633–654. https://doi.org/10.1007/s00107-022-01918-z

A.Pranata, Y., Suryoatmono, B., Hassan, R., Pattipawaej, O. C., & Ahmad, Z. (2025). Structural behavior of beam-to-column glued laminated timber connection using double steel plates. *BioResources*, *20*. https://doi.org/10.15376/biores.20.4.8551-8565

Blass, H. J., & Görlacher, R. (2004). *Design of connections in timber structures* (tech. rep.). COST Action E35. Karlsruhe, Germany.

Blomgren, H.-E., Barber, D., & Montgomery, G. (2023). Fire design of glulam connections with timber-to-timber bearing interfaces. *Proceedings of the 13th World Conference on Timber Engineering (WCTE 2023)*, 1798–1806. https://doi.org/10.52202/069179-0238

CEN. (2004). *Eurocode 5: Design of timber structures — part 1-2: General — structural fire design*.

CEN. (2025). *Design of timber structures – part 1-1: General rules and rules for buildings* [Swedish adoption: SS-EN 1995-1-1:2025]. European Committee for Standardization.

Conway, M., Mehra, S., Harte, A. M., & O'Ceallaigh, C. (2021). Densified wood dowel reinforcement of timber perpendicular to the grain: A pilot study. *Journal of Structural Integrity and Maintenance*, *6*(3), 177–186. https://doi.org/10.1080/24705314.2021.1906090

du Plessis, M., Streicher, D., & Walls, R. (2025). Experimental testing on concealed beam hanger mass timber connections considering the influence of gap size and intumescent sealants. *Fire Technology*, *61*(7), 5185–5210. https://doi.org/10.1007/s10694-025-01782-2

Fragiacomo, M., & Batchelar, M. (2012). Timber frame moment joints with glued-in steel rods. ii: Experimental investigation of long-term performance. *Journal of Structural Engineering*, *138*(6), 802–811. https://doi.org/10.1061/(ASCE)ST.1943-541X.0000517

Ganjali, H., Tong, F., & Tannert, T. (2025). Biaxial resistance of pre-engineered beam hangers in glulam. *Buildings*, *15*(3). https://doi.org/10.3390/buildings15030440

Gauthier-Turcotte, É., Sylvain, M., & Fiset, M. (2022). Strength and behaviour of spruce-pine glulam timber 1 moment connections using glued-in steel rods. *Journal of Structural Engineering*, *148*. https://doi.org/10.1061/(ASCE)ST.1943-541X.0003486

Hawasly, F., Matsumoto, N., Koshihara, M., & Adachi, K. (2023). Wood-only timber frame joints inspired by trees' branch model, part 1: Structural system and bending performance. *AIJ Journal of Technology and Design*, *29*(73), 1296–1301. https://doi.org/10.3130/aijt.29.1296

Jockwer, R., & Dietsch, P. (2018). Review of design approaches and test results on brittle failure modes of connections loaded at an angle to the grain. *Engineering*

*Structures*, *171*, 362–372. https://doi.org/https://doi.org/10.1016/j.engstruct.2018.05.061

Kanagaki, D., Totsuka, M., Hirashima, T., & Kato, H. (2025). Reinforcement for compression perpendicular to grain in column-base and -beam joints using partially threaded and fully threaded screws. *Engineering Structures*, *324*, 119334. https://doi.org/https://doi.org/10.1016/j.engstruct.2024.119334

Kuda, D., & Petřičková, M. (2020). Modular timber structures. *IOP Conference Series: Materials Science and Engineering*, *800*. https://doi.org/10.1088/1757-899X/800/1/012033

Leichti, R. J., Hyde, R. A., French, M. L., & Camillos, S. G. (2000). The continuum of connection rigidity in timber structures. *Wood and Fiber Science*, *32*(1), 11–19. https://wfs.swst.org/index.php/wfs/article/view/2185

Madland, H., Fischer, E. C., & Sinha, A. (2023a). Cyclic testing of glue-laminated beam-to-column connections. *Journal of Structural Engineering*, *149*(4), 04023013. https://doi.org/10.1061/JSENDH.STENG-11865

Madland, H., Fischer, E. C., & Sinha, A. (2023b). Monotonic testing of glue-laminated beam-to-column connections. *Journal of Structural Engineering*, *149*(5), 04023039. https://doi.org/10.1061/JSENDH.STENG-11816

MathWorks. (2025). *Ga — find minimum of function using genetic algorithm (r2025b)* [Accessed Month Day, Year]. https://se.mathworks.com/help/releases/R2025b/gads/ga.html

Pasca, D. P., Massaro, F. M., De Santis, Y., Stamatopoulos, H., Ljungdahl, J., & Aloisio, A. (2024). Deformation level and specimen geometry in compression perpendicular to the grain of solid timber, glt and clt timber products. *Engineering Structures*, *321*, 118972. https://doi.org/https://doi.org/10.1016/j.engstruct.2024.118972

Reboucas, A. S., Mehdipour, Z., Branco, J. M., & Lourenco, P. B. (2022). Ductile moment-resisting timber connections: A review. *MDPI*, *12*. https://doi.org/10.3390/buildings12020240

Stamatopoulos, H., Malo, K. A., & Vilguts, A. (2022). Moment-resisting beam-to-column timber connections with inclined threaded rods: Structural concept and analysis by use of the component method. *Construction and Building Materials*, *322*, 126481. https://doi.org/https://doi.org/10.1016/j.conbuildmat.2022.126481

Steiger, R., Serrano, E., Stepinac, M., Rajčić, V., O'Neill, C., McPolin, D., & Widmann, R. (2015). Strengthening of timber structures with glued-in rods. *Construction and Building Materials*, *97*, 90–105. https://doi.org/10.1016/j.conbuildmat.2015.03.097

Swedish Wood. (2022). *Design of timber structures. volume 1: Structural aspects of timber construction* (3rd ed.).

Walters, L., Nasiri, H. R., Tong, F., & Tannert, L. W. T. Impacts of beam hanger rotational stiffness on column resistance of post-and-beam frames. In: World Conference on Timber Engineering (WCTE), 2025. https://doi.org/10.52202/080513-0484

Wang, T., Wang, Y., Crocetti, R., Honfi, D., Wålinder, M., Olsson, A., & Horney, E. (2025a). Glued-in hardwood rods as reinforcements for compression perpendicular to the grain: Single fastener to global loading cases. *Engineering Structures*, *344*, 121312. https://doi.org/10.1016/j.engstruct.2025.121312

Wang, T., Wang, Y., Crocetti, R., Honfi, D., Wålinder, M., Olsson, A., & Horney, E. (2025b). Reinforcement for compression perpendicular to the grain by means of adhesively bonded birch timber products. *Proceedings of the World Conference on Timber Engineering (WCTE)*. https://doi.org/10.52202/080513-0560

Woods, J. E., & Wierzbowski, A. (2026). Cyclic performance of pre-engineered beam-column connections for mass timber and hybrid mass timber-steel structures. *Engineering Structures*, *347*, 121683. https://doi.org/https://doi.org/10.1016/j.engstruct.2025.121683

WoodWorks. (2024). *Woodworks index of mass timber connections* (Accessed Month Day, Year). WoodWorks. https://www.woodworks.org/wp-content/uploads/wood_solution_paper_Index_Mass_Timber_Connections_05.2024.pdf

# Appendix A

## REFERENCE PROJECT

## LOADS: EN 1990

$f_{Ed.b} := 100\ \frac{kN}{m}$

$N_{Ed} := 3\ MN$

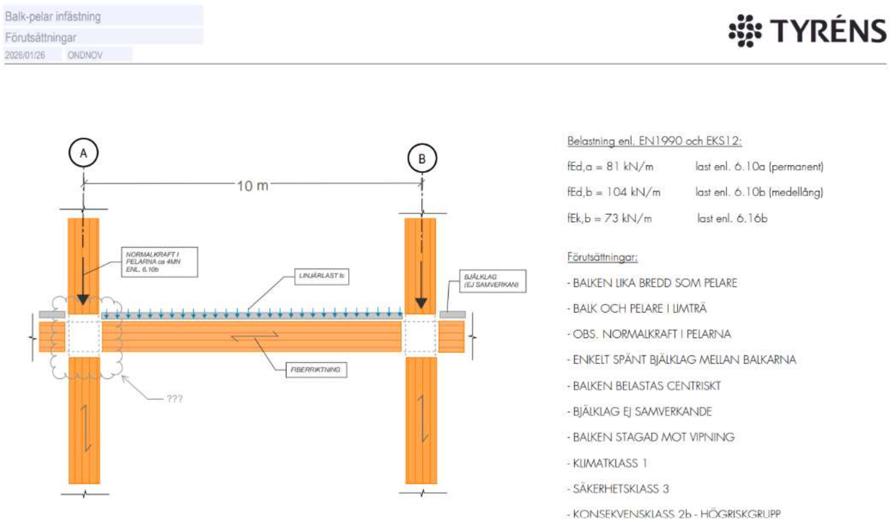


## PREREQUISITES

Service class 1 - medellång

$k_{mod} := 0.8$

$\gamma_M := 1.25$

## CROSS-SECTIONS

### GLULAM BEAM

$h_b := 1100\ mm$ $\quad b_b := 400\ mm$

$A_b := h_b \cdot b_b$ $\quad L_b := 10\ m$

### GLULAM COLUMN

$h_c := 400\ mm$ $\quad b_c := 400\ mm$

$A_c := h_c \cdot b_c$ $\quad L_c := 3\ m$

### GL32h

$f_{mk} := 32\ MPa$ $\quad f_{c.0k} := 32\ MPa$

$f_{vk} := 3.5\ MPa$ $\quad E_{0.05} := 11800\ MPa$

### SIZE EFFECTS

```
if h_b < 600 mm                      = 1
    k_h := min([ (600 / h_b)^0.1 ; 1.1 ])
else
    k_h := 1
```

$$\text{if } h_b < 600\ mm \quad k_h := \min\left(\left[\begin{matrix}\left(\frac{600}{h_b}\right)^{0.1} \\ 1.1\end{matrix}\right]\right) \text{ else } k_h := 1 \quad = 1$$

### DESIGN STRENGTHS

$$f_{md} := \frac{f_{mk} \cdot k_{mod} \cdot k_h}{\gamma_M} = 20.48\ MPa \qquad f_{vd} := \frac{f_{vk} \cdot k_{mod}}{\gamma_M} = 2.24\ MPa$$

$$f_{c.0d} := \frac{f_{c.0k} \cdot k_{mod}}{\gamma_M} = 20.48\ MPa$$

### DESIGN SHEAR AND MOMENT LOAD EFFECTS - PINNED

$$V_{Ed} := \frac{f_{Ed.b} \cdot L_b}{2} = 500\ kN$$

$$M_{Ed} := \frac{f_{Ed.b} \cdot L_b^2}{8} = 1250\ kN\ m$$

## ULS

### BEAM BENDING CAPACITY

$k_{crit} := 1$

$$W_b := \frac{b_b \cdot h_b^2}{6} = 8.0667 \cdot 10^7\ mm^3$$

$$M_{Rd} := f_{md} \cdot W_b \cdot k_{crit} = 1652.0533\ kN\ m$$

$$\frac{M_{Ed}}{M_{Rd}} = 0.7566$$

OK!

$$\text{if } \frac{M_{Ed}}{M_{Rd}} < 1 \quad \text{"OK"} \quad \text{else} \quad \text{"Not OK"} \quad = \text{"OK"}$$

II

## BEAM SHEAR CAPACITY

$$k_{cr} := \min\left(\begin{bmatrix} \dfrac{3.0\ \text{MPa}}{f_{vk}} \\ 1.00 \end{bmatrix}\right) = 0.8571$$

$t_f := 30\ \text{mm}$ $\quad b_p := 283\ \text{mm}$

$t_s := 15\ \text{mm}$

$h_s := 923\ \text{mm}$

$t_{fb} := 58.5\ \text{mm}$ Filler block - based on charring depth

$$A_1 := b_p \cdot \left(t_f + t_{fb}\right)$$

$$A_2 := t_s \cdot h_s$$

$$A_{rem} := A_1 + A_2$$

$$A_{red} := A_b - A_{rem}$$

$$A_{ef} := k_{cr} \cdot A_{red}$$

$$V_{Rd} := \frac{A_{ef} \cdot f_{vd}}{1.5} = 513.4202\ \text{kN}$$

$$\frac{V_{Ed}}{V_{Rd}} = 0.9739$$

OK!

```
if V_Ed / V_Rd < 1  = "OK"
  "OK"
else
  "Not OK"
```

## COLUMN COMPRESSION PARALELL TO FIBRES

$$I := \frac{b_c \cdot h_c^{\,3}}{12} = 2.13 \cdot 10^{9}\ \text{mm}^4$$

$$\text{i} := \sqrt{\frac{I}{A_c}} = 115.47\ \text{mm}$$

$$\lambda := \frac{0.5 \cdot L_c}{\text{i}} = 12.99$$

Fixed-Fixed columns assumption

$$\beta_c := 0.1$$

$$\lambda_{rel} := \frac{\lambda}{\pi} \cdot \sqrt{\frac{f_{c.0k}}{E_{0.05}}} = 0.22$$

$$k := 0.5 \cdot \left(1 + \beta_c \cdot \left(\lambda_{rel} - 0.3\right) + \lambda_{rel}^{\,2}\right) = 0.519$$

$$\begin{array}{l} \text{if } \lambda_{rel} > 0.3 \qquad = 1 \\ \quad k_c := \dfrac{1}{k + \sqrt{k^2 - \lambda_{rel}^{\,2}}} \\ \text{else} \\ \quad k_c := 1 \end{array}$$

$$N_{c.0Rd} := f_{c.0d} \cdot A_c \cdot k_c = 3276.8\ \text{kN}$$

$$\frac{N_{Ed}}{N_{c.0Rd}} = 0.9155$$

OK!

```
if N_Ed / N_c.0Rd < 1 = "OK"
  "OK"
else
  "Not OK"
```

III

# CONNECTION DESIGN - Bearing plate - column side
# According to SS-EN 1995-1-1:2025

### Load and prerequisites

$q := 100\ \frac{kN}{m}$ Line load beam

$L := 10\ m$ Beam span

$V_{Ed} := q \cdot \frac{L}{2} = 500\ kN$ Shear force

$k_{mod} := 0.8$ Modification factor

$\gamma_M := 1.25$ Table 4.4. - Glulam partial factor

$\gamma_R := 1.3$ Table 4.4 - Partial factor - connections with dowel-type fasteners

$\gamma_{M1} := 1.1$ Table 4.4 - Partial factor - Steel design resistance

### Beam dimensions

$h_{beam} := 1100\ mm$

$b_{beam} := 400\ mm$

$E_s := 210000\ MPa$

## Design of flanges according to EN 1995 - 1 -2: 2004

### Table 3.1: Design charring rates

$\beta_0 := 0.65\ \frac{mm}{min}$

$\beta_n := 0.7\ \frac{mm}{min}$

Glulam charring rates - density over 290 kg/m3

### 3.4.2 Surfaces unprotected throughout the time of fire exposure

$time := 90\ min$ Time of fire exposure - 90 min (simon)

$d_{char.0} := \beta_0 \cdot time = 58.5\ mm$ (3.1) - design charring depth

### Key parameters - Dowelled connection - Units in mm, N, Nmm, N/mm2, kg/m3
## 11.2.3 in 1995-1-1:2025
### From Table 11.6: Characteristic embedment strength

$d := 10$ Fastener diameter

$\rho_k := 440$ Timber density GL32h, in kg/m3

$\alpha := 0\ deg$ Angle of the load to the grain

$\varepsilon_c := 90\ deg$ Insertion angle to grain

$$f_{h\alpha k} := \frac{0.082 \cdot (1 - 0.01 \cdot d) \cdot \rho_k}{2.5 \cdot \cos(\varepsilon_c)^2 + \sin(\varepsilon_c)^2} = 32.472$$ (21) - Embeddment strength timber - predrilled

IV

**Steel plate**

$t_p := 15$

Steel plate thickness

```
if  t_p ≤ 0.5                    = 1
  k_plt := 0.5
else
  if  t_p > 1.0
    k_plt := 1
  else
    "Interpolate"
```

$f_{hk} := k_{plt} \cdot 600 = 600$

(1) - Embeddment strength steel - predrilled inner plate

**From Table 11.3: Characteristic yield and tensile strength - screws**

$f_{uk} := 1240$

$f_{yk} := f_{uk} \cdot 0.9 = 1116$

**From Table 11.7: Characteristic yield moment - Screws**

```
d_1 := if (3.5 ≤ d) ∧ (d ≤ 5)        = 6.5
         d_1 := d · 0.6
     else
       if (5 < d) ∧ (d ≤ 10)
         d_1 := d · 0.65
       else
         if (10 < d) ∧ (d ≤ 14)
           d_1 := d · 0.6
         else
           d_1 := d · 0.75
```

Inner thread diameter -
Table 11.7 (4)

$M_{yk} := 0.3 \cdot f_{uk} \cdot d_1^{2.6} = 48318.9699$

(3) - Screw yield moment

**Embeddment depths**

**Embeddment strength definitions**

$f_{h1k} := f_{h\alpha k}$

Timber member

$f_{h2k} := f_{hk}$

Steel member

$\beta := \frac{f_{h2k}}{f_{h1k}} = 18.4775$

(11.15)

**From Table 11.4: Required minimum embedment depth, ensures failure mode f)**

$t_{h1.req.f} := 1.15 \cdot 2 \cdot \sqrt{\frac{M_{yk}}{f_{h1k} \cdot d}} \cdot \left( \frac{\sqrt{\beta}}{\sqrt{1+\beta}} + 1 \right) = 55.3831$

(3)

$t_{h2.req.f} := 1.15 \cdot 2 \cdot \sqrt{\frac{M_{yk}}{f_{h2k} \cdot d}} \cdot \left( \frac{1}{\sqrt{1+\beta}} + 1 \right) = 8.0059$

(4)

V

**From Table 11.5: Required minimum embedment depth, failure mode d)**

$$t_{h1.req.d} := 1.05 \cdot \sqrt{2} \cdot \sqrt{\frac{M_{yk}}{f_{h1k} \cdot d}} \cdot \left( \frac{\sqrt{\beta}}{\sqrt{1+\beta}} \right) = 17.6426 \qquad (1)$$

$$t_{h2.req.d} := 1.05 \cdot \sqrt{2} \cdot \sqrt{\frac{M_{yk}}{f_{h2k} \cdot d}} \cdot \left( \frac{1}{\sqrt{1+\beta}} + \sqrt{2} \right) = 6.9142 \qquad (2)$$

**From Table 11.5: Required minimum embedment depth, failure mode e)**

$$t_{h1.req.e} := 1.05 \cdot \sqrt{2} \cdot \sqrt{\frac{M_{yk}}{f_{h1k} \cdot d}} \cdot \left( \frac{\sqrt{\beta}}{\sqrt{1+\beta}} + \sqrt{2 \cdot \beta} \right) = 127.7572 \qquad (3)$$

$$t_{h2.req.e} := 1.05 \cdot \sqrt{2} \cdot \sqrt{\frac{M_{yk}}{f_{h2k} \cdot d}} \cdot \left( \frac{1}{\sqrt{1+\beta}} \right) = 0.9548 \qquad (4)$$

**Final minimum required embeddment depths**

$$t_{h1.req} := \max \left( \begin{bmatrix} t_{h1.req.f} \\ t_{h1.req.d} \\ t_{h1.req.e} \end{bmatrix} \right) = 127.7572$$

$$t_{h2.req} := \max \left( \begin{bmatrix} t_{h2.req.f} \\ t_{h2.req.d} \\ t_{h2.req.e} \end{bmatrix} \right) = 8.0059$$

**Final embeddment depths**

$$t_{emb.c} := 20 \cdot d = 200$$

Maximum according to axial stiffness equations - 11.

```
t_h1 := if t_emb.c ≥ t_h1.req        = 200
            t_h1 := t_emb.c
        else
            t_h1 := t_h1.req
```

Embeddmenet depth column, depends on screw penetration

```
t_h2 := if t_p ≥ t_h2.req        = 15
            t_h2 := t_p
        else
            t_h2 := t_h2.req
```

Embeddment depth steel plate - Can be increased

VI

**Failure modes a) to f) for fastnener in single shear according to (11.14) and Figure 11.6**

$$F_{Dk} := \begin{bmatrix} f_{h1k} \cdot t_{h1} \cdot d \\ f_{h2k} \cdot t_{h2} \cdot d \\ \dfrac{f_{h1k} \cdot t_{h1} \cdot d}{1+\beta} \cdot \left( \sqrt{\beta + 2 \cdot \beta^{2} \cdot \left( 1 + \dfrac{t_{h2}}{t_{h1}} + \left( \dfrac{t_{h2}}{t_{h1}} \right)^{2} \right) + \beta^{3} \cdot \left( \dfrac{t_{h2}}{t_{h1}} \right)^{2}} - \beta \cdot \left( 1 + \dfrac{t_{h2}}{t_{h1}} \right) \right) \\ \dfrac{1.05 \cdot f_{h1k} \cdot t_{h1} \cdot d}{2+\beta} \cdot \left( \sqrt{2 \cdot \beta \cdot (1+\beta) + \dfrac{4 \cdot \beta \cdot (2+\beta) \cdot M_{yk}}{f_{h1k} \cdot d \cdot t_{h1}^{2}}} - \beta \right) \\ \dfrac{1.05 \cdot f_{h1k} \cdot t_{h2} \cdot d}{1 + 2 \cdot \beta} \cdot \left( \sqrt{2 \cdot \beta^{2} \cdot (1+\beta) + \dfrac{4 \cdot \beta \cdot (1 + 2 \cdot \beta) \cdot M_{yk}}{f_{h1k} \cdot d \cdot t_{h2}^{2}}} - \beta \right) \\ 1.15 \cdot \sqrt{\dfrac{2 \cdot \beta}{1+\beta}} \cdot \sqrt{2 \cdot M_{yk} \cdot f_{h1k} \cdot d} \end{bmatrix} \text{N}$$

$$F_{Dk} = \begin{bmatrix} 64.944 \\ 90 \\ 27.5966 \\ 28.1594 \\ 14.0985 \\ 8.8735 \end{bmatrix} \text{kN}$$

$F_{Dk} := \min\left(F_{Dk}\right) = 8.8735\ \text{kN}$ Governing failure mode f)

$F_{Dd} := \dfrac{k_{mod} \cdot F_{Dk}}{\gamma_M} = 5.6791\ \text{kN}$ Dowel-effect contribution per fastener, per shear plane

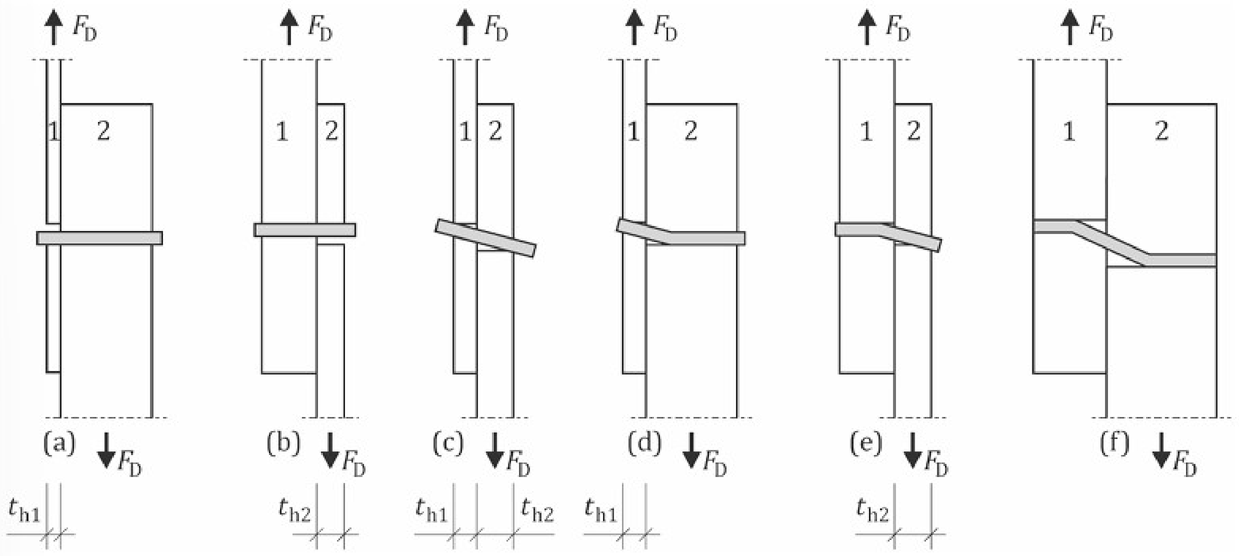


**Figure 11.6 — Possible failure modes a) – f) for a fastener loaded in single shear**

### 11.2.2.3 Withdrawal resistance

$k_{screw} := 8.2$ Factor for the characteristic withdrawal strength

$k_w := 1$ Parameter for angle between fastener to grain

$t_{lamella} := 45\ \mathrm{mm}$ Typical lamella thickness: From swedish wood

$n_p := \dfrac{t_{h1}\ \mathrm{mm}}{t_{lamella}} = 4.4444$ Number of penetraded lamellas as decimal number

$$k_{mat.wk} := \begin{cases} k_{mat.wk} := 1 + \dfrac{\ln(n_p)}{12} & \text{if } 1 + \dfrac{\ln(n_p)}{12} \le 1.15 \\ 1.15 & \text{else} \end{cases} = 1.1243$$

Material parameter for number of laminations

$k_p := 1.1$

$f_{w.k} := k_{screw} \cdot k_w \cdot k_{mat.wk} \cdot (d)^{-0.33} \cdot \left(\dfrac{\rho_k}{350}\right)^{k_p} \dfrac{\mathrm{N}}{\mathrm{mm}^2} = 5.5465\ \mathrm{MPa}$ Table 11.2 (4)

$l_w := t_{h1}\ \mathrm{mm} = 200\ \mathrm{mm}$ Withdrawal length

$F_{w.k.col} := \pi \cdot d\ \mathrm{mm} \cdot l_w \cdot f_{w.k} = 34.8498\ \mathrm{kN}$ Withdrawal strenght (11.3)

### 11.2.2.4 Steel tensile resistance

$A_s := \pi \cdot \left(\dfrac{d_1}{2}\right)^2 = 33.1831$

$F_{t.k} := 0.9 \cdot A_s \cdot f_{uk}\ \mathrm{N} = 37.0323\ \mathrm{kN}$

### 11.2.3.8 Rope-effect contribution

$\gamma_{M2} := 1.25$ Table 4.4 - Partial factor, steel in tension

$k_{rp1} := 0.25$ Table 11.8

$k_{rp2} := 1$ Table 11.9

$$F_{ax.t.d} := \min\left(\begin{bmatrix} \dfrac{k_{mod}}{\gamma_R} \cdot \max\left(\begin{bmatrix} F_{w.k.col} \end{bmatrix}\right) \\ \dfrac{F_{t.k}}{\gamma_{M2}} \end{bmatrix}\right) = 21.4461\ \mathrm{kN}$$

(11.1) Design axial tensile resistance

$$F_{rp.d} := \min\left(\begin{bmatrix} k_{rp1} \cdot F_{ax.t.d} \\ k_{rp2} \cdot F_{Dd} \end{bmatrix}\right) = 5.3615\ \mathrm{kN}$$

(11.19) Rope effect contribution

### 11.2.3.1 General: Design lateral resistance per shear plane of a single fastener

$F_{vd} := F_{Dd} + F_{rp.d} = 11.0406\ \mathrm{kN}$ (11.13)

VIII

**Minimum spacings and edge and end distances for screws, Predrilled Table 11.16**

$a_{1.min} := 5 \cdot d\ \mathrm{mm} = 50\ \mathrm{mm}$ Paralell to grain

$a_{2.min} := 4 \cdot d\ \mathrm{mm} = 40\ \mathrm{mm}$ Perpendicular to grain

$a_{3.t.min} := 12 \cdot d\ \mathrm{mm} = 120\ \mathrm{mm}$ Loaded end - parallel to grain

$a_{3.c.min} := 7 \cdot d\ \mathrm{mm} = 70\ \mathrm{mm}$ Unloaded end - parallell to grain

$a_{4.t.min} := 7 \cdot d\ \mathrm{mm} = 70\ \mathrm{mm}$ Loaded edge - perpendicular to grain

$a_{4.c.min} := 5 \cdot d\ \mathrm{mm} = 50\ \mathrm{mm}$ Unloaded edge - perpendicular to grain

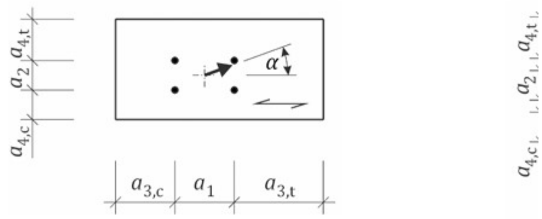


**a) Nails, screws, rods with wood screw thread, dowels, bolts and bonded-in rods**

**Key**

$a_{1/2}$ spacing of dowel-type fasteners parallel/perpendicular to grair

$a_{3,t/c}$ loaded/unloaded end distance parallel to grain

$a_{4,t/c}$ loaded/unloaded edge distance perpendicular to grain

$\alpha$ load to grain angle

$\theta$ staple crown to grain angle

**Table 11.16 — Minimum spacings, edge and end distances for laterally-loaded dowel-type fasteners and shear connectors in SL, PL, PW, OSB, HB, MB, MDF, RPB and CPB**

| SL, PL, PW, OSB, HB, MB, MDF, RPB and CPB<br>Type | Spacing / distance<br>Criteria | $a_{1,min}$ | $a_{2,min}$ | $a_{3,t,min}$ (loaded end) | $a_{3,c,min}$ (unloaded end) | $a_{4,t,min}$ (loaded edge) | $a_{4,c,min}$ (unloaded edge) |
|---|---|---|---|---|---|---|---|
| **Not predrilled** | | | | | | | |
| Nails, screws and rods with wood screw thread | $\rho_k \le 430\ kg/m^3$ | $10d$ | $5d$ | $15d$ | $10d$ | $7d$ | $5d$ |
| Nails, screws | $\rho_k > 430\ kg/m^3$<br>$\rho_k \le 500\ kg/m^3$ | $15d$ | $7d$ | $20d$ | $15d$ | $12d$ | $7d$ |
| Staple legs | $\rho_k \le 500\ kg/m^3$ | $15d$ | $5d$ | $15d$ | $10d$ | $7d$ | $5d$ |
| **Predrilled** | | | | | | | |
| Nails, screws and rods with wood screw thread | | $5d$ | $4d$ | $12d$ | $7d$ | $7d$ | $3d$ |
| Dowels and bonded-in rods | | $5d$ | $3d$ | max ($7d$; 80 mm) | $4d$ | $4d$ | $3d$ |
| Bolts | | $5d$ | $4d$ | max ($7d$; 80 mm) | $4d$ | $4d$ | $3d$ |
| Ring and shear plate connectors | | $2d_{con}$ | $3d_{con}$ | $1,5d_{con}$ | $2d_{con}$ | $0,6d_{con}$ | $0,6d_{con}$ |
| Toothed plate connectors | | $1,5d_{con}$ | $1,2d_{con}$ | $2,0d_{con}$ | $2d_{con}$ | $0,8d_{con}$ | $0,6d_{con}$ |

$t_f := 30\ \mathrm{mm}$

**Plate dimensions and number of fasteners connected to column**

$h_p := h_{beam} - 2 \cdot d_{char.0} - t_f = 953\ \mathrm{mm}$ Height of plate

$b_{90.c} := b_{beam} - 2 \cdot d_{char.0} = 283\ \mathrm{mm}$ Width of plate

$n_0 := 13$ Number of fastener paralell to grain - column

$n_{90} := 4$ Number of fasteners perpendicular to grain - column

$n := n_0 \cdot n_{90} = 52$

$a_{end} := 20\ \mathrm{mm}$

**Chosen spacings**

Unloaded end - top

$a_{3.c} := a_{3.c.min} = 70\ \mathrm{mm}$

$a_{4.c} := a_{4.c.min} = 50\ \mathrm{mm}$

Loaded end - bottom

$a_{3.t} := a_{3.t.min} = 120\ \mathrm{mm}$

$a_{4.t} := a_{4.t.min} = 70\ \mathrm{mm}$

$a_1 := \text{if } \dfrac{h_p - 2 \cdot a_{end}}{n_0 - 1} > a_{1.min} = 76.0833\ \mathrm{mm}$ Spacing paralell to grain

$\qquad a_1 := \dfrac{h_p - 2 \cdot a_{end}}{n_0 - 1}$

$\quad \text{else}$

$\qquad a_1 := a_{1.min}$

IX

$$a_2 := \text{if } \frac{b_{90.c} - 2 \cdot a_{2.min}}{n_{90} - 1} > a_{2.min} = 67.6667 \text{ mm}$$

$$a_2 := \frac{b_{90.c} - 2 \cdot a_{2.min}}{n_{90} - 1}$$

else

$$a_2 := a_{2.min}$$

Spacing perpendicular to grain

**Check that spacing fits**

Paralell to grain arrangement

$$\text{if } 2 \cdot a_{end} + \left(n_0 - 1\right) \cdot a_1 \le h_p = \text{"OK"}$$

"OK"

else

"Not OK"

Perpendicular to grain arrangement

$$\text{if } 2 \cdot a_{2.min} + \left(n_{90} - 1\right) \cdot a_2 \le b_{90.c} = \text{"OK"}$$

"OK"

else

"Not OK"

X

# Shear force validation - equal distribution

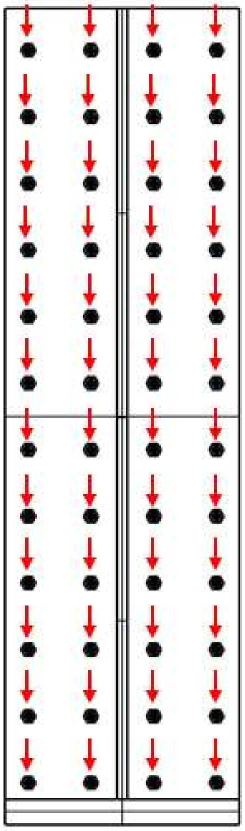

**Bracket geometry**

$t_f := 30\ \mathrm{mm}$

$l_f := 320\ \mathrm{mm}$

$b_f := 283\ \mathrm{mm}$

$h_p = 953\ \mathrm{mm}$

$t_p\ \mathrm{mm} = 15\ \mathrm{mm}$

$h_s := h_p - t_f = 923\ \mathrm{mm}$

$t_s := 15\ \mathrm{mm}$

**Screw configuration**

$n_0 = 13$ $\qquad a_1 = 76.0833\ \mathrm{mm}$

$n_{90} = 4$ $\qquad a_2 = 67.6667\ \mathrm{mm}$

$n = 52$

**Design shear force in each screw -
symmetric internal beam shoe -> no group effect considered**

$$F_v := \frac{V_{Ed}}{n} = 9.6154\ \mathrm{kN}$$

# Axial force validation - Rigid body assumption

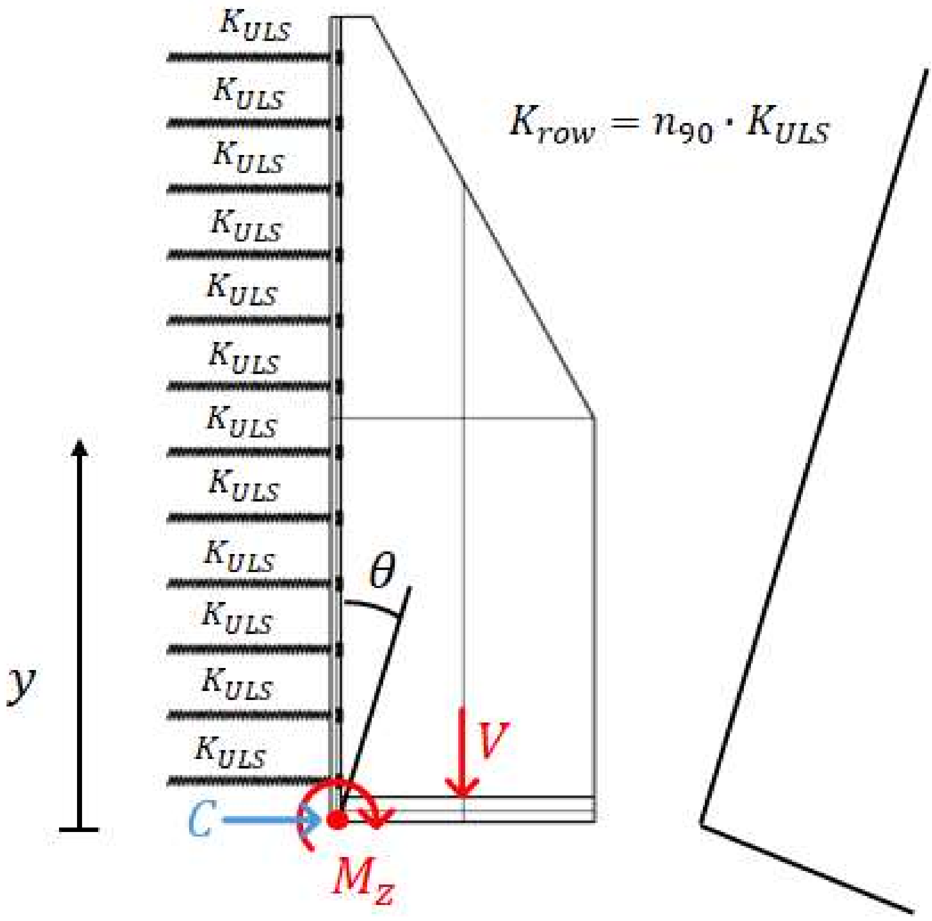


### Bracket load and resulting moment

$t_p := t_p \ \mathrm{mm} = 15 \ \mathrm{mm}$

$e_x := \dfrac{l_f}{2} + t_p = 175 \ \mathrm{mm}$

$M_z := V_{Ed} \cdot e_x = 8.75 \cdot 10^{7} \ \mathrm{N \ mm}$

### Load introduction - Stiffener to backplate

$y_a := \dfrac{1}{3} \cdot h_s = 307.6667 \ \mathrm{mm}$ Assumption, stiffener introduces opening at ya from bottom

$y_0 := 0 \ \mathrm{mm}$

$y_{RC} := y_0$ Rotation about the toe

## Screw properties

Screw axial stiffness - built in units mm, kg/m3 - Table 11.3

$d = 10$

$l_w := t_{h1} = 200$

$\rho_{mean} := 490$

$k_{SLS.ax} := 2 \cdot d^{0.6} \cdot l_w^{0.6} \cdot \rho_{mean}^{0.9} = 50445.7363$

$k_{ULS.ax} := \dfrac{k_{SLS.ax}}{1.5} \dfrac{\mathrm{N}}{\mathrm{mm}} = 33630.4908 \dfrac{\mathrm{N}}{\mathrm{mm}}$

XII

Screw laterall stiffness - built in units mm, kg/m3 - Used as input in Abaqus - Table 11.12

$$k_{SLS.lat} := \text{if } t_p \geq 1 \cdot d \text{ mm} \quad 2 \cdot 60 \cdot d_1^{1.7} \cdot \left(\frac{\rho_{mean}}{420}\right)^{1.1} \quad \text{else} \quad 60 \cdot d_1^{1.7} \cdot \left(\frac{\rho_{mean}}{420}\right)^{1.1} = 3425.9058$$

If sufficienty clamped - > * 2!

$$k_{ULS.lat} := \frac{k_{SLS.lat}}{1.5} \frac{\text{N}}{\text{mm}} = 2283.9372 \frac{\text{N}}{\text{mm}}$$

$$K_{row} := n_{90} \cdot k_{ULS.ax} = 1.3452 \cdot 10^5 \frac{\text{N}}{\text{mm}}$$

Row stiffness

**Screw coordinates and lever arms to RC**

Vertical coordinate of row r

Lever arms from RC to each row

$$r := [1 .. n_0]$$

$$y_r := t_f + a_{end} + (r-1) \cdot a_1 = \begin{bmatrix} 50 \\ 126.0833 \\ 202.1667 \\ 278.25 \\ 354.3333 \\ 430.4167 \\ 506.5 \\ 582.5833 \\ 658.6667 \\ 734.75 \\ 810.8333 \\ 886.9167 \\ 963 \end{bmatrix} \text{mm}$$

$$y_{i\,r} := y_r - y_0 = \begin{bmatrix} 50 \\ 126.0833 \\ 202.1667 \\ 278.25 \\ 354.3333 \\ 430.4167 \\ 506.5 \\ 582.5833 \\ 658.6667 \\ 734.75 \\ 810.8333 \\ 886.9167 \\ 963 \end{bmatrix} \text{mm}$$

Lever arms above RC

$$y_{pos\,r} := \text{Max}\left(\begin{bmatrix} y_{i\,r} \\ 0 \end{bmatrix}\right)$$

Sum lever arms for equillibrium

$$y_{\Sigma.t} := \sum_{r=1}^{n_0} \left( \left( y_{pos\,r} \right)^2 \right) = 4.3886 \text{ m}^2$$

## Moment equiliibrium about RC - compression toe

$N_r := k_{ULS.ax} \cdot \delta_r$ Withdrawal force in one screw in row r

$T := n_{90} \cdot N_r$ Total withdrawal force in in row r

$C := \sum_{r=1}^{n_0} T_r$ From horizontal equillibrium we get C = sum(T)

$\delta_r := \theta_z \cdot y_{pos_r}$ Axial displacement from rigid body rotation assumption

Moment eq. about RC gives, with summation of axiall row forces and their respective lever arms

$$M_z := \sum_{r=1}^{n_0} T \cdot y_{pos_r}$$

Row forces * lever arms

Expand T

$$M_z := \sum_{r=1}^{n_0} \left( n_{90} \cdot k_{ULS.ax} \cdot \theta_z \cdot y_{pos_r} \right) \cdot y_{pos_r}$$

With known moment

$$M_z := V_{Ed} \cdot e_x = 87.5 \text{ kN m}$$

We get the rigid body rotation angle from known moment

$$\theta_z := \frac{M_z}{n_{90} \cdot k_{ULS.ax} \cdot \sum_{r=1}^{n_0} \left( \left( y_{pos_r} \right)^2 \right)} = 0.0001$$

Rigid body rotation - analytical simplified assumption of an infinetly stiff plate

**Axial displacemnt per screw in row r**

$\delta_r := \theta_z \cdot y_{pos_r}$

**Axial force per screw in row r**

$N_r := k_{ULS.ax} \cdot \delta_r$

**Total axial force in all screws in row r**

$$T_r := n_{90} \cdot N_r = \begin{bmatrix} 0.9969 \\ 2.5139 \\ 4.0308 \\ 5.5478 \\ 7.0647 \\ 8.5817 \\ 10.0986 \\ 11.6156 \\ 13.1325 \\ 14.6495 \\ 16.1665 \\ 17.6834 \\ 19.2004 \end{bmatrix} \text{ kN}$$

**Total compression force at toe**

$$C := \sum_{r=1}^{n_0} T_{r_r} = 131.2823 \text{ kN}$$

# Bearing plate validation - Bending stresses

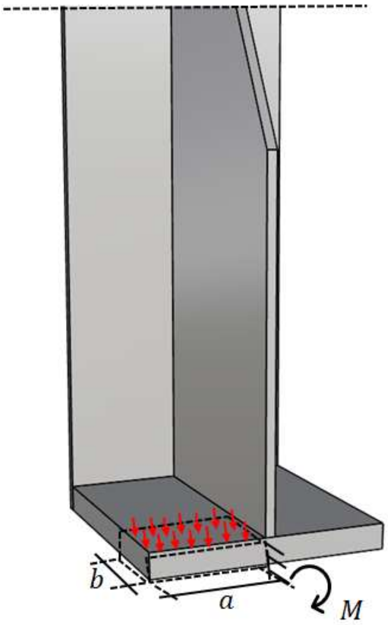


$b := 10\ \mathrm{mm}$ Width strip

$a := \dfrac{b_{90.c} - t_s}{2} = 134\ \mathrm{mm}$ Length strip

$q_p := \dfrac{V_{Ed}}{2 \cdot l_f \cdot a} = 0.0058\ \dfrac{\mathrm{kN}}{\mathrm{mm}^2}$ Load strip

$M_{p.Ed} := \dfrac{q_p \cdot a^2}{2} \cdot b = 523.4375\ \mathrm{kN\ mm}$ Design moment

$W_{p.el} := \dfrac{b \cdot t_f^2}{6} = 1500\ \mathrm{mm}^3$ Section modulus - strip

$\sigma_p := \dfrac{M_{p.Ed}}{W_{p.el}} = 348.9583\ \mathrm{MPa}$ Maximum stress strip

$f_y := 355\ \mathrm{MPa}$ Steel quality

# Design resistance checks - Numerical model

### EN 1995 - 1 - 1: 2025: 11.2.3 Lateral resistance of a fastener per shear plane

$F_{v.FEM} := 10.06\ \mathrm{kN}$

$\dfrac{F_{v.FEM}}{F_{vd}} = 0.9112$ OK!

### Check against maximum axial capacity - Eq: (11.1)

$F_{ax.FEM} := 9.03\ \mathrm{kN}$

$\dfrac{F_{ax.FEM}}{F_{ax.t.d}} = 0.4211$ OK!

### Interaction of axial and lateral forces - top inner screw

$F_{v.FEM.top} := 9.7\ \mathrm{kN}$ Corresponding worst combination screw lateral force

$\left(\dfrac{F_{v.FEM.top}}{F_{vd}}\right)^2 + \left(\dfrac{F_{ax.FEM}}{F_{ax.t.d}}\right)^2 = 0.9492$ OK!

### Bearing plate bending stresses

$\sigma_{z.FEM} := 340.2\ \mathrm{MPa}$

$\dfrac{\sigma_{z.FEM}}{f_y} = 0.9583$ OK!

XV

**DEPARTMENT OF ARCHITECTURE AND CIVIL ENGINEERING**
**CHALMERS UNIVERSITY OF TECHNOLOGY**
Gothenburg, Sweden 2026
www.chalmers.se

CHALMERS
UNIVERSITY OF TECHNOLOGY